Zirconium metal organic frameworks as heterogeneous catalysts for Meerwein-Ponndorf-Verley reactions

Hans-Hilmar Mautschke

Doctoral Thesis

September 2019

Valencia

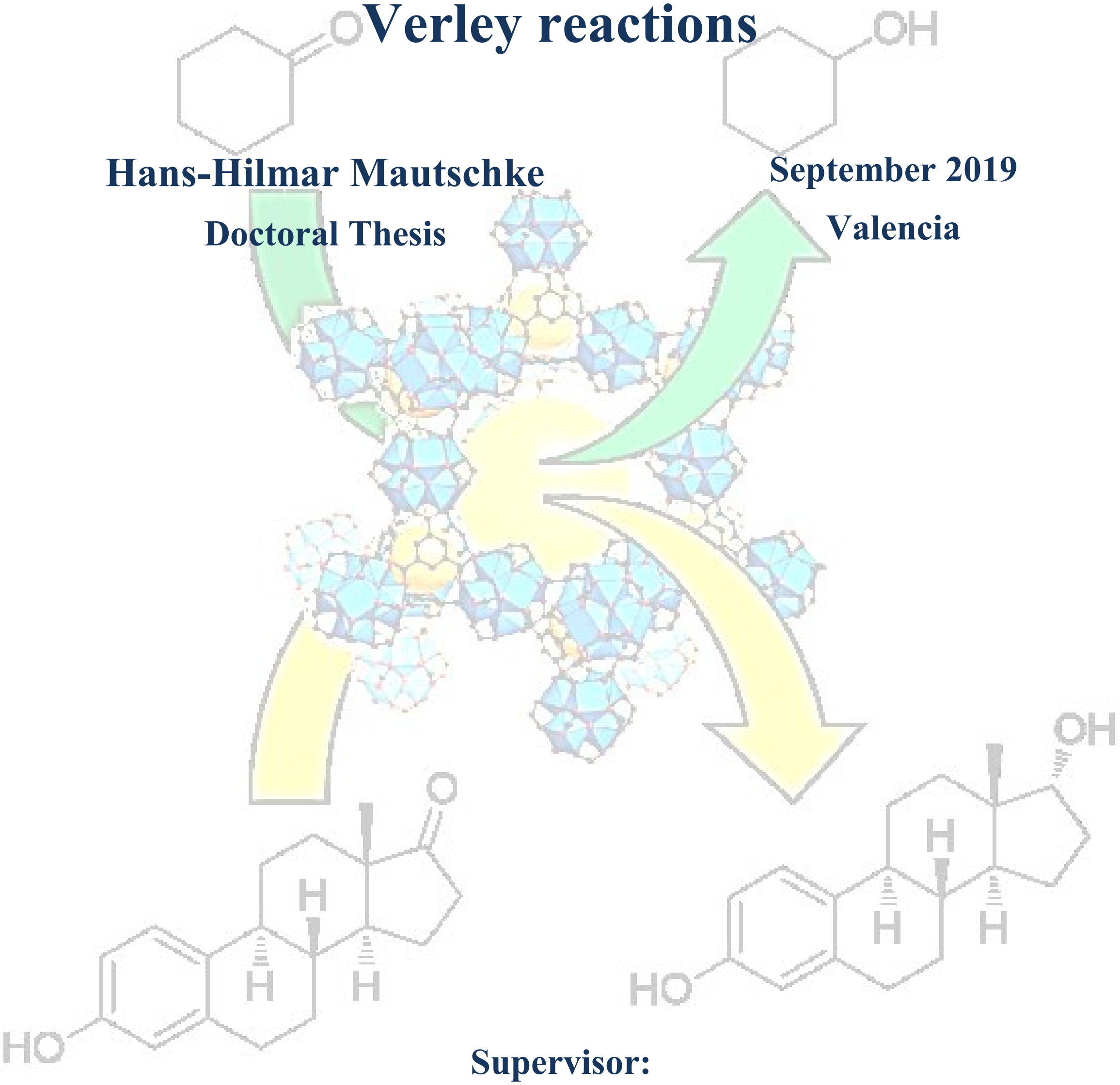

Supervisor:

Dr. Francesc X. Llabrés i Xamena

INSTITUTO DE TECNOLOGÍA QUÍMICA
CSIC
CONSEJO SUPERIOR DE INVESTIGACIONES CIENTÍFICAS
UNIVERSITAT POLITÈCNICA DE VALÈNCIA

UNIVERSITAT POLITÈCNICA DE VALÈNCIA

Instituto Universitario Mixto de Tecnología Química

(UPV-CSIC)

ZIRCONIUM METAL ORGANIC FRAMEWORKS AS HETEROGENEOUS CATALYSTS FOR MEERWEIN-PONNDORF-VERLEY REACTIONS

Doctoral Thesis

Hans-Hilmar Mautschke

Supervisor:

Dr. Francesc X. Llabrés i Xamena

September 2019

Valencia

Francesc X. Llabrés i Xamena, Tenured Scientist at the Instituto Universitario Mixto de Tecnología Química (UPV-CSIC), hereby

CERTIFY: That the thesis entitled "**Zirconium Metal Organic Frameworks as Heterogeneous Catalysts for Meerwein-Ponndorf-Verley Reactions**" has been carried out under my supervision by Mr. Hans-Hilmar Mautschke at the Instituto Universitario Mixto de Tecnología Química

Dr. Francesc X. Llabrés i Xamena

Acknowledgements

I want to thank the European Union's Horizon 2020 research and innovation program for a contract under the Marie Sklodowska-Curie grant agreement No. 641887 (Project acronym: DEFNET).

I want to give a special thanks to Francesc X. Llabrés i Xamena who trusted me with this project and guided me through the last years during my work at the ITQ. It was definitely a great experience to work on this project in the group of Metal-Organic Frameworks. I also would like to thank A. Eduardo Palomares for accepting me as a tutor during my stay at the ITQ.

I want to thank Fran who introduced me into the lab work and also all the others who helped me if there were any barriers to cross. I am very happy that I could meet so many new nice people during the last years, inside and outside the ITQ.

I also want to thank Prof. Richard Fischer and those responsible at Clariant, Heufeld, especially, Andreas Reitzmann and Andreas Berger, who enabled this industrial secondment for me and introduced me into the work with zeolites and the work in an industrial environment. I am very glad that I could also make this experience during the DEFNET project.

Also I want to thank the whole DEFNET team. There were alot of interesting workshops and it was always very nice to get so much scientific input apart from the work at the ITQ. Further it was so nice to meet with all the other PhDs and postdocs during this time.

I want to thank Germán Sastre at the ITQ for the computational work that is finally included in Chapter 5 and 6 of this thesis.

Last, I also want to thank my family. Knowing that I always can count on their support also made all of this possible for me.

Resumen

Se han preparado varios materiales metal orgánicos de circonio MOF-808 para evaluar sus propiedades catalíticas en reacciones tipo Meerwein-Ponndorf-Verley (MPV) para la reducción de compuestos carbonílicos.

En particular, se han sintetizado compuestos tipo MOF-808 modificados en los que una pequeña fracción de los ligandos trimesato presentes en el MOF original se ha reemplazado por ligandos dicarboxilato, como una estrategia para inducir la creación controlada de defectos estructurales. Los ligandos utilizados han sido: isoftalato (MOF-808-IPA), 3,5-piridindicarboxilato (MOF-808-Pydc), 5-aminoisoftalato (MOF-808-NH_2) y 5-hidroxiisoftalato (MOF-808-OH). Todos los materiales obtenidos presentan una elevada cristalinidad y son isoreticulares respecto al MOF-808 original.

Se ha evaluado la actividad catalítica del MOF-808 original y de los materiales modificados en reacciones tipo MPV, utilizando ciclohexanona como compuesto modelo. Todos los materiales presentan una elevada actividad catalítica, superior a la del tereftalato de circonio UiO-66 utilizado como referencia. Esta mayor actividad catalítica se corresponde a un mayor número de iones Zr^{4+} con insaturación coordinativa presentes en el MOF-808 con respecto al UiO-66. Además, los materiales MOF-808-IPA y MOF-808-Pydc presentan una mayor actividad que el MOF-808 original, lo que se debe a la presencia de centros activos menos congestionados estéricamente debido a la introducción de los ligandos dicarboxilato. Una ventaja adicional de compuestos MOF-808 con respecto al UiO-66 es su sistema de poros más grande, lo que permite la conversión de moléculas de mayor tamaño. Para evaluar esta característica, se ha utilizado un compuesto de gran tamaño, la estrona, capaz de penetrar en los poros del MOF-808 pero no en el UiO-66. En consecuencia, el MOF-808 es capaz de convertir por completo la estrona de forma selectiva a estradiol, mientras que el UiO-66 apenas presenta actividad. Además, cuando se usa el MOF-808 como catalizador, se produce una cantidad considerable del isómero 17α-estradiol, difícil de obtener por otros medios, por lo que las propiedades de diastereoselectividad del MOF-808 en reacciones MPV resultan de gran interés preparativo.

Con el fin de estudiar en mayor detalle la diastereoselectividad de reacciones MPV catalizadas por MOF-808, se ha estudiado la reducción de ciclohexanonas substituidas: 3-metilciclohexanona (3MeCH), 2-metilciclohexanona (2MeCH) y 2-fenil-ciclohexanona (2PhCH). En función del alcohol utilizado como reductor y de la posición del grupo substituyente en la ciclohexanona, el MOF-808 favorece selectivamente la formación de uno u otro isómero, con una diastereoselectividad variable: 82%, 61% y 94%, respectivamente para 3MeCH, 2MeCH y 2PhCH. Es posible racionalizar estos resultados considerando la formación preferencial de uno u otro estado de transición en el espacio confinado disponible dentro de los poros del MOF. Las características energéticas del proceso se han analizado mediante el uso combinado de estudios cinéticos y cálculos teóricos.

Finalmente, en vista las interesantes propiedades del MOF-808 como catalizador para reacciones MPV, se ha extendido con éxito el uso de este material a la preparación de

compuestos hidroxiesteroides de difícil obtención y de interés farmacológico mediante la reducción quimio-, regio- y diastereoselectiva del correspondiente oxoesteroide. De esta forma, se han conseguido obtener en un solo paso de reacción y con una elevada selectividad los siguientes compuestos: 17α-estradiol, 5α-androstan-3β,17α-diol y epitestosterona, lo que demuestra el potencial del MOF-808 como catalizador para la síntesis de compuestos de alto valor añadido.

Abstract

Various zirconium-containing MOF-808 compounds have been prepared as potential catalysts for the Meerwein-Ponndorf-Verley (MPV) reduction of carbonyl compounds.

Modified MOF-808 have been synthethized in which a small fraction of the trimesate ligands present in pristine MOF-808 has been replaced by dicarboxylate ligands, as a strategy to induce a controlled creation of defects. The linkers used are: isophthalate (MOF-808-IPA), 3,5-pyridinedicarboxylate (MOF-808-Pydc), 5-aminoisophthalate (MOF-808-NH_2) and 5-hydroxyisophthalate (MOF-808-OH). All these compounds are highly crystalline and isoreticular with pristine MOF-808.

The catalytic activity of pristine and defect engineered MOF-808 has been evaluated for MPV reactions, using cyclohexanone as model substrate. All the materials show a higher catalytic activity than that of zirconium terephthalate UiO-66 used as reference. This higher activity is attributed to the higher amount of coordinatively unsaturated Zr^{4+} ions in MOF-808 than in UiO-66. Moreover, MOF-808-IPA and MOF-808-Pydc are more active than pristine MOF-808, which is due to the creation of less sterically crowded sites due to the introduction of defective dicarboyxlate linkers. A further advantage of MOF-808 over UiO-66 is the presence of a wider pore system, which allows converting bulkier substrates. To evaluate this characteristic, a bulky ketone has been used; estrone, which can enter the pores of MOF-808 but not those of UiO-66. Accordingly, MOF-808 can fully convert estrone selectively to estradiol, while UiO-66 shows barely any catalytic activity. Interestingly, when MOF-808 is used as catalysts, a noticeable amount of the isomer 17α-estradiol is produced, which is difficult to obtain by other means. Therefore, the diastereoselective properties of MOF-808 for MPV reactions are interesting from the preparative point of view.

In order to investigate in more detail the diastereoselective properties of MOF-808 for MPV reactions, various substituted cyclohexanones have been considered: 3-methylcyclohexanone (3MeCH), 2-methylcyclohexanone (2MeCH) and 2-phenylcyclohexanone (2PhCH). Depending on the alcohol used as reducing agent and the position of the substituent in the cyclohexanone molecule, MOF-808 selectively favors the formation of one isomer or the other with a different diastereoselectivity: 82%, 61% and 94%, respectively for 3MeCH, 2MeCH y 2PhCH. These results can be rationalized by considering the preferential formation of a given transition state in the confined space available inside the MOF pores. The energetic characteristics of the process have been analyzed by a combined use of kinetic studies and theoretical calculations.

Finally, in view of the interesting properties of MOF-808 as catalyst for MPV reactions, this material has been successfully applied to the preparation of a number of challenging hydroxysteroid compounds with pharmacologic interest through a chemo-, regio- and diastereoselective reduction of the corresponding oxosteroid. In this way, it has been possible to prepare in one single reaction step the following compounds: 17α-estradiol, 5α-androstan-3β,17α-diol and epitestosterone. This demonstrates the high potential of MOF-808 as a catalysts for the synthesis of high added value compounds.

Resum

S'han preparat varis materials metall orgànics de zirconi MOF-808 per avaluar les seves propietats catalítiques en reaccions tipus Meerwein-Ponndorf-Verley (MPV) per a la reducció de composts carbonílics.

En particular, s'han sintetitzat composts tipus MOF-808 modificats en els que una petita fracció dels lligands trimesat presents en el MOF original s'han reemplaçat per lligands dicarboxilats, com una estratègia per induir la creació controlada de defectes estructurals. Els lligands utilitzats han sigut: isoftalat (MOF-808-IPA), 3,5-piridindicarboxilat (MOF-808-Pydc), 5-aminoisoftlatat (MOF-808-NH_2) i 5-hidroxiisoftalat (MOF-808-OH). Tots els materials preparats presenten una elevada cristal·linitat i són isoreticular respecte al MOF-808 original.

S'ha avaluat l'activitat catalític del MOF-808 original i dels materials modificats en reaccions tipus MPV, utilitzant ciclohexanona com a compost model. Tots els materials presenten una elevada activitat catalítica, superior a la del tereftalat de zirconi UiO-66 utilitzat com a referència. Aquesta major activitat catalítica es correspon a un major nombre d'ions Zr^{4+} amb insaturació coordinativa presents en el MOF-808 respecte a l'UiO-66. A més, els materials MOF-808-IPA i MOF-808-Pydc presenten una major activitat que el MOF-808 original, el que és debut a la presència de centres actius menys congestionats estèricament debut a la introducció dels lligands dicarboxilat. Un avantatge addicional dels MOF-808 respecte a l'UiO-66 és el seu sistema de porus més gran, que permet la conversió de molècules de major tamany. Per avaluar aquesta característica, s'ha utilitzat un compost de gran taman, l'estrona, capaç de penetrar en els porus del MOF-808 però no en els de l'UiO-66. En conseqüència, el MOF-808 és capaç de convertir completament l'estrona de forma sel·lectiva a l'estradiol, mentre que l'UiO-66 gairebé no presenta activitat catalítica. A més, quan s'usa el MOF-808 com a catalitzador, es produeix una quantitat considerable de l'isòmer 17α-estradiol, difícil d'obtenir per altre medis, de manera que les propietats de diastereoselectivitat del MOF-808 en reaccions MPV resulten de gran interès preparatiu.

Per tal d'estudiar en major detall la diastereoselectivitat de reaccions MPV catalitzades per MOF-808, s'ha estudiat la reducció de ciclohexanones substituïdes: 3-metilciclohexanona (3MeCH), 2-metilciclohexanona (2MeCH) i 2-fenil-ciclohexanona (2PhCH). En funció de l'alcohol usat com a reductor i de la posició del grup substituent en la ciclohexanona, el MOF-808 afavoreix selectivament la formació d'un o de l'altre isòmer, amb una diastereoselectivitat variable: 82%, 61% y 94%, respectivament per a 3MeCH, 2MeCH y 2PhCH. És possible racionalitzar aquest resultats considerant la formació preferent d'un o l'altre estat de transició en l'espai confinat disponible dins dels porus del MOF. Les característiques energètiques del procés s'han analitzat mitjançant l'ús combinat d'estudis cinètics i càlculs teòrics.

Finalment, en vista de les interessants propietats del MOF-808 com a catalitzador per a reaccions MPV, s'ha estès amb èxit l'ús d'aquest material a la preparació de composts hidroxiesteroids de difícil obtenció i d'interès farmacològic mitjançant la reducció quimio-, regio- i diastereoselectiva del corresponent oxoesteroid. D'aquesta manera, s'ha aconseguit obtenir en un únic pas de reacció i amb una elevada selectivitat els següents composts: 17α-estradiol, 5α-androstan-3β,17α-diol i epitestosterona, el que demostra el potencial del MOF-808 com a catalitzador per a la síntesi de composts d'alt valor afegit.

List of symbols and abbreviations

$\Delta G^{\ddagger}$	Gibbs free energy of activation
$\Delta H^{\ddagger}$	Enthalpy of activation
$\Delta S^{\ddagger}$	Entropy of activation
Δ^1-T	Δ^1-testosterone
17-OH	17-hydroxysteroid
17-OXO	17-oxosteroid
5-HMF	5-(hydroxymethyl)furan-2-carbaldehyde
A4	Δ^4-androstene-3,17-dione
Ac	acetate
ADD	$\Delta^{1,4}$-Androstadiene-3,17-dione
AES	atomic emission spectroscopy
AlTPPCl	5,10,15,20-tetraphenylporphynatoaluminiumchloride
ANGELS	activators of non-genomic estrogen-like signaling
a.u.	arbitrary unit
BDC	benzene-1,4-dicarboxylate, terephthalate
BEA	beta polymorph A
BET	BRUNAUER-EMMETT-TELLER
BPDC	[1,1'-biphenyl]-4,4'-dicarboxylate, 4,4'-biphenyldicarboxylate
BPin	4,4,5,5-tetramethyl-1,3,2-dioxaborolane
BSE	backscattered electrons
BTC	benzene-1,3,5-tricarboxylate
Bu	butyl
c	concentration
Cbz	benzyl carbamate
CH	cyclohexanone
CHol	cyclohexanol
CTH	catalytic transfer hydrogenation
cus	coordinatively unsaturated sites
CWA	chemical warfare agents

D	dimensionality
DE	defect-engineered, defect engineering
DEC	diethyl carbonate
DHT	dihydrotetosterone
DIBAL-H	diisobutylaluminum hydride
DMC	dimethyl carbonate
DMF	*N,N*-dimethylformamide
DMMP	dimethyl methylphosphonate
DMNP	dimethyl 4-nitrophenyl phosphate
DMSO	(methylsulfinyl)methane, dimethyl sulfoxide
d.r.	diastereomeric ratio
DRIFTS	diffuse reflectance infrared fourier transform spectroscopy
DTTDC	dithieno[3,2-b;2',3'-d]-thiopheno-2,6-dicarboxylate,
DUT	Dresden University of Technology
E	epitestosterone
E1	estrone
E2	estradiol
EDS	energy dispersive x-ray spectroscopy
e.g.	for example
EL	ethyl 4-oxopentanoate, ethyl levulinate
EMC	ethyl methyl carbonate
E-P	EYRING-POLANYI
EPIA	epiandrosterone
EPIAdiol	androstane-3β,17-diol
equiv.	equivalents
ER	estrogen receptor
Et	ethyl
et al.	and others
FESEM	field emission scanning electron microscopy

FID	flame ionization detector
FTIR	fourier-transform infrared spectroscopy
GA	(*RS*)-Ethyl *N*,*N*-Dimethylphosphoramidocyanidate, Tabun
GC	gas chromatography
GD	3,3-Dimethylbutan-2-yl methylphosphonofluoridate, Soman
Gly	glycine
GVL	5-methyldihydrofuran-2(3*H*)-one, γ-valerolactone
h	hours
HKUST	Hong Kong University of Science and Technology
HOMO	highest occupied molecular orbital
HPW	12-tungstophoric acid
i	*iso*
ICP	inductively coupled plasma
IPA	benzene-1,3-dicarboxylate, isophthalate
IR	infrared
IRMOF	isoreticular metal-organic framework
L	ligand
LA	4-oxopentanoic acid, levulinic acid
LUMO	lowest unoccupied molecular orbital
M	molarity
MCM	Mobile Composition of Matter
MIL	Matériaux de l'Institut Lavoisier
MPAK/ERK	mitogen-activated protein kinases/extracellular signal-regulated kinases
MOF	metal-organic framework
MPV(O)	Meerwein-Ponndorf-Verley(-Oppenauer) reaction
MWW	Mobile tWenty tWo
NAD(P)H	Nicotinamidadenindinukleotid(phosphat), reduced form
NBO	natural bond orbital

NMR	nuclear magnetic resonance spectroscopy
NP	nanoparticle
NU	Northwestern University
p	*para*
PCN	porous coordination network
PE	petroleum ether
Pent	pentyl
Ph	phenyl
PIZOF	porous interpenetrated zirconium-organic-framework
POM	polyoxometalate
POST	Pohang University of Science and Technology
POX	diethyl (4-nitrophenyl) phosphate, paraoxon
Pr	propyl
PSLE	post-synthesis ligand exchange
PSM	postsynthetic modification
PTSA	4-methylbenzene-1-sulfonic acid, *p*-toluenesulfonic acid
Pydc	pyridine-1,3-dicarboxylate
PW	paddlewheel
(P)XRD	x-ray (powder) diffraction
r	radius
SA	2-hydroxybenzaldehyde, salicylaldehyde
SBA	Santa Barbara Amorphous type material
SBU	secondary building unit
SEM	scanning electron microscopy
SI	salicylimine
t	*tert*
T	testosterone
TCH	4-(*tert*-butyl)cyclohexan-1-one
TCPP	tetrakis(4-carboxyphenyl)porphyrin

TDC	thiophene-2,5-dicarboxylate
TFA	trifluoroacetic acid
TGA	thermal gravimetric analysis
THF	tetrahydrofuran
TMA	*N,N*-dimethylmethanamine, trimethylamine
TMB	3,3’,5,5’-tetramethyl[1,1’-biphenyl]-4-4’-diamine
TMEDA	*N*,*N*,*N*′,*N*′-Tetramethylethane-1,2-diamine
TON	turnover number
TOF	turnover frequency
TPD-MS	temperature programmed decomposition/mass spectrometry
TPDC	[1,1’:4’,1’’-terphenyl]-4,4’’-dicarboxylate,4,4’,4’’-triphenyldicarboxylate
TS	transition state
TUD	Dresden University of Technology
UHV-FTIR	ultrahigh vacuum fourier-transform infrared spectroscopy
UiO	University of Oslo
UV-Vis	ultraviolet-visible
ν	wavenumber
VM	*S*-[2-(Diethylamino)ethyl] *O*-ethyl methylphosphonothioate
VNU	Vietnam National University
VX	ethyl ({2-[bis(propan-2-yl)amino]ethyl}sulfanyl)(methyl)phosphinate
ZIF	zeolitic imidazolate framework

Table of contents

Acknowledgements I
Resumen V
Abstract XI
Resum XV
List of symbols and abbreviations XXI
Table of contents XXIX
Chapter 1. General introduction 1
 1.1. Introduction 3
  1.1.1. Metal-Organic Frameworks (MOFs) 3
   1.1.1.1 Isoreticular synthesis 4
   1.1.1.2 Postsynthetic modification (PSM) 6
    a) PSM at the inorganic SBU 6
    b) PSM at the organic linker 8
   1.1.1.3 Encapsulation 9
   1.1.1.4 Defects 11
  1.1.2. MOFs as heterogeneous catalysts 15
   1.1.2.1 Zr-containing MOFs 16
    a) UiO-66 17
    b) MOF-808 19
    c) Other Zr-MOFs 20
  1.1.3. Catalytic reactions with MOF-808 21
  1.1.4. MEERWEIN-PONNDORF-VERLEY (MPV) reduction 27
 1.2. References 30
Chapter 2. Objectives 39
 2.1. General objectives 41
  2.1.1. Chapter 4 41
  2.1.2. Chapter 5 41
  2.1.3. Chapter 6 41
Chapter 3. Synthesis and characterization techniques 43
 3.1. Synthesis 45

3.2. X-ray powder diffraction (PXRD) 46
3.3. Infrared (IR) analysis 48
3.4. N_2-adsorption/desorption experiments 49
3.5. Thermogravimetric analysis (TGA) 50
3.6. Nuclear magnetic resonance spectroscopy (NMR) analysis 50
3.7. Gas Chromatography (GC) 51
  3.7.1. Gas chromatography coupled with mass spectrometry (GC-MS) 52
3.8. Scanning electron microscopy (SEM) 52
3.9. Catalytic reactions 53
3.10. References 53
Chapter 4. Catalytic properties of pristine and DE MOF-808 materials 55
4.1. Introduction 57
4.2. MPV reduction of cyclohexanone (CH) 58
4.3. DE MOF-808-x materials 59
  4.3.1. Catalytic results for the MPV reduction of CH using pristine and DE MOF-808 materials 61
  4.3.2. Catalytic results for the MPV reduction of estrone (E1) 66
4.4. Conclusions 68
4.5. References 69
Chapter 5. Diastereoselective MPV reduction of substituted cyclohexanones over MOF-808 73
5.1. Introduction 75
5.2. Results and discussion 79
  5.2.1. Reduction of 3-methylcyclohexanone (3MeCH) 79
  5.2.2. Reduction of 2-methylcyclohexanone (2MeCH) 82
  5.2.3. Reduction of 2-phenylcyclohexanone (2PhCH) 83
  5.2.4. Kinetic analysis 85
  5.2.5. Computational study 88
5.3. Conclusions 89
5.4. References 90

Chapter 6. One-step chemo-, regio- and stereoselective reduction of ketosteroids to hydroxysteroids over MOF-808 93

6.1. Introduction 95

6.2. Catalytic results (reduction of 17-OXOs) 103

6.2.1. Diastereoselective reduction of estrone (E1) 103

6.2.1.1 Influence of the reaction temperature *106*

a) Kinetic analysis 106

6.2.2. Diastereoselective reduction of 5α-androstan-3β-ol,17-one (or epiandrosterone, EPIA) 110

6.2.3. Regio-, chemo- and diastereoselective reduction of Δ^4-androstene-3,17-dione (A4) 112

6.3. Conclusions 115

6.4. References 115

Chapter 7. Conclusions 119

Chapter 8. Annexes 125

8.1. General information 127

8.1.1. Synthesis of materials 127

8.1.1.1 UiO-66: Used in Chapter 4 and 5 .... *127*

8.1.1.2 MOF-808: Used in Chapter 4, 5 and 6 .... *127*

8.1.1.3 DE MOF-808-x (x = IPA, Pydc, OH or NH_2): Used in Chapter 4 .... *127*

8.1.1.4 DUT-67: Used in Chapter 4 .... *128*

8.1.1.5 Zr-BEA: Used in Chapter 5 and 6 .... *129*

a) Synthesis of dealuminated Zr-BEA seeds 129

b) Synthesis of aluminium-free Zr-BEA zeolite 129

8.1.2. General procedure for the thermal activation of MOF catalysts 129

8.2. Additional information for Chapter 4. Catalytic properties of pristine and DE MOF-808 materials 130

8.2.1. Characterization of catalysts 130

8.2.1.1 XRD *130*

8.2.1.2 ^{1}H-NMR *130*

8.2.1.3 FESM *131*

8.2.1.4 N_2-adsorption/desorption isotherms *133*

8.2.1.5 FTIR and CO adsorption ... 134

8.2.2. General procedure for the reduction of cyclohexanone (CH) ... 136

8.2.3. General procedure for the reduction of estrone (E1) ... 136

8.2.4. Structural analysis of estradiols (E2) and determination of diastereoselective ratio (d.r.) ... 136

8.2.5. Characterization of steroids from the reduction of E1 (^{1}H-NMR spectra of individual compounds) ... 137

8.3. Additional information for Chapter 5. Diastereoselective MPV reduction of substituted cyclohexanones ... 138

8.3.1. General procedure for the reduction of substituted cyclohexanones ... 138

8.3.2. $NaBH_4$ reduction of 2PhCH ... 139

8.3.3. Time-conversion plots of 2MeCH and 3MeCH over MOF-808 using ^{i}PrOH or ^{s}BuOH at 353 K ... 139

8.3.4. Procedure for the kinetic analysis of 2MeCH and 3MeCH reduction ... 139

8.3.5. EYRING-POLANYI plots obtained from the reduction of 2MeCH and 3MeCH over MOF-808 using ^{i}PrOH or ^{s}BuOH as reducing agent ... 142

8.3.6. Computational analysis ... 142

8.4. Additional information for Chapter 6. One-step chemo-, regio- and stereoselective reduction of ketosteroids to hydroxysteroids ... 144

8.4.1. General procedure for the reduction of steroids ... 144

8.4.2. $NaBH_4$ reduction of E1 and EPIA ... 145

8.4.3. Procedure for the kinetic analysis of E1 ... 145

8.4.4. EYRING-POLANYI plots obtained from the reduction of E1 ... 146

8.4.5. Structural analysis of hydroxysteroids and determination of diastereoselective ratio (d.r.) ... 146

8.4.6. Characterization of steroids from the reduction of EPIA (^{1}H-NMR spectra of individual compounds) ... 146

8.4.7. Characterization of steroids from the reduction of A4 (GC analysis of reaction and ^{1}H- and ^{13}C-NMR spectra of individual compounds) ... 147

8.4.8. Computational analysis ... 149

8.5. References ... 150

Chapter 1

General introduction

1.1. Introduction

1.1.1. *Metal-Organic Frameworks (MOFs)*

Metal-organic frameworks (MOFs) are a class of solid and crystalline materials, which are built up from either metal ions (or metal oxoclusters) interconnected through multidentate ligands by coordination bonds, to form mono-, bi- or tridimensional networks as shown schematically in Figure 1.1. The metal nodes of a MOF are commonly called secondary building units (SBUs) of the material, while the organic ligands are usually referred to as "struts". MOFs can feature exceptional high surface areas and pore volumes and a vast diversity, concerning their pore structure, chemical composition as well as chemical and physical properties. For instance, the material known as NU-110 (NU = Northwestern University)[1] has a specific surface area (S_{BET}) of up to 7000 m^2g^{-1} and a pore volume of over 4 cm^3g^{-1}. Thereby, MOFs have attracted a lot of interest during the last decades and a lot of effort has been made in evaluating their applicability in different fields, such as molecular adsorption and separation,[2] catalysis,[3,4] sensing,[5] or drug delivery.[6] The versatility of MOFs also arises from the high number of different metals that can be used in the synthesis of MOFs, in various oxidation states (such as M^{2+}, M^{3+} and M^{4+})[7] and together with the variation of organic linker molecules and the coordination geometry, an exceptionally high amount of different compositions and pore architectures can be formed. Various topologies are possible even when the same combination of SBUs and organic struts are used, as shown for example in the case of the two structure isomers MIL-101[8] and MIL-88B,[9] as well as the MIL-53[10] (MIL = Matériaux de l'Institut Lavoisier) (see Figure 1.2). Thus, MIL-101 and MIL-88B are constructed from the same metal-oxo clusters, which are connected through benzene-1,4-dicarboxylate (BDC) linker molecules, but they significantly differ in their structure, as MIL-101 is a mesoporous and rigid structure, whereas MIL-88B has much smaller pores and shows breathing (flexible) behavior. Unlike the isolated metal-oxo clusters in MIL-101 and MIL-88B, MIL-53 consists of 1-

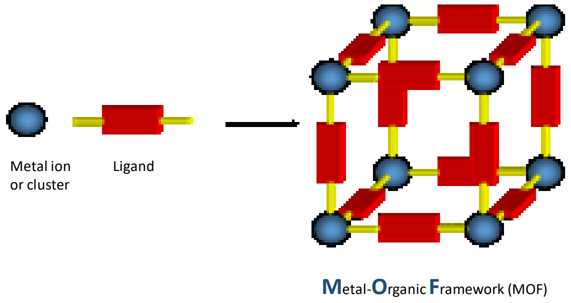

Figure 1.1. Representation of a MOF constructed from metal nodes connected by ligand molecules

dimensional metal-oxo chains, which are interconnected through BDC linker molecules, to form a 3-dimensional network. Concerning the inorganic subnetwork in MOFs, the dimensionality can be increased from a 0D coordination polymer to 3D.[11] In the last two decades or so, different strategies have been devised to increase even further the MOF tunability and versatility in view of potential applications. Most relevant tools include: Isoreticular synthesis, post-synthesis modification, encapsulation and controlled defect production.

1.1.1.1 Isoreticular synthesis

Isoreticular synthesis is an approach for altering or fine-tuning chemical and structural properties of MOF materials while maintaining the same network topology. Regarding the "modular" concept of MOF formation,[12–14] on the one hand different metal ions can be used for constructing the same type of SBUs. This approach is especially interesting, as materials with the same topology can be prepared, but the variation of metal ions can introduce different reactive sites on the SBU, such as Lewis acid sites or redox active sites. For instance, the SBU of isoreticular UiO-66 compounds (UiO = University of Oslo) can be formulated as $[M_6O_4(OH)_4]^{12+}$, in which M can be Zr, Hf, U, Th or Ce.[15–19] The hexanuclear metal oxide clusters are connected to twelve linker molecules to form a cubic closed packed structure. Although mixed metal compounds like UiO-66(Zr/Hf), UiO-66(Zr/Ti)[20] or UiO-66(Zr/Ce)[21,22] have been reported in the literature, not all of them can be synthesized directly, but must be obtained from a preformed MOF by post-synthesis modification (see later). Thus, UiO-66(Zr/Ti) for example was prepared through a modification of UiO-66(Zr) where titanium introduces additional photocatalytic activity.

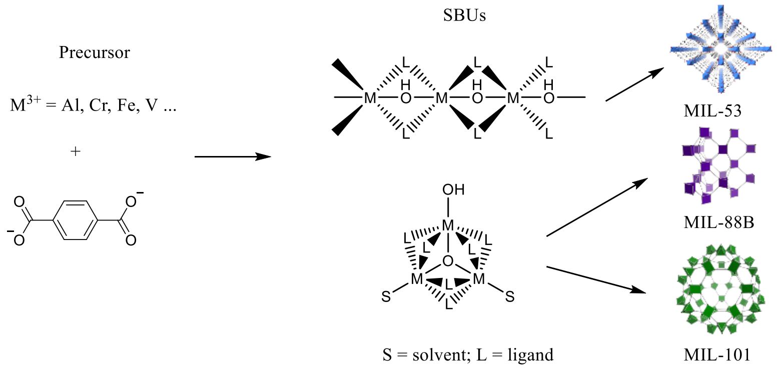

Reprinted (adapted) with permission from (*Cryst. Growth Des.*, **2013**, *13*, 5036–5044). Copyright (2013) American Chemical Society

Figure 1.2. Structural isomers build from the same metal and ligand

Alternatively to the variation of metal ions, different linker molecules of various dimensions and functionalities but geometrically equivalent can be used to synthesize isoreticular MOFs. A prominent example was provided by YAGHI *et al.*, who reported the isoreticular synthesis of several compounds, analogous to MOF-5, containing Zn_4O clusters in a simple cubic net (**pcu**),[23] collectively denoted IRMOF-n.[24] In a similar way, isoreticular compounds of UiO-66 for instance consist of the same inorganic hexanuclear building blocks and their 12-fold connectivity by organic linker molecules, which keeps the overall structure of the materials unchanged. The use of linker molecules of different lengths on the other hand changes the porosity of the material, since pore opening and size varies with the length of the organic linker molecule. Therefore, the BDC linker of UiO-66 was replaced by [1,1'-biphenyl]-4,4'-dicarboxylate (BPDC) or [1,1':4',1''-terphenyl]-4,4''-dicarboxylate (TPDC) to form isoreticular compounds named UiO-67 and UiO-68. The BET surface area increases from 1187 m^2g^{-1} to 3000 m^2g^{-1} and 4170 m^2g^{-1} and the pore openings increase from 6 Å to 8 Å and 10 Å for UiO-66, UiO-67 and UiO-68, respectively (see Figure 1.3).[15] The pore openings are also a crucial factor in catalysis, as they determine whether a molecule of a given size has access to the internal surface area of the material or not. Thus, more open frameworks can be derived from expanded linker molecules, which is a way to overcome diffusion limitations. Although this approach can be very useful in the construction of more open frameworks, it was shown that the stability for expanded materials such as UiO-67 decreased.[25–27]

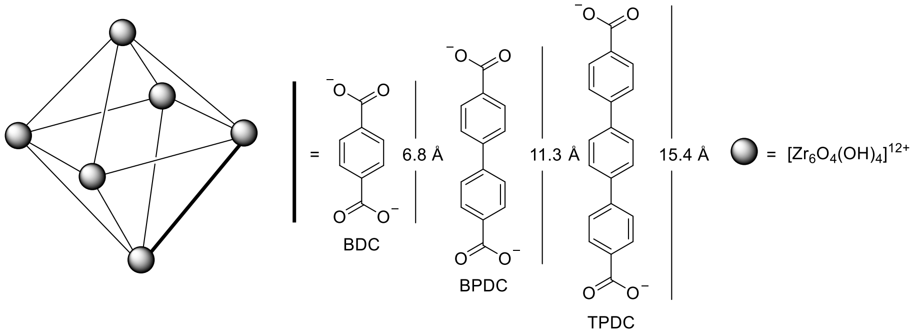

Figure 1.3. UiO-type MOFs, constructed from different linker molecules

Isoreticular synthesis can also be used for the introduction of a number of functionalized linkers.[24] Functional moieties on linker molecules can alter or introduce additional physical and chemical properties in the MOF and can be a necessary first step in postsynthetic modification of materials (see later). For example, introduction of electron-withdrawing groups (F, Cl, Br, NO_2) on the BDC linker of UiO-66 was shown to increase the catalysts LEWIS acidity of the resulting UiO-66 derivative and its activity in the 3,7-dimethyloct-6-enal (or citronellal) cyclization.[28] The strongest effect was observed for the NO_2 group with a 56-fold increase in rate with respect to non-functionalized compounds. The selectivity to 5-methyl-2-(prop-1-en-2-yl)cyclohexan-1-ol (or isopulegol) also increased up to 81%, which is typical for LEWIS acid catalysts. It was shown, that in UiO-66-NO_2 the adsorption of isopulegol is stronger, due to stronger LEWIS acidity. Also the transition state (TS) becomes more stabilized, due to electrostatic interactions of the adsorbate and the NO_2 group. On another scenario, NH_2 groups on the BDC linker showed also to have a beneficial effect in catalysis, such as in the esterification of 4-oxopentanoic acid (or levulinic acid, LA) with ethanol catalyzed by Zr-containing UiO-66 compounds. It was shown, that the NH_2 group leads to a dual activation of the reactant and alcohol molecules due to formation of a network of hydrogen bonds, which is not possible within pristine UiO-66, lacking the NH_2 groups. Further, ab initio calculations recently concluded that UiO-66 can act as a catalyst with combined LEWIS/BRØNSTED acid sites. While LEWIS acidity was provided by coordinatively unsaturated Zr^{4+} sites, strongly adsorbed water molecules induced a noticeable BRØNSTED acidity, which was shown to be enhanced by the presence of NH_2 groups on the BDC linkers.[29,30]

1.1.1.2 Postsynthetic modification (PSM)

Preformed MOFs can be modified postsynthetically which introduces an additional dimension to MOF tunability. According to their complex structures, there are several opportunities for post-synthetic modification (PSM) on MOFs. These include modification on the metal cluster and linker molecule of MOFs. In this way chemical and physical properties of MOFs can be altered using the PSM approach. Further, MOFs can be used as a heterogeneous support for different types of catalysts, which are postsynthetically introduced into the porous structure of the MOF. Early reports on PSM of MOFs basically consisted in non-covalent modifications, such as exchange of guest molecules or ion-exchange. Only recently scientists realized that MOFs can actually be treated like chemical substrates and be submitted to more complex covalent modifications, of either SBUs or organic linkers.

a) PSM at the inorganic SBU

In some cases, isoreticular compounds with a specific topology are not accessible via direct synthesis by simply varying the metal source. Transmetalation of a preexisting MOF can be a way to obtain novel materials with new properties through isomorphous substitution of one metal by another. Even though metal exchange is not always quantitative and mixed metal MOFs are commonly obtained using this approach, synthesis of mixed metal MOFs can be also of advantage, as it can improve stability of materials or introduce novel properties.[20,31] For instance, the titanium analogue of UiO-66 could not be prepared with other existing direct methods, as Ti(IV) is not known to form the hexanuclear SBU metal cluster, present in UiO-66. Nevertheless, treatment of preexisting Zr-containing UiO-66 with $TiCl_4$ led to partial substitution of Zr(IV) by Ti(IV) forming a mixed metal (Zr/Ti)UiO-66. Later a mixed linker UiO-66 MOF was prepared and partially exchanged with Ti^{IV} using the same strategy to yield

$Zr_{4.3}Ti_{1.7}O_4(OH)_4(BDC\text{-}NH_2)_{5.17}(BDC\text{-}(NH_2)_2)_{0.83}$.[32] Postsynthesis metal exchange was conducted by introducing the MOF in a solution of $TiCl_4(THF)_2$ in *N,N*-dimethylformamide (DMF) at 358 K for 5 days. The resulting catalyst was studied in the CO_2 photocatalytic reduction to HCOOH under visible light irradiation in a solution of acetonitrile with 2,2',2''-nitrilotris(ethan-1-ol) and 0.1 M 1-benzyl-1,4-dihydropyridine-3-carboxamide. The catalytic activity of the mixed-metal mixed-ligand MOF was superior to that of UiO-66(Zr/Ti)-NH_2 MOF, containing only BDC-NH_2 linkers. The catalyst was even found to be more stable than UiO-66(Zr/Ti)-NH_2 and maintained its crystallinity and morphology over three catalytic cycles. The bis-amino-substituted linkers introduced new energy levels and increased light absorption. Introduction of titanium also greatly affects the catalytic properties, since the $Zr_6O_4(OH)_4$ SBU of UiO-66 cannot efficiently accept electrons from the BDC linker, due to its redox potential energy level, which lies above the LUMO of the BDC linker.[33]

–OH groups on the Zr-cluster and terminal –OH/H_2O groups of defective zirconium MOFs can also be used for further postsynthesis functionalization. In this case, the solid structure of the MOF acts as a support for introducing a catalytic metal species by anchoring to these –OH sites (Metalation).[34] The obtained new material exhibits completely new reactivity, as the metal is different to the metal present in the SBU of the MOF. Different metals have been attached to the nodes of Zr-MOFs, such as Ti^{IV} (UiO-66),[35] V^{V} (UiO-66),[36] Al^{III} & Zn^{II} (NU-1000).[34]

In a different approach, the inorganic building brick of UiO-66 was modified by AMELOOT *et al.,*[37] by reacting the bridging μ_3-OH groups with an alkoxide base. The $Zr_6O_4(OH)_4$ cluster of UiO-66 were first dehydrated and then contacted with LiO^tBu afterwards. Assuming that two –OH groups per cluster can be replaced by $^tBuO^-$, approximately 25% of the available sites were replaced during LiO^tBu treatment. The crystalline structure of the MOF was retained during PSM. Further analysis showed an excess of up to one Li per cluster, which was assigned to partial deprotonation of terminal –OH groups during materials activation. UiO-66@LiO^tBu was used later with improved phosphotriesterase catalytic activity in the hydrolysis of chemical-warfare agents (CWAs).[38] In this study, doping of UiO-66 with basic lithium alkoxide led to much higher activity compared to compounds such as parent UiO-66 and porous ZrO_2.

Finally, another possibility for modifying the SBUs of preformed MOFs is by grafting active groups onto coordinatively unsaturated sites (*cus*) created upon evacuation of labile ligands (such as weakly coordinated H_2O molecules)[39] or at defect positions.[40] LI *et al.* for example prepared a bifunctional acid/base catalyst following a three-step PSM procedure starting from (Cr)MIL-101 (see Scheme 1.1).[41] The final catalyst features acidic SO_3H sites on the BDC linker and basic NH_2 sites through anchoring of ethane-1,2-diamine to *cus* of (Cr)MIL-101. The catalyst was tested in a deacetalization/HENRY reaction tandem process. Whereas a mixture of 4-methylbenzene-1-sulfonic acid/*N,N*-dimethylmethanamine (PTSA/TMA) was almost fully inactive, MIL-101-SO_3H-NH_2 almost quantitatively converted

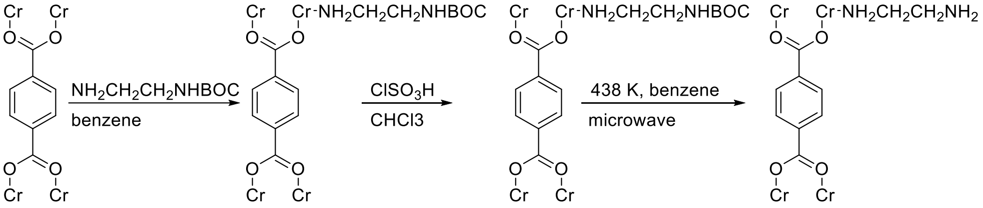

Reprinted (adapted) with permission from (*Chem. Commun.*, **2012**, *48*, 6151-6153). Copyright (2012) The Royal Society of Chemistry

Scheme 1.1. Preparation of MIL-101-SO_3H-NH_2 from (Cr)MIL-101

(dimethoxymethyl)benzene into (*E*)-(2-nitrovinyl)benzene. Addition of PTSA or TMA to MIL-101-SO_3H-NH_2 stopped the activity, probably due to formation of ion pairs. Introduction of an organic acid group was also beneficial for the first reaction step compared to parent (Cr)MIL-101.

b) PSM at the organic linker

The first example of covalent PSM of organic linkers was reported by KIM *et al.* in 2000.[42] Those authors described the synthesis of a 2D homochiral MOF, named POST-1 (POST = Pohang Universiy of Science and Technology), built from Zn^{2+} trimeric SBUs and enantiopure tartrate derivative containing pyridyl pendant groups. Treatment of POST-1 with CH_3I led to the efficient methylation of pyridyl groups, while XRD analysis revealed that the crystalline structure of the solid was maintained.[42] PSM can be used as well for the preparation of mixed ligand MOFs. Thus, post-synthesis ligand exchange (PSLE) represents an interesting alternative to direct synthesis of mixed-linker MOFs (which is not always feasible). PSLE can be achieved by simple contacting the MOF with a solution containing a new geometrically equivalent ligand under appropriate conditions, or even by directly contacting two solid isoreticular MOFs,[20,43] as shown in Scheme 1.2. PSLE was initially demonstrated on different robust and water stable materials such as UiO-66(Zr), MILs and ZIFs (ZIF = zeolitic imidazolate framework). KIM *et. al.* also used the PSLE for the preparation of mixed linker UiO-66(Zr) materials containing hydroxyl or azide groups.

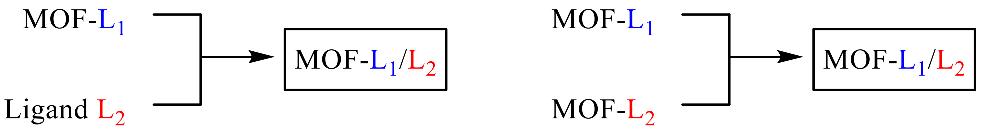

Scheme 1.2. Strategies for the preparation of mixed-ligand MOFs

PSM of ligands can also be used for the introduction of metal complexes, which can be anchored to the organic linker of the MOF. In this way, a homogeneous catalyst can be attached to a heterogeneous support (heterogeneization), which provides a means for preparing well-defined single-site catalysts based on MOFs.[4] Although there are several possibilities to attach metal complexes to the organic linker of MOFs, one approach is the modification of an amino-functionalized linker molecule, the formation of an imine and subsequent anchoring of a metal-complex. IRMOF-3 (isoreticular metal-organic framework-3) for instance (the aminoterephthalate analogue of MOF-5), was successfully used in the postsynthetic introduction of metal complexes. Thus, the 2-NH_2-BDC linker was reacted with 2-hydroxybenzaldehyde (or salicylaldehyde, SA) to form a salicylimine (SI), which serves as an anchoring point for metal complexation. The strategy was used for anchoring an Au(III)-complex[44] and a V(O)$acac_2$-complex[45] to IRMOF-3-SI, which are heterogenized structural analogs of the well known salen-type homogeneous catalyst.[46] IRMOF-3-SI-Au for instance was used in the multicomponent domino coupling and cyclization of *N*-protected ethylaniline, aldehyde and amine. Its activity was superior to various catalysts including the analogous homogeneous gold(III) Schiff base complex. The catalyst could be reused for the reaction and no leaching of gold was observed. The catalyst was also active in the hydrogenation of 1,3-butadiene with very high selectivities (up to 97%) to but-1-ene and (*E*)-but-2-ene.

1.1.1.3 Encapsulation

Encapsulation uses the huge porous structure of the MOF as a support where functional moieties are immobilized. One prominent example is the encapsulation of metal nanoparticles (NPs) inside the MOF pores, that can be prepared following two main approaches. First the ship-in-a-bottle approach, in which NPs are constructed inside the structure of a preformed MOF, or second a bottle-around-the-ship approach, where the MOF structure is constructed around preformed NPs.[47] In the first case, a suitable metallic precursor (e.g., an organometallic compound or a metal salt) is first adsorbed inside the MOF pores. This can be achieved mainly by impregnation/adsorption from solution or by chemical vapor deposition.[48] Then, NPs are formed by in-situ reduction of the metallic precursor by any suitable means, including the use of reducing agents (H_2, $NaBH_4$, etc.) or either thermal or photochemical decomposition. In the case of encapsulation of preformed NPs, the process is usually favored by using capping agents (such as polyvinylpyrolidine) to stabilize metal NPs, which are then contacted with solutions containing the metal and ligand precursor of the MOF. The mixture is then submitted to appropriate conditions to favor the MOF synthesis, which crystallizes around the NPs.

Regardless of the method used, either ship-in-a-bottle or bottle-around-the-ship, stabilization of metal NPs inside the cavities of a porous support such as a MOF prevents agglomeration and sintering of the metal NPs, which would lead to an unwanted decrease of the metal dispersion (i.e., the fraction of atoms exposed to the surface of the NP), with the concomitant loss of activity. The strategy of encapsulation has been already exploited using zeolites, mesoporous aluminosilicates and other porous organic or inorganic materials.[49–52] Due to their high porosity and structure diversity, MOFs offer interesting possibilities as host materials for metal NPs. Entrapment of metal NPs inside MOFs can

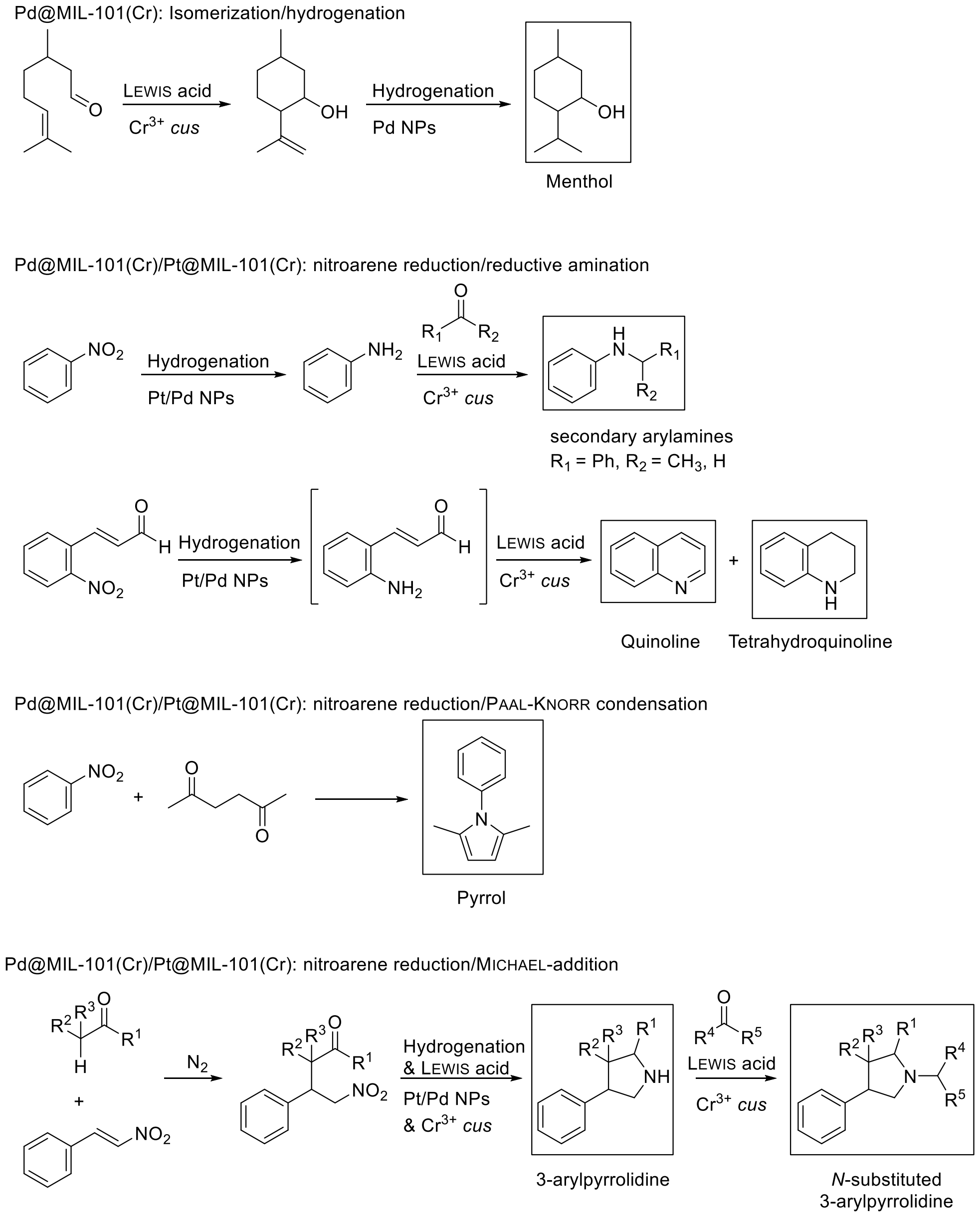
Pd@MIL-101(Cr): Isomerization/hydrogenation
LEWIS acid
Cr3+ cus
OH
Hydrogenation
Pd NPs
Menthol
Pd@MIL-101(Cr)/Pt@MIL-101(Cr): nitroarene reduction/reductive amination
NO2
Hydrogenation
Pt/Pd NPs
NH2
R1 R2
LEWIS acid
Cr3+ cus
secondary arylamines
R1 = Ph, R2 = CH3, H
Hydrogenation
Pt/Pd NPs
LEWIS acid
Cr3+ cus
Quinoline
Tetrahydroquinoline
Pd@MIL-101(Cr)/Pt@MIL-101(Cr): nitroarene reduction/PAAL-KNORR condensation
Pyrrol
Pd@MIL-101(Cr)/Pt@MIL-101(Cr): nitroarene reduction/MICHAEL-addition
N2
Hydrogenation
& LEWIS acid
Pt/Pd NPs
& Cr3+ cus
LEWIS acid
Cr3+ cus
3-arylpyrrolidine
N-substituted 3-arylpyrrolidine

Reprinted (adapted) with permission from (*ChemCatChem* **2013**, *5*, 538–549). Copyright (2013) American Chemical Society

Scheme 1.3. Multistep reactions with Pd@MIL-101(Cr) and Pt@MIL-101(Cr)

not only prevent agglomeration of particles due to physical confinement but also can control the dimension and size of metal NPs, due to the regular size and shape of pore and channel structures of the host material. A 3-dimensional pore system is usually preferred for encapsulation, since channels allow migration of NPs, which finally can result in particle agglomeration at the external surface of the MOF, as well as leaching of the metal to the surroundings. Therefore, mesoporous structures surrounded by smaller windows like MIL-100 and MIL-101 can form good platforms for NP incorporation.[53,54] Moreover, the larger pore size and high porosity of MOFs further improves diffusion of reaction substrates and enables the accessibility of active sites within the material. However, one drawback of using MOFs as matrices for encapsulation as compared to materials such as zeolites, is their lower stability. Therefore, preparation methods have to be selected in which the MOF matrix is stable, to benefit from their advantages. Also leaching of the metal and stability issues have to be addressed during or after the catalytic reaction. For instance, MOFs such as MOF-5 show low stability in H_2O and other solvents[55], so their use as supports for metal NPs is not advisable for catalytic applications. Introduction of metal NPs inside the MOF offers the highly demanded possibility to develop multifunctional catalysts, in which the inherent functionalities of the MOF components (either SBU or ligand functional groups) are combined with the catalytic properties of the newly introduced metal NPs. In this way, it is possible to carry out multi-step transformations in one pot, as in the representative examples shown in Scheme 1.3. Besides encapsulation of metal (and metal oxide) NPs, MOFs can also be used for encapsulation of many other discrete moieties, including polyoxometalates, porphyrines and metallo-porphyrins, or other molecular catalysts, such as chiral JACOBSEN'S catalyst.[56] Encapsulation can then be used as a means for immobilization of molecular catalytic moieties, which could otherwise lose their activity if they were in solution due to mutual deactivation. For instance, when soluble Mn-salen complexes are used as homogeneous epoxidation catalysts, a drop of the activity over time is usually observed. This is attributed to the oxidation of the salen ligand, which is facilitated by reactive encounters with other catalyst molecules in solution. Catalyst isolation by encapsulation can thus prevent or minimize unwanted deactivation pathways.

1.1.1.4 Defects

The "ideal" structure of a crystal with a perfect periodic repetition of structural building blocks in many cases does not exist, due to some irregularities or defects produced within the structure. These structural irregularities or defects in MOFs can originate from missing or dislocated atoms or ions. Structural irregularities within MOFs have been classified recently as, point defects (e.g., vacancies), line defects (e.g., dislocations), planar defects (e.g., boundaries and stacking faults) and micro-, mesoscale volume defects (e.g., inclusions and voids). Defects have been shown to greatly influence chemical and physical properties of MOFs. It is also well known, that defects can be the origin of unique properties of certain materials. Defects can be formed during synthesis as inherent defects, resulting from misconnections or dislocations during crystallization.

In addition, efforts have been made to intentionally introduce defects during synthesis or postsynthetic treatment. This approach usually refers to as "*defect engineering* (DE)" of MOFs. In catalysis, defects can be of great importance, as they can act as catalytic active sites within the structure.[57]

Zr^{4+} open metal sites within the UiO-66 structure display one example, as they were found to act as Lewis acid sites. Since the pristine UiO-66 typically displays no open metal sites, these open metal sites can be described as point defects. They arise from the presence of missing linker defects that can be created during synthesis or by post treatment leading to the formation of Zr^{4+} open metal sites. Vermoortele *et al.* examined the correlation between defects in the UiO-66 structure and its catalytic activity for the citronellal cyclization.[58] To favor defect formation, a modulated synthesis procedure using trifluoroacetic acid (TFA) was applied. TFA replaced small amounts of BDC linker molecules during the synthesis of the MOF and the use of HCl as a crystallizing agent further enhanced the effect of linker replacement by TFA. Activation of materials at high temperatures led to dehydroxylation on the SBU and removal of the TFA molecules which creates open metal sites on the cluster of UiO-66. With increasing TFA concentration (0-20 equiv. with respect to BDC) the catalytic activity increased gradually. For UiO-66-10 (10 equiv. of TFA) an increased number of missing linkers was also confirmed by thermogravimetric analysis (TGA). Addition of 1 equiv. of HCl (for UiO-66-10$_{\text{HCl}}$) led to further linker deficiency, which was confirmed by TGA analysis and a higher catalytic activity in the citronellal cyclization. Enhanced catalytic activity for UiO-66-10$_{\text{HCl}}$ and its nitro analogue UiO-66-NO_2-10$_{\text{HCl}}$ was observed for the Meerwein-Ponndorf-Verley (MPV) reduction of 4-(*tert*-butyl)cyclohexan-1-one (TCH) with ^{i}PrOH, as compared to UiO-66 and UiO-66-NO_2.

Cirujano *et al.* also examined the influence of missing linker defects on the catalytic activity of UiO-66 and UiO-66-NH_2 for the esterification of LA with various alcohols.[29] Therefore, a series of UiO-66 and UiO-66-NH_2 batches were synthesized using a non-modulated synthesis procedure and their catalytic activity was tested for the esterification reaction of LA with EtOH. Different amounts of defects were formed during synthesis, due to stochastic variations of the temperature, time or reactant concentrations. The amount of defects was further analyzed by TGA measurements. Typically, one missing linker leads to formation of two defect sites on the SBU, which are occupied by terminal H_2O molecules, giving rise to two open metal sites upon water

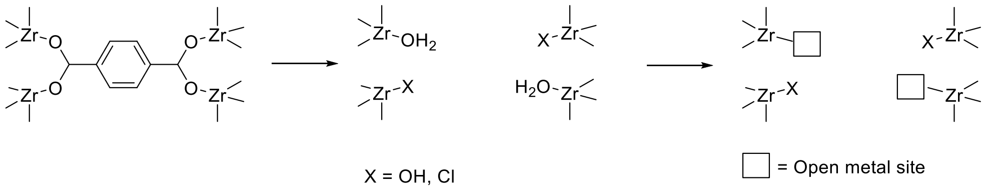

Scheme 1.4. Formation of defects in UiO-66 by missing linkers

removal, as shown in Scheme 1.4. Charge neutrality is obtained by two additional terminal –OH groups (or Cl anions present during the synthesis). In both cases (UiO-66 & UiO-66-NH_2), the reaction rate constant increased with an increasing number of defects (missing linkers).

A mixed linker approach can be used to introduce modified coordinatively unsaturated sites (M-*cus*) at the paddle-wheel units of [$M_3(BTC)_2$] (M = Cu, Ru; BTC = benzene-1,3,5-tricarboxylate) and other MOFs. Defective linker molecules are selected having the same coordination geometry and dimensions as the native ligand of the MOF, but missing one (or more) coordinating groups. In this way, it is possible to partially replace BTC ligands of the parent MOF, up to a certain limit without affecting too much the crystalline structure. The lack of one coordination site on defective linker molecules leads to creation of a defect at the metal node of the MOF. In this way, up to 50% of pyridine-3,5-dicarboxylate ligands (Pydc) were introduced into $Cu_3(BTC)_2(H_2O)_3$ by MARX *et al.* It was found that the coordination number at the Cu atoms is reduced for samples with higher substitution (30% and 50%). Moreover, CO adsorption showed formation of defective Cu^{1+}/Cu^{2+} pairs, which are almost completely absent in the parent Cu-BTC MOF. Partially reduction of the Cu^{2+} to Cu^{+} is necessary to keep the electrical neutrality of the system, due to the lower charge of Pydc defective ligands with respect to the parent BTC. Significant changes in reactivity and selectivity for the toluene oxidation in acetonitrile were observed for Cu-BTC-Pydc materials, due to a different chemical and electronic environment at the metal centers, which also modifies the accessibility during catalysis.[59] The approach was extended to a series of defective linker molecules, such as substituted isophthalates (5-X-IPA; X = OH, CN and NO_2). Also the formation of mesopores was observed, which can result from missing coordinating sites of defective linker molecules as well as from missing metal clusters.[60]

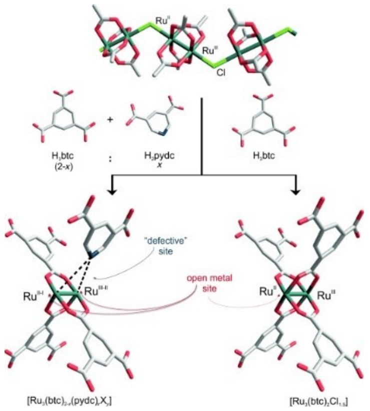

Reprinted (adapted) with permission from (*Angew. Chem. Int. Ed.*, **2014**, *53*, 7058–7062). Copyright (2014) WILEY-VCH Verlag GmbH & KGaA

Figure 1.4. left) defective cluster and right) none-defective cluster on HKUST-1

The same concept was used by KOZACHUK *et al.* in the synthesis of a series of DE [$Ru_3(BTC)_{2-x}(Pydc)_xX_y$] MOFs (X = Cl, OH, OAc; x = 0.1, 0.2, 0.6, 1; $0 \leq y \leq 1.5$).[61] As shown in Figure 1.4, partially reduced $Ru^{\delta+}$ was observed for DE samples, similar to what was found in the case of Cu-BTC MOFs commented above. Significant changes were observed in CO_2 adsorption, hydrogenation of 1-octene and ethylene adsorption.

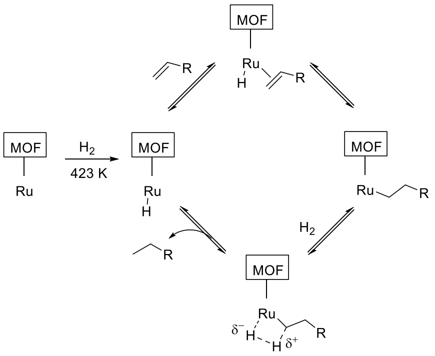

Reprinted (adapted) with permission from (*Angew. Chem. Int. Ed.*, **2014**, *53*, 7058–7062). Copyright (2014) WILEY-VCH Verlag GmbH & KGaA

Scheme 1.5. Olefin hydrogenation invlolving base-assisted heterolytic splitting of H_2 over defect-engineered Ru-MOFs

Introduction of defects for instance led to an increase in olefin hydrogenation. The observed catalytic activity for DE Ru-BTC samples for oct-1-ene hydrogenation was explained in terms of the formation of Ru-H intermediate species at the undercoordinated Ru species upon H_2 treatment (see Scheme 1.5). In contrast, such Ru-H species were totally absent in pristine Ru-BTC compound, resulting in a much lower catalytic activity. Also a dissociative chemisorption of CO_2 at 100 K was observed by UHV-FTIR in the dark, which leads to formation of CO.

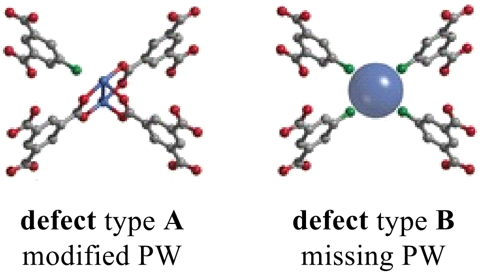

Reprinted (adapted) with permission from (*Chem. Eur. J.*, **2016**, *22*, 14297–14307). Copyright (2016) WILEY-VCH Verlag GmbH & KGaA

Figure 1.5. Different defect types found in Ru-DEMOFs (PW = paddelwheel)

In a subsequent study by the same authors, Ru-DEMOFs were prepared with 5-X-IPA (X = H, OH, NH_2, Br) as defective linker molecules. These materials feature type A defects (with reduced $Ru^{\delta+}$) and type B defects (with missing clusters) as shown in Figure 1.5. High concentrations of defective linkers, as well as small non coordinating groups on defective linkers, such as 5-X-IPA (X = H) were found to favor formation of missing cluster defects. Especially with 5-X-IPA (X = OH) a large number of reduced $Ru^{\delta+}$ was formed. Ru-DEMOFs with a larger number of type A defects (reduced $Ru^{\delta+}$ sites) were found to be more active in the ethylene polymerization and a significant increase in TOF value was observed. In the PAAL-KNORR synthesis it is assumed that –OH groups on the defective linkers introduce more steric hindrance. Type B defects with missing nodes might decrease steric hindrance at the metal nodes and increase the catalytic activity.

1.1.2. *MOFs as heterogeneous catalysts*

As commented earlier, MOFs are of particular interest for catalytic applications due to their high porosity, crystallinity and the possibility to fine-tune the chemical and physical properties of materials. Catalytically active sites can be introduced at: i) the metallic nodes[62] of the structure, ii) the linker molecules, or iii) encapsulated inside the pores of the material.[4] Two or more functional groups within one material can be combined, to form multifunctional MOFs. Different active centers can for instance act in a synergistic way (e.g., dual activation of reaction substrates) or they can be used in cascade reactions, where multiple reactions take place successively on various active sites as shown above (see Scheme 1.3). Nevertheless, MOFs also have some disadvantages, compared to other heterogeneous catalysts, which are already used in industrial applications. Since other catalysts, such as zeolites show much higher tolerance towards thermal and chemical stability, the advantages of MOFs are clearly in the possibility of fine-tuning the chemical environment and their structure in terms of pore size, shape and dimensionality. The costs in production of MOFs are also higher compared to other heterogeneous catalysts (e.g., mineral acids and bases, metal salts and complexes and zeolites). Therefore, the use of MOFs should be focused on for example highly chemo- and regioselective reactions, where a given functional group is transformed in the presence of other functionalities and undesired side products and reactions become suppressed. This is often the case in the production of high added value fine chemicals, where polyfunctional substrates are usually involved. Also in the production of chiral drugs MOFs can be of interest, as they can function as a chiral catalyst in (enantio)selective catalysis in contrast with the major challenge for preparing chiral zeolites.[63,64] As an alternative to homogeneous catalysts, MOFs facilitate work up procedures, lead to cleaner products and can be useful in the development of more economic processes such as one-pot procedures.

Early reports on MOF-based catalysis were merely proof of concept studies, in which the main scope was to show that those MOFs contained the necessary active sites to catalyze a certain reaction. However, the performance obtained with these MOFs was generally very poor and serious concerns existed on materials stability under reaction conditions. This pessimistic situation started to change with the preparation of more robust compounds (such as MIL-101 or UiO-66). Today, more than one decade ago from the pioneering works on MOF catalysis, the catalytic use of these compounds is well established for a large number of reactions. We have fastly evolved from poor "proof of concept" solids to highly active and selective catalysts, in some cases with performances comparable to (or even surpassing) alternative state-of-the-art catalysts.[65]

Among the large number of MOFs described so far as potential heterogeneous catalysts, Zr-containing compounds deserve a special mention. These compounds, with the archetype UiO-66 in a relevant position, show in general elevated chemical, thermal and mechanical stability, thanks to the presence of Zr_6 SBUs with a high connectivity. Besides UiO-66 type compounds, other families of Zr-containing compounds include some PCN-ns (prepared by the group of H. C. ZHOU; PCN = porous coordination network), NU-ns (prepared by the group of J. T. HUPP and O. K. FARHA), DUT-ns (prepared by the group of S. KASKEL; DUT = Dresden University of Technology), *etc.* In this thesis, we have focused on the catalytic properties of one particular type of Zr-trimesate compound, named MOF-808, first prepared by YAGHI.[66,67] In the following, we will briefly describe the main characteristics of these Zr-MOFs.

1.1.2.1 Zr-containing MOFs

Zr-containing MOFs attracted a lot of interest, due to their high stability compared with other previously synthesized MOFs. The key feature for the high stability of Zr-MOFs is the high oxidation state of the Zr(IV) ions as compared to M(I), M(II) or M(III) metals present in other MOFs. The Zr(IV) ions are highly oxygen affine because of strong bond polarization.[68] The coordination bonds between carboxylate oxygen and Zr(IV) are usually very strong and further in line with the PERSON'S hard/soft, acid/base concept.[69] Therefore, Zr(IV) ions and carboxylate ligands are considered as hard acid and hard base, respectively. Most Zr-MOFs are found to be stable in organic solvents and water and even in acidic aqueous solution. The lower stability towards basic media can be described by the natural bond orbital (NBO) theory.[26,68–70] The NBO charge of oxygen in ^{-}OH anions is stronger than in the carboxylate group, which results in stronger bonding of ^{-}OH anions towards Zr(IV), which leads to the formation of zirconium (oxo)hydroxide and to decomposition of the MOF materials.

The Zr_6O_8 cluster is the most common SBU found in Zr-MOFs. This cluster consists of a Zr_6-octahedron where zirconium atoms are coordinated to eight oxygen atoms, forming a square-antiprismatic coordination. UiO-66 with a $[Zr_6O_4(OH)_4]^{12+}$ inorganic building brick, 12-fold connected to BDC linker molecules, was the first MOF constructed from a Zr_6-cluster (see Figure 1.6). Later, a large number of MOFs has been discovered consisting of the same Zr_6-cluster but varying in the type of linker molecule, number of coordinated linker molecules per cluster and denticity of linker molecules, such as bidentate, tridentate or tetradentate ligands, consisting of two, three or four carboxylic acid groups per molecule, respectively. A large structure variety already exists within

Zr-MOFs.[71] Some relevant examples of the already extended family of Zr-MOFs are listed in Table 1.1.

Table 1.2. Relevant Zr-MOFs with a Zr_6-cluster and different connectivity

12 connected	8 connected	6 connected
UiO-66	PCN-700	MOF-808
UiO-67	PCN-222	
PIZOFs	NU-1000	
	DUT-51	
	DUT-67	

Besides the Zr_6O_8 cluster, other SBUs are found in MOFs, such as the Zr_8O_6 cluster in PCN-221 reported by FENG *et al.*[72] A ZrO_6 core was found for instance in zirconium-phosphonate frameworks where the ZrO_6 octahedra form a 0D metal cluster[73] or 1D metal-oxo chains.[74] A ZrO_7 core was found in form of two parallel corner-sharing chains or chains of edge-sharing dimers of zirconium polyhedra within isoreticular MIL-140A-D[75] and also a ZrO_8 core was found in form of edge-sharing polyhedra, constructing 1D metal-oxo chains, as for instance in MIL-163.[76] In the following, a brief description of some prominent Zr-containing MOFs is given, including MOF-808, which has been focus of the present thesis.

a) UiO-66

UiO-66 was the first described member of this family containing a $[Zr_6O_4(OH)_4]^{12+}$ cluster in which triangular faces of the Zr_6-octahedron are alternatively capped by four μ_3-O and four μ_3-OH groups (four protons on the cluster are needed to achieve charge neutrality). Here, the symbol μ_3 indicates that oxygen atoms are shared by three Zr atoms defining the triangular faces of the octahedron. The cluster is coordinated to twelve BDC linker molecules. The SBUs organize in a face centered cubic packing, defining two types of cages, tetrahedral cages of 8 Å and octahedral cages of 11 Å, which are accessible through triangular windows of around 7 Å (see Figure 1.6). It has been shown, that upon heating the material to T > 523 K, dehydroxylation occurs on the metal cluster. Therefore, two of the μ_3-OH groups and two hydrogens of the remaining two μ_3-OH groups are eliminated from the SBU, which results in the formation of two H_2O molecules. The process is completed at 573 K to form a distorted $[Zr_6O_6]^{12+}$ cluster,

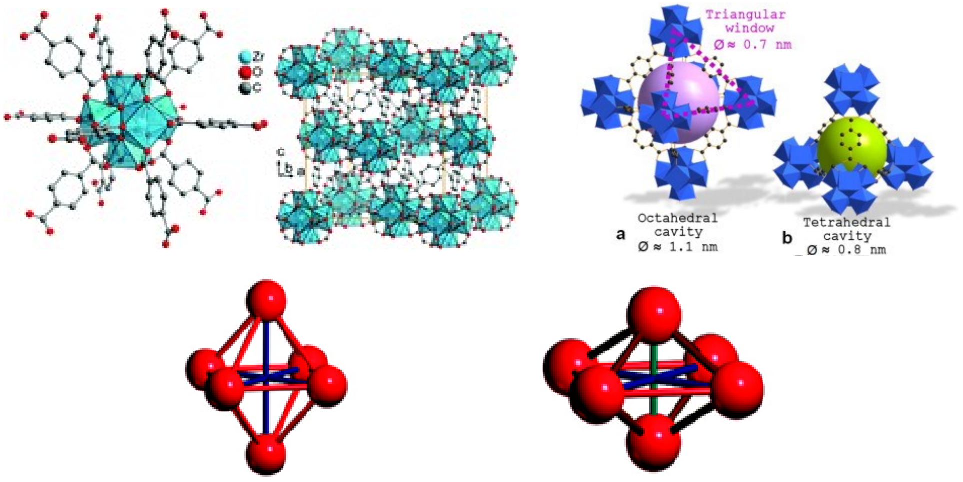

Reprinted (adapted) with permission from (*CrystEngComm.*, **2017**, *19*, 4092–4117). Copyright (2017) The Royal Society of Chemistry; (*Microporous and Mesoporous Materials*, **2011**, *139*, 67–73). Copyright (2010) Elsevier Inc.; (*Chem. Mater.*, **2011**, *23*, 1700–1718). Copyright (2011) American Chemical Society

Figure 1.6. UiO-66: SBU and 3D network (left, top); octahedral and tetrahedral caavities (right, top) and Zr_6-cluster before (left, bottom) and after (right, bottom) dehydroxylation

where the Zr-O coordination number is reduced to seven. The process is fully reversible and upon exposure to water vapor the initial $[Zr_6O_4(OH)_4]^{12+}$ cluster is formed (see Figure 1.6). UiO-66 shows a remarkable thermal stability, with a decomposition temperature of 813 K in air, is stable at pressures up to 10000 $kgcm^{-2}$ and is further stable in different solvents, such as DMF, H_2O, benzene and propan-2-one (or acetone).[15] Given this remarkable thermal, mechanical and chemical stability, UiO-66 was one of the first Zr-MOFs to be considered for catalysis. UiO-66 could be used successfully in a number of reactions as catalyst, such as epoxide ring-opening reaction[77], cross-aldol condensation[78], citronellal cyclization[28], acetalization[79], esterification[29] and others.[80–82] Although the catalytic applicability of UiO-66 has been proved in a number of reactions, relatively small pore size and openings limit reactions to small substrates since larger compounds will not have access to the active sites located at the internal surface of the material. Further, the ideal cluster in UiO-66 is connected to 12 BDC linker molecules, which leads to occupation of all coordination positions of zirconium atoms by the carboxylate groups of BDC linker molecules. As commented in the previous section, the lack of open metal sites in the ideal structure of UiO-66 limits the number of reactive Zr^{4+} centers to those associated to missing linker defects, which usually represent less than 20% of the total Zr atoms of the solid.

b) MOF-808

MOF-808[83] is a six connected Zr-containing MOF. The $[Zr_6O_4(OH)_4(HCO_2)_6]^{6+}$ SBUs are connected to six BTC linker molecules to form a 3-dimensional network. The remaining coordination positions of Zr^{4+} ions not connected by the BTC linkers are saturated by formate anions bridging two Zr sites, which can be removed by simple washing during activation.[84] This leaves two coordination unsaturated positions on every Zr^{4+} ion, which are occupied by one ^{-}OH anion (to keep the electric neutrality of the material) and one labile H_2O molecule. Then, MOF-808 contains intrinsic open metal sites due to the SBU's structure, in sharp contrast with UiO-66 in which open metal sites are only possible at defective positions associated with missing linkers. MOF-808 crystallizes in **spn** topology and forms a β-cristobalite network. The Zr_6 SBUs built fully staggered supertetrahedra with **D_{3d}** (antiprismatic) topology (see Figure 1.7). It is the smaller isoreticular analogue of the mesoporous zirconium metal-organic framework, PCN-777.[85] MOF-808 features big adamantane-shaped cages with a diameter of 18.4 Å and an aperture of 14 Å and small tetrahedral cages with an internal pore diameter of 4.8 Å and an aperture of 1.2 Å.

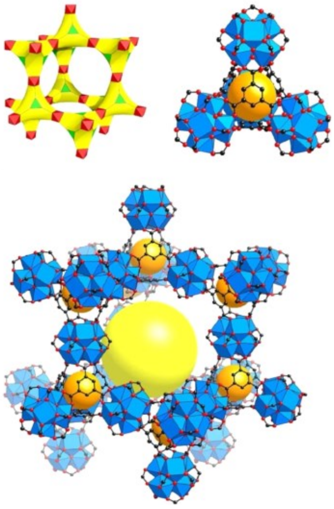

Reprinted (adapted) with permission from (*J. Am. Chem. Soc.*, **2014**, *136*, 4369–4381). Copyright (2014) American Chemical Society

Figure 1.7. MOF-808: spn topology (top, left); small tetrahedral cage (top, right) and large adamantane shaped cage (bottom)

c) Other Zr-MOFs

The replacement of the linear BDC linkers found in UiO-66 by geometrically equivalent highly elongated linker molecules resulted in the formation of a family of compounds called Porous Interpenetrated Zirconium-Organic-Frameworks (PIZOFs),[86] where a second identical framework is formed (interpenetrated) inside the first one. Elongated linker molecules of sufficient length create large tetrahedral windows that allow three linkers to pass, which results in the formation of an interpenetrated framework. The bended linker molecules in the framework create two types of tetrahedral pores. Smaller concave ones of around 14 Å and bigger convex ones of around 19 Å (see Figure 1.8). The SBUs of the second framework are occupying the concave pores. This results in the formation of an additional tetrahedral pore by reduction of the octahedral pore. PIZOFs were also synthesized with different functionalized linkers[86] and have a **fcu** topology with a 12 connected Zr_6-cluster as for UiO-66.

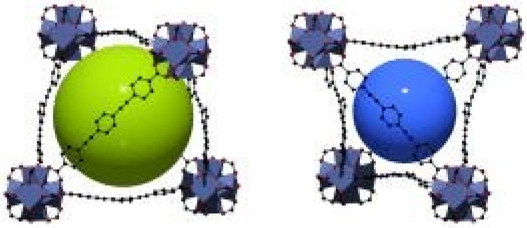

Reprinted (adapted) with permission from (*Chem. Eur. J.*, **2011**, *17*, 9320–9325). Copyright (2011) Wiley-VCH Verlag GmbH & Co. KGaA, Weinheim

Figure 1.8. Representation of convex cavity (left) and concave cavity (right) present in the structure of PIZOFs

With the use of tetradentate carboxylate ligands the connectivity of the Zr_6-cluster was reduced from twelve (as in UiO-66) to eight as in the case of PCN-222[87] and NU-1000.[34] Each tetradentate ligand is connecting four different SBUs and in total 8 linker molecules are connected to every SBU. Originally, for both MOFs the cluster was described as a $[Zr_6(\mu_3\text{-OH})_8(OH)_8]^{8+}$ cluster. Later a $[Zr_6(\mu_3\text{–}O)_4(\mu_3\text{–}OH)_4(OH)_4(OH_2)_4]^{8+}$ cluster was proposed for NU-1000, which underwent dehydroxylation upon thermal treatment leading to a $[Zr_6(\mu_3\text{–}O)_8]^{8+}$ cluster, which was consistent with diffuse reflectance infrared fourier transform spectroscopy (DRIFTS) and TGA analysis.[88] The tetrakis(4-carboxyphenyl)porphyrin (TCPP) linker in PCN-222 enables incorporation of additional metals, such as Fe, Mn, Co, Ni, Cu and Zn to the porphyrin position of the linker molecule.[34]

The connectivity of the Zr_6-cluster was also reduced using different bidentate ligands. In the group of S. KASKEL two different MOFs were prepared using DTTDC (dithieno[3,2-b;2',3'-d]-thiopheno-2,6-dicarboxylate) and TDC (thiophene-2,5-dicarboxylate) as linker molecules for DUT-51[89] and DUT-67,[90] respectively (see Figure 1.9). DUT-67 can be seen as the smaller analogue of DUT-51, as both linkers are bent due to the thiophene moiety but vary in length. The connectivity on the $Zr_6(\mu_3–O)_6(\mu_3–OH)_2$ cluster is reduced to eight and the compounds crystallize in **reo** topology.

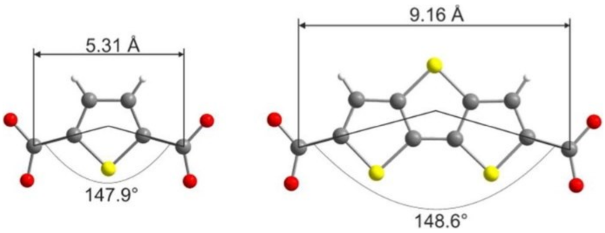

Reprinted (adapted) with permission from (*Cryst. Growth. Des.*, **2013**, *13*, 1231–1237). Copyright (2013) American Chemical Society

Figure 1.9. Geometry of linkers: TDC (left) and DTTDC (right)

In PCN-700[91] the connectivity on the $Zr_6(\mu_3–O)_4(\mu_3–OH)_4$ cluster is also reduced to eight, but different to DUT-51 and -67, PCN-700 crystallizes in a **bcu** topology. The MOF was synthesized with substituted 2,2'-biphenyl-4,4'-dicarboxylate linker molecules (Me_2-BPDC), where the two methyl groups introduce two off-plane carboxylate groups.

1.1.3. *Catalytic reactions with MOF-808*

The main focus of this thesis is to evaluate the catalytic properties of MOF-808. When this thesis was started, some precedents on this topic already existed in the bibliography, which will be shortly reviewed in the following.

The first report describing the use of MOF-808 as catalyst was published by JIANG *et al.*[67] These authors showed that as-prepared MOF-808 was rather inactive in the citronellal cyclization (only 8% conversion after 8 h), which is typically catalyzed by a LEWIS acid catalyst. The lack of activity of MOF-808 was probably due to the blocking of the Zr^{4+} open metal sites by formate anions used as modulators during the MOF synthesis. In order to improve the catalytic performance of MOF-808, those authors used this compound as a platform to coordinate sulfuric acid to the MOF structure by replacement of formate anions (see Figure 1.10, left). Due to the accessibility of all formate groups by the large pores and the three-fold connectivity by BTC linker molecules, it was assumed that exchange of formate groups by sulfuric acid should be possible without destruction of the framework. Therefore, different materials were prepared with a maximum loading of 2.5 sulfate groups per SBU, yielding a compound with the composition $[Zr_6O_5(OH)_3(BTC)_2(SO_4)_{2.5}(H_2O)_{2.5}]$, (MOF-808-2.5$SO_4$). Coordination of sulfuric acid leads to an increase in BRØNSTED acidity and sulfated MOFs with 1.3 and 2.5 sulfate ligands per SBU were found to be in the superacidic region, with a HAMMETT acidity function $H_0 \leq -14.5$. Citronellal conversion increased to 98% for MOF-808-2.5SO_4. Further the selectivity in the citronellal cyclization towards (±)-isopulegol monotonically decreases with increasing sulfate content (55% for MOF-808-2.5SO_4), which is indicative for BRØNSTED acidity. LEWIS acids typically give high selectivities (≥ 75%) towards (±)-isopulegol. MOF-808-2.5SO_4 further showed full conversion for the isomerization of α-pinene with selectivities towards 2,2-dimethyl-3-methylidenebicyclo[2.2.1]heptane (or camphene) and 1-methyl-4-(prop-1-en-2-yl)cyclohex-1-ene (or limonene) comparable to sulfated zirconia. As-prepared MOF-808 on the contrary was completely inactive. The catalytic activity of sulfated MOF-808 was further tested in different types of reactions, such as FRIEDEL–CRAFTS acylation of anisole, esterification of (9*Z*)-octadec-9-enoic acid, isomerization of limonene and in the conversion of methylcyclopentane into various hydrocarbons at 423–473 K. The catalyst was found to be a reusable and heterogeneous catalyst, with much higher activity than as-prepared MOF-808.

YEN *et al*[92] used sulfated MOF-808 in the synthesis of quinazolinones from β ketoesters and benzamides, as well as for the synthesis of benzimidazoles from β-ketoesters and *o*-phenylenediamines in propane-1,2,3-triol (or glycerol) as a green solvent. It was shown that the catalyst can be reused several times without significant loss of activity and that the catalyst crystallinity remains during reactions. Also the reaction was of true heterogeneous nature, as removal of the catalyst leads to no further conversion of substrates. The study was further expanded to the synthesis of benzothiazoles via the reaction of 2-aminobenzene-1-thiol with β-diketones. Sulfated MOF-808 was a more active catalyst in the cyclocondensation than many heterogeneous and homogeneous catalysts and could be used with glycerol as an environmentally benign solvent. MOF-808-2.5SO_4 was also found to be active in the solvent free benzoxazole synthesis through a heterocyclization of substituted 2-aminophenols and aldehydes.[93] Nevertheless, its catalytic activity was surpassed by its hafnium analogue, namely VNU-11-SO_4 (VNU = Vietnam National University).

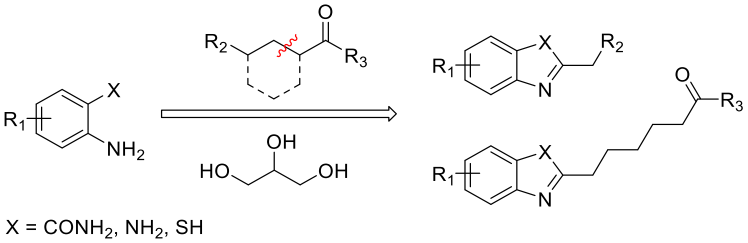

Reprinted (adapted) with permission from (*Journal of Industrial and Engineering Chemistry*, **2018**, *64*, 107–115). Copyright (2018) The Korean Society of Industrial and Engineering Chemistry

Scheme 1.6. Synthesis of quinazolinones, benzimidazoles or benzothiazoles from corresponding starting compounds

Ji *et al.*[94] were further able to convert the $Zr_6(\mu_3\text{-}O)_4(\mu_3\text{-}OH)_4(HCO_2)_6$ nodes in MOF-808 into an alkylated Zr-Me species. The resultant MOF (ZrMe-BTC) was active in the ethylene polymerization. The authors also reported the synthesis of $ZrCl_2$-BTC and $ZrMe_2$-BTC MOF. $ZrMe_2$-BTC was inactive as catalyst due to coordinative saturation at the anionic $ZrMe_2$ centers. ZrMe-BTC on the contrary contained neutral Zr-monoalkyl centers with open coordination sites. This represented the first MOF using metal SBUs as the active sites in a polymerization reaction (see Figure 1.10, right).

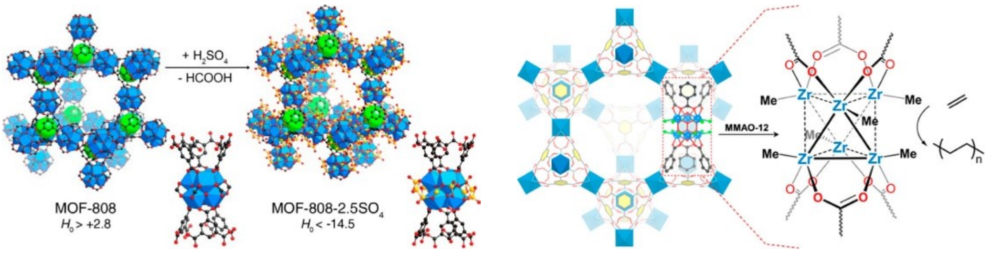

Reprinted (adapted) with permission from (*J.Am. Chem. Soc.*, **2014**, *136*, 12844–12847). Copyright (2014) American Chemical Society; (*J.Am. Chem. Soc.*, **2017**, *139*, 11325–11328). Copyright (2017) American Chemical Society

Figure 1.10. formation of sulfated MOF-808 from parent MOF-808 (left) and formation of ZrMe-BTC from $ZrCl_2$-BTC (right)

The same group reported the step-wise transformation on metal nodes of $Zr_6(\mu_3\text{-}O)_4(\mu_3\text{-}OH)_4(HCO_2)_6(BTC)_2$ into $[Zr^{III}{}_6(\mu_3\text{-}O)_4(\mu_3\text{-}ONa)_4H_6Na_6(BTC)_2$.[95] Therefore, the oxidation state of zirconium changed from IV^+ in parent MOF-808 to III^+ in Zr^{III}H-BTC. Zr^{3+} centers are usually difficult to obtain in homogeneous catalysts, coordinatively saturated and/or chemically unstable. The catalyst was found to be very active in the hydroboration and hydrosilylation of pyridines and quinolones. Also the catalyst was the most productive hydroboration catalyst of pyridine at that time. In the reaction with 4,4,5,5-tetramethyl-1,3,2-dioxaborolane (BPin) a TON of 365 was obtained. The compound also retained its crystallinity during catalytic reactions and was found to be a reusable and heterogeneous catalyst, without significant drop of activity and selectivity after up to five reuses.

Formate ions, which are typically coordinated after synthesis to the hexanuclear zirconium cluster in parent MOF-808 can be readily removed by heating the material in fresh solvent. This leads to removal of formate and coordination of –OH groups and H_2O molecules to undercoordinated metal sites. The –OH groups are needed to maintain charge neutrality within the structure. This form is usually described as MOF-808-a, the activated form of MOF-808. MOF-808-a has been used lately for the degradation of CWAs and some simulants. Some substrates that have been tested are summarized in Figure 1.11.The high number of open metal sites within the structure as well as the open framework with apertures and pores of sufficient size lead to good activity of MOF-808-

a in the hydrolysis of CWAs and simulants.[84] MOF-808 was tested in different reaction media and for a number of compounds and was also compared with different Zr-MOFs, such as UiO-66, UiO-66-NH_2, NU-1000, PCN-777, DUT-84 *etc*. MOON *et al.* used MOF-808 for the hydrolysis of the nerve-agent simulant DMNP in an aqueous buffer solution.[96] The study was extended to the use of a plug-flow reactor under continuous flow conditions and the catalyst could be reused as well. KALINOVSKYY *et al.* showed later that MOF-808-a can be used for the hydrolysis of the V-series agent VM in the absence of buffer in H_2O.[97] They also used a different activation procedure, as MOF-808 was activated in a microwave, suspended in distilled H_2O. KONING *et al.* also tested

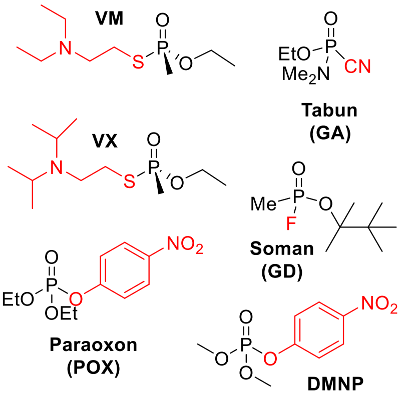

Figure 1.11. Representation of CWAs with leaving groups marked in red

MOF-808-a for the hydrolysis of a series of compounds (VX, GA, POX and GD) in H_2O and in an aqueous buffer solution.[98] Whereas the degradation in alkaline buffer solution proceeded in all cases very easy, the absence of a buffer led to much slower conversion or even stopped the reaction completely. It is further proposed that the basic function in VX and GA have a beneficial effect on the hydrolysis rate. A reaction mechanism on Zr-MOFs was proposed by PLONKA *et al.* for dimethyl methylphosphonate (DMMP) under vapor-phase conditions. The mechanism consists of two steps: (i) nucleophilic addition of the hydroxide ligand to DMNP and formation of a pentacoordinated phosphorus intermediate and (ii) decomposition of the pentacoordinated intermediate *via* elimination of methanol as the leaving group.[99] They further showed that the derived phosphonic acid product upon decomposition of reagents might be strongly bound to the catalyst. Therefore, catalytic processes are being inhibited, which is in contrast to catalytic processes reported for many examples in solution.

Another work by LY *et al.* showed that the hydrolysis of a series of dipeptides (Gly-X) and hen egg white lysozyme protein can be catalyzed by non activated MOF-808.[100] MOF-808 showed to be applicable at different pD values and could be reused without significant loss of crystallinity and activity. The good reusability outperformed other catalysts such as Zr(IV)-substituted polyoxometalates (POMs), which can form catalytically inactive dimers during reaction.

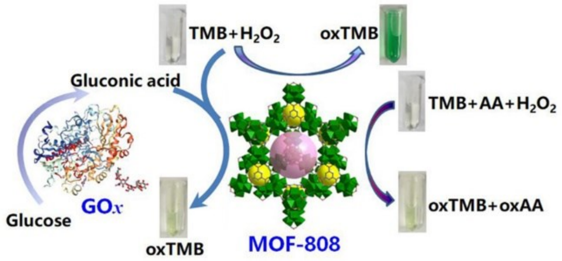

Reprinted (adapted) with permission from (*Inorg. Chem.*, **2018**, *57*, 9096–9104). Copyright (2018) American Chemical Society

Figure 1.12. MOF-808-a as peroxidase-like catalyst

Activated MOF-808 was also used by ZHENG *et al.* as a peroxidase-like catalyst at neutral pH (see Figure 1.12).[101] Although a number of peroxidase mimetics are known, including different MOFs, their optimal catalytic activity is often restricted to acidic conditions with pH values around 3-4. For applications in biological systems on the other hand it is required to work at near-neutral pH values (pH 5.0-7.4) and the exploration of suitable peroxidase mimics is still of great interest. 3,3',5,5'-tetramethyl[1,1'-biphenyl]-4-4'-diamine (TMB) could be oxidized by MOF-808 in a pH range of 3-10 when H_2O_2 served as oxidant. Because TMB oxidation is indicated by a color change, MOF-808 was also used as a sensor for H_2O_2, L-ascorbic acid and D-gluconic acid concentration during TMB oxidation. D-gluconic acid is the product of glucose oxidation catalyzed by glucose oxidase and the detection of D-gluconic acid therefore is an indicator for D-glucose concentration.

MOF-808 was also used by GONG *et al.* in the production of 5-(hydroxymethyl)furan-2-carbaldehyde (or 5-hydroxymethylfurfural, 5-HMF) from glucose.[102] MOF-808 showed higher conversion compared to UiO-66. Nevertheless, the recyclability and stability was lower compared to UiO-66, which was attributed to the hydrolytic conditions (DMSO-d_6/water, 39/1) which led to partial decomposition of MOF-808.

DESIDERY *et al.* used amphoteric MOF-808 in the transesterification of dimethyl carbonate (DMC) to a mixture of diethyl carbonate (DEC) and ethyl methyl carbonate (EMC).[103] Transesterification reactions can be catalyzed by both, bases and acids, as the carboxyl group of the ester and the hydroxyl group of the alcohol can be activated to facilitate the nucleophilic substitution. MOF-808 features Lewis acid sites at the Zr atoms and basic sites at the bridging O atoms at the Zr_6-cluster. MOF-808 successfully catalyzed the transesterification of DMC and its activity was superior to any other commercially available catalyst.

MOF-808-a was also used as support to incorporate Pd nanoparticles, yielding Pd/MOF-808-a.[104] The resulting material was used as catalyst for the base-free Heck- reaction and the oxidation of alcohol in a one-pot tandem reaction (see Figure 1.13). Heck-reaction is an effective way to increase C-C chain lengths and bases are usually added for the neutralization of the halogen acid and reexposing of the catalytic center. It was shown that the terminal –OH groups in activated MOF-808 exhibit Brønsted basicity and can replace additional bases during reaction. Brønsted basicity was proved by different techniques such as CO_2-TPD-MS, in situ DRIFTS and acid-base titration. Accordingly, the catalytic activity of Pd/MOF-808-a for the production of (*E*)-1,2-diphenylethene under base-free conditions was very high (yield of 93,6%). On the contrary, Pd/MIL-101 and Pd/UiO-66, which show no Brønsted basicity, had very low activity under base-free conditions. The Pd/MOF-808-a catalyst could be reused and showed high activity for up to 10 cycles. No significant loss of crystallinity was observed after the 10th cycle. The catalytic activity was further tested for substituted phenyl containing olefins, acrylates and linear olefins. Pd/MOF-808a could further catalyze the oxidation of phenylmethanol to benzaldehyde and subsequent reaction with methanol to methyl benzoate. Conversions and yield of final product methyl benzoate were higher than for Pd/MIL-101 and Pd/UiO-66.

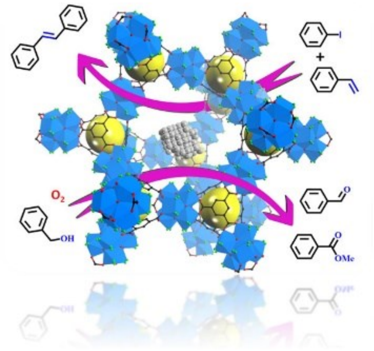

Reprinted (adapted) with permission from (*Inorg. Chem.*, **2018**, *57*, 8033–8036). Copyright (2018) American Chemical Society

Figure 1.13. Pd/MOF-808-a as catalyst for the Heck-reaction and production of methyl benzoate from benzyl alcohol

Ullah *et al.* used MOF-808 further as a support for the 12-tungstophoric acid complex (HPW), which was encapsulated inside the pores of the MOF.[105] HPW@MOF-808 was used in the Friedel-Crafts acylation of anisole with benzoyl chloride to (4-methoxyphenyl)(phenyl)methanone. With a loading of 28.2 wt% the catalytic system had a yield of 97.9% and was competitive with reported and conventional catalytic systems. The catalyst was reused four times without significant loss of activity and selectivity and removal of the catalyst from the reaction mixture resulted in no further conversion, indicating that the reaction is of true heterogeneous character.

As it will be described in more detail in the following, the MPV reduction of carbonyl compounds is attractive, as it avoids using precious metals, molecular H_2 used in alternative reduction methods, and is chemically highly (chemo)selective. A few reports exist on the use of MOF-808 as MPV catalysts, which represent an important precedent for the present thesis. Thus, MOF-808 was used as an efficient catalyst in the catalytic transfer hydrogenation (CTH) of ethyl 4-oxopentanoate (or ethyl levulinate, EL) to 5-methyldihydrofuran-2(3*H*)-one (or γ-valerolactone, GVL) by VALEKAR *et al.*[106] EL was first reduced in a MPV reduction to ethyl 4-hydroxypentanoate, which cyclizes in a subsequent step to GVL.

PLESSERS *et al.* used MOF-808 as a catalyst in the MPV reduction of various α,β-unsaturated aldehydes and ketones.[107] The reduction of challenging substrates such as (*R*)-2-methyl-5-(prop-1-en-2-yl)cyclohex-2-en-1-one (*or R*-carvone) could be improved further by removal of reacted reducing agent (acetone) and the use of 2,3-dihydro-1*H*-inden-1-ol (or (*S*)-1-indanol) as a stronger reducing agent. The large BET surface area and low connectivity of MOF-808 showed to be beneficial in the MPV reduction compared to other Zr-containing catalysts such as UiO-66. It has to be mentioned that diastereoselectivity was induced by the MOF-808 catalyst in the reduction of *R*-carvone. With the strong reducing agent (*S*)-1-indanol (see Scheme 1.7) yields were increased to 73% with a diastereomeric excess of 90% towards the *cis* isomer.

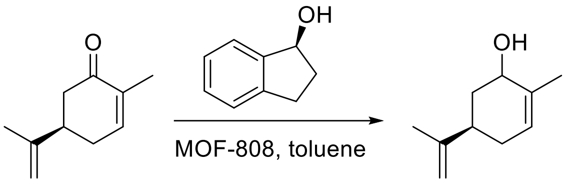

Scheme 1.7. MPV reduction of *R*-carvone using strong reducing agent (*S*)-1-indanol

1.1.4. *MEERWIN-PONNDORF-VERLEY (MPV) reduction*

The MEERWEIN-PONNDORD-VERLEY (MPV) reaction implies the reduction of a ketone or an aldehyde to the corresponding alcohol (secondary or primary, respectively) in the presence of a sacrificial alcohol as a source of the hydride ions, as shown in Scheme 1.8. The opposite reaction, i.e., the oxidation of a secondary alcohol to a ketone, is also possible and is known as OPPENAUER oxidation. Both reduction-oxidation reactions are thus collectively referred to as MEERWEIN-PONNDORF-VERLEY-OPPENAUER (MPVO) reaction.

The MPVO reaction was first reported in 1925[108–110] using aluminium alkoxides as catalysts, first in the reduction of aldehydes and later using easily oxidizable secondary alcohols and their aluminium alkoxides, such as $Al(O^iPr)_3$, in the reduction of ketones. The reduction reaction was shown to be reversible and was used later for instance in the oxidation of steroids for the synthesis of progesterone.[111,112]

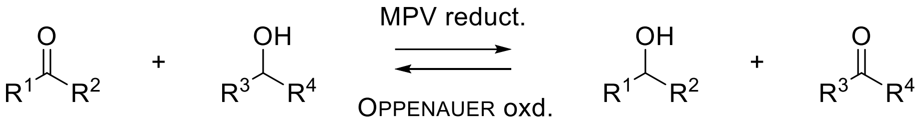

Scheme 1.8. MPVO transfer hydrogenation

The reduction reaction is chemoselective; i.e., it can be carried out in the presence of other easily reducible functional groups such as conjugated and unconjugated unsaturated C-C bonds, esters and nitro groups. This is a clear advantage of the MPVO reaction with respect to other reduction methods, such as direct hydrogenation with H_2 or reduction with other reducing agents, such as $NaBH_4$. In oxidation reactions, no overoxidation towards the carboxylic acids takes place, which can be a drawback when other oxidation reactions are used. Also the reaction proceeds under mild reaction conditions, which is favorable for the synthesis of natural products. The use of easily reducible oxidants, like quinones, benzophenone and cyclohexanone allowed also the oxidation of primary alcohols to aldehydes.

However, a main drawback of MPVO reactions is that it often requires the use of stoichiometric amounts of the alkoxides. Therefore, development of new catalysts with improved properties has been actively pursued to date. In this way, the use of metal alkoxides has been expanded to transition metal complexes of titanium,[113] zirconium,[114] hafnium[113] or iridium,[115] lanthanide alkoxides,[116] alkali metal alkoxides[117] and heterogeneous systems. Alkali alkoxides for instance were found to be useful in the conversion of *N*-containing substrates.[117] Strategies for improving the conversion in a MPVO reaction include the use of stronger oxidants/reductants, usually in a large excess, that can be removed from the reaction mixture after use.

Given the pro-chiral nature of the carbonyl group, the MPVO reaction can be used in diastereoselective reduction reactions, while also chiral reducing agents or catalysts can be used to introduce enantioselectivity. To attain higher diastereomeric ratios, lower reaction temperatures, shorter reaction times and low amounts of catalyst might be favored, to avoid racemization towards the thermodynamic equilibrium.

Different heterogeneous systems have been tested with some success, including for instance γ-Al_2O_3,[118] and other metal oxides, such as La_2O_3,[119] MgO[120] and hydrous zirconium oxide.[121,122] Also zeolites[123] have been used in the MPVO reaction, and BEA-zeolite[124] (BEA = Beta polymorph A) was found to be a highly active catalyst. Calcination of the catalyst at high temperature led to an increase in activity and formation of octahedral aluminium atoms, which were proposed to be the active sites in the reaction. Titanium was incorporated as a LEWIS acid center into BEA-zeolite and it was found to be active in the MPVO reaction.[125,126] An advantage compared to BEA-zeolite was found in the tolerance of H_2O. The BRØNSTED acid sites within BEA-zeolite lead to an increased water sorption and blocking of active aluminium sites. The nearly all-silica Ti-BEA zeolite on the contrary is much more hydrophobic and keeps its activity better after addition of water to the reaction mixture. An improvement compared to Ti-BEA zeolite was found for the Sn-BEA zeolite.[127] Tin has a higher electronegativity than titanium and thus should be a better catalyst for the MPVO reaction, which was indeed found for Sn-BEA zeolite. The aluminium-free Sn-BEA zeolite was more active than Al-BEA and Ti-BEA catalysts. A further improvement was found for the Zr-BEA zeolite.[128,129] Zr-BEA zeolite showed very high activity for the MPVO reaction and also tolerance to for instance water and pyridine. Besides Ti, Sn and Zr, other metals with high charge to radius ratio were tested, such as Nb and Ta.[130] The resulting Nb- and Ta-BEA zeolites are active in the MPVO reaction and Ta-BEA zeolite showed good activity and selectivity in a domino etherification/MPV reduction reaction.

An important feature of BEA zeolites with respect to homogeneous catalysts is that the MPVO reaction takes places inside the restricted space of the BEA channels. Thus, a bulky substrate such as 1-(3,5-di-*tert*-butylphenoxy)propan-2-one is not converted in H-BEA zeolite but it was in a mesoporous MCM-41 (MCM = Mobile Composition of Matter) (Scheme 1.9).[124] Further, the confined space of the zeolite channels can introduce important constraints driving the reaction to the formation of specific stereoisomers. Thus, TCH is converted to the *cis* 4-(*tert*-butyl)cyclohexan-1-ol with high selectivity, due to transition-state selectivity.[124] The TS leading to the *cis* product is much less bulky than the TS leading to the *trans* product. The selectivity was also found in the oxidation reaction in a mixture of *cis* and *trans* 4-(*tert*-butyl)cyclohexan-1-ol. Here the *cis* isomer was converted preferentially over the *trans* isomer.[128]

Besides BEA-type zeolites, tetravalent metals such as Ti,[131] Zr[132] and Sn[133] have been also incorporated into MWW zeolite (MWW = Mobile tWenty tWo). Zr-MWW[132] was shown to be active in the MPV reduction of cyclohexanone (CH) with comparable reactivity to Zr-BEA zeolite. Because of slightly smaller channels, reaction times were longer than for Zr-BEA zeolite. In comparison with Ti-BEA zeolite, a Ti-MCM-41 zeolite[125] was not active in the MPV reduction of TCH with ^{i}PrOH.

Mesoporous silicates, such as MCM-41 have been used for grafting metal alkoxides, such aluminium-[134] and zirconium-alkoxides[135] or zirconium- and hafnium-alkyl complexes[136] and are active catalysts in the MPV reduction. MCM-41 with grafted zirconium- and hafnium-alkoxides or -metallocenes have been used for instance in the reduction of α,β-unsaturated ketones.

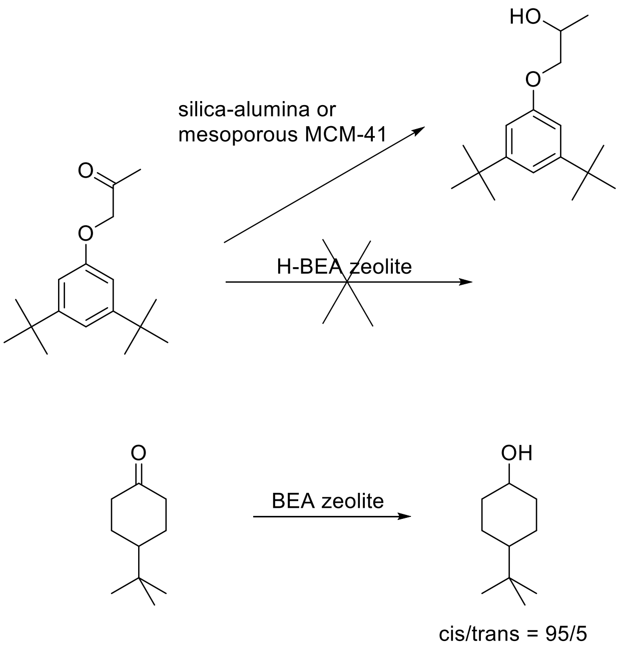

Scheme 1.9. MPV reduction of carbonyl compounds using zeolitets of different pore size and structure

As hydrous zirconium oxide and Zr-containing zeolites were shown to be active catalysts in the MPVO reaction, it was suggested that MOFs containing for instance zirconium-oxo clusters could be feasible catalysts for the MPVO reaction. The structural diversity within MOFs was found to be beneficial as increased activity in the OPPENAUER oxidation of geraniol with furfural was found for UiO-66-NO_2, the nitro analogue of UiO-66.[28] Defective UiO-66-NO_2-10_{HCl} was more active in the reduction of TCH with ^{i}PrOH compared to defective UiO-66-10_{HCl}.[58] As it has been commented above, MOF-808 was also used in the MPV reduction of a number of α,β-unsaturated carbonyl compounds to the corresponding alcohols, including *R*-carvone, using (*S*)-1-indanol as a strong reducing agent.[107]

1.2. References

1. Farha, O. K. *et al. J. Am. Chem. Soc.* **2012**, *134*, 15016.
2. Suh, M. P.; Park, H. J.; Prasad, T. K. & Lim, D. W. *Chem. Rev.* **2012**, *112*, 782.
3. Corma, A.; Garcia, H. & Llabrés i Xamena, F. X. *Chem. Rev.* **2010**, *110*, 4606.
4. Rogge, S. M. J. *et al. Chem. Soc. Rev.* **2017**, *46*, 3134.
5. Kreno, L. E. *et al. Chem. Rev.* **2012**, *112*, 1105.

6. Horcajada, P. *et al. Chem. Rev.* **2012**, *112*, 1232.
7. Devic, T. & Serre, C. *Chem. Soc. Rev.* **2014**, *43*, 6097.
8. Férey, G. *et al. Science* **2005**, *309*, 2040.
9. Surblé, S.; Serre, C.; Mellot-Draznieks, C.; Millange, F. & Férey, G. *Chem. Commun.* **2006**, *0*, 284.
10. Serre, C. *et al. J. Am. Chem. Soc.* **2002**, *124*, 13519.
11. Férey, G. *Chem. Soc. Rev.* **2008**, *37*, 191.
12. Batten, S. R.; Hoskins, B. F. & Robson, R. *J. Am. Chem. Soc.* **1995**, *117*, 5385.
13. Hoskins, B. F. & Robson, R. *J. Am. Chem. Soc.* **1990**, *112*, 1546.
14. Hoskins, B. F.; Robson, R. & Scarlett, N. V. Y. *Angew. Chem. Int. Ed.* **1995**, *34*, 1203.
15. Cavka, J. H. *et al. J. Am. Chem. Soc.* **2008**, *130*, 13850.
16. Jakobsen, S. *et al. Phys. Rev. B - Condens. Matter Mater. Phys.* **2012**, *86*, 1.
17. Falaise, C. *et al. Chem. Eur. J.* **2013**, *19*, 5324.
18. Falaise, C.; Charles, J. S.; Volkringer, C. & Loiseau, T. *Inorg. Chem.* **2015**, *54*, 2235.
19. Lammert, M. *et al. Chem. Commun.* **2015**, *51*, 12578.
20. Kim, M.; Cahill, J. F.; Fei, H.; Prather, K. A. & Cohen, S. M. *J. Am. Chem. Soc.* **2012**, *134*, 18082.
21. Ebrahim, A. M. & Bandosz, T. J. *ACS Appl. Mater. Interfaces* **2013**, *5*, 10565.
22. Nouar, F. *et al. Chem. Commun.* **2015**, *51*, 14458.
23. Li, M.; Li, D.; O'Keeffe, M. & Yaghi, O. M. *Chem. Rev.* **2014**, *114*, 1343.
24. Eddaoudi, M. *et al. Science* **2002**, *295*, 469.
25. Decoste, J. B. *et al. J. Mater. Chem. A* **2013**, *1*, 5642.
26. Shufen, W. *et al. Dalt. Trans.* **2015**, *44*, 8049.
27. Lawrence, M. C.; Schneider, C. & Katz, M. J. *Chem. Commun.* **2016**, *52*, 4971.
28. Vermoortele, F. *et al. Angew. Chem. Int. Ed.* **2012**, *51*, 4887.
29. Cirujano, F. G.; Corma, A. & Llabrés i Xamena, F. X. *Chem. Eng. Sci.* **2015**, *124*, 52.
30. Caratelli, C. *et al. J. Catal.* **2017**, *352*, 401.
31. Deria, P. *et al. Chem. Soc. Rev.* **2014**, *43*, 5896.
32. Lee, Y.; Kim, S.; Kang, J. K. & Cohen, S. M. *Chem. Commun.* **2015**, *51*, 5735.

33. Silva, C. G.; Luz, I.; Llabrés i Xamena, F. X.; Corma, A. & García, H. *Chem. Eur. J.* **2010**, *16*, 11133.

34. Mondloch, J. E. *et al. J. Am. Chem. Soc.* **2013**, *135*, 10294.

35. Nguyen, H. G. T. *et al. Catal. Sci. Technol.* **2015**, *5*, 4444.

36. Nguyen, H. G. T. *et al. ACS Catal.* **2014**, *4*, 2496.

37. Ameloot, R. *et al. Chem. Eur. J.* **2013**, *19*, 5533.

38. López-Maya, E. *et al. Angew. Chem. Int. Ed.* **2015**, *54*, 6790.

39. Hwang, Y. K. *et al. Angew. Chem. Int. Ed.* **2008**, *47*, 4144.

40. Deria, P. *et al. J. Am. Chem. Soc.* **2013**, *135*, 16801.

41. Li, B. *et al. Chem. Commun.* **2012**, *48*, 6151.

42. Seo, J. S. *et al. Nature* **2000**, *404*, 982.

43. Kim, M.; Cahill, J. F.; Su, Y.; Prather, K. A. & Cohen, S. M. *Chem. Sci.* **2012**, *3*, 126.

44. Zhang, X.; Llabrés i Xamena, F. X. & Corma, A. *J. Catal.* **2009**, *265*, 155.

45. Ingleson, M. J.; Barrio, J. P.; Guilbaud, J. B.; Khimyak, Y. Z. & Rosseinsky, M. J. *Chem. Commun.* **2008**, *0*, 2680.

46. Baleizão, C. & Garcia, H. *Chem. Rev.* **2006**, *106*, 3987.

47. Juan-Alcañiz, J.; Gascon, J. & Kapteijn, F. *J. Mater. Chem.* **2012**, *22*, 10102.

48. Rösler, C. & Fischer, R. A. *CrystEngComm* **2015**, *17*, 199.

49. Astruc, D.; Lu, F. & Aranzaes, J. R. *Angew. Chem. Int. Ed.* **2005**, *44*, 7852.

50. Campelo, J. M.; Luna, D.; Luque, R.; Marinas, J. M. & Romero, A. A. *ChemSusChem* **2009**, *2*, 18.

51. Corma, A. & Garcia, H. *Chem. Soc. Rev.* **2008**, *37*, 2096.

52. Xuan, W.; Zhu, C.; Liu, Y. & Cui, Y. *Chem. Soc. Rev.* **2012**, *41*, 1677.

53. Cirujano, F. G.; Llabrés i Xamena, F. X. & Corma, A. *Dalt. Trans.* **2012**, *41*, 4249.

54. Gascon, J.; Corma, A.; Kapteijn, F. & Llabre i Xamena, F. X. *ACS Catal.* **2014**, *4*, 361.

55. Dhakshinamoorthy, A. & Garcia, H. *Chem. Soc. Rev.* **2012**, *41*, 5262.

56. Bogaerts, T. *et al. Chem. Commun.* **2013**, *49*, 8021.

57. Fang, Z.; Bueken, B.; Vos, D. de & Fischer, R. A. *Angew. Chem. Int. Ed.* **2015**, *54*, 7234.

58. Vermoortele, F. *et al. J. Am. Chem. Soc.* **2013**, *135*, 11465.

59. Marx, S.; Kleist, W. & Baiker, A. *J. Catal.* **2011**, *281*, 76.
60. Fang, Z. *et al. J. Am. Chem. Soc.* **2014**, *136*, 9627.
61. Zhang, W. *et al. Chem. Eur. J.* **2016**, *22*, 14297.
62. Valvekens, P.; Vermoortele, F. & Vos, D. de *Catal. Sci. Technol.* **2013**, *3*, 1435.
63. Wang, C.; Zheng, M. & Lin, W. *J. Phys. Chem. Lett.* **2011**, *2*, 1701.
64. Falkowski, J. M.; Liu, S. & Lin, W. *CHAPTER 11 Asymmetric Catalysis with Chiral Metal Organic Frameworks* In: Llabrés i Xamena, F. & Gascon, J. (Eds.) *Metal Organic Frameworks as Heterogeneous Catalysts*, The Royal Society of Chemistry, Cambridge, 2013, 344.
65. Llabrés i Xamena, F. X.; Luz, I. & Cirujano, F. G. *CHAPTER 7 Strategies for Creating active Sites in MOFs* In: Llabres i Xamena, F. & Gascon, J. (Eds.) *Metal Organic Frameworks as Heterogeneous Catalysts*, The Royal Society of Chemistry, Cambridge, 2013, 237.
66. Furukawa, H.; Ga, F.; Hudson, M. R. & Yaghi, O. M. *J. Am. Chem. Soc.* **2014**, *136*, 4369.
67. Jiang, J. *et al. J. Am. Chem. Soc.* **2014**, *136*, 12844.
68. Zhang, M. *et al. Angew. Chem. Int. Ed.* **2014**, *53*, 815.
69. Pearson, R. G. *J. Am. Chem. Soc.* **1963**, *85*, 3533.
70. Lu, P. *et al. J. Mater. Chem. A* **2014**, *2*, 16250.
71. Bai, Y. *et al. Chem. Soc. Rev.* **2016**, *45*, 2327.
72. Feng, D. *et al. Inorg. Chem.* **2013**, *52*, 12661.
73. Taddei, M. *et al. Chem. Commun.* **2014**, *50*, 5737.
74. Taddei, M. *et al. Chem. Commun.* **2014**, *50*, 14831.
75. Campo, B. *et al. Angew. Chem. Int. Ed.* **2012**, *124*, 9401.
76. Mouchaham, G. *et al. Angew. Chem. Int. Ed.* **2015**, *54*, 13297.
77. Liu, Y.; Klet, R. C.; Hupp, J. T. & Farha, O. *Chem. Commun.* **2016**, *52*, 7806.
78. Vermoortele, F.; Ameloot, R.; Vimont, A.; Serre, C. & Vos, D. de *Chem. Commun.* **2011**, *47*, 1521.
79. Timofeeva, M. N. *et al. Appl. Catal. A Gen.* **2014**, *471*, 91.
80. Goh, T. W.; Xiao, C.; Maligal-Ganesh, R. V.; Li, X. & Huang, W. *Chem. Eng. Sci.* **2015**, *124*, 45.
81. Dissegna, S. *et al. Cryst. Eng. Comm.* **2017**, *19*, 4137.
82. Luz, I.; Rösler, C.; Epp, K.; Llabrés i Xamena, F. X. & Fischer, R. A. *Eur. J. Inorg.*

Chem. **2015**, *2015*, 3904.

83. Furukawa, H. *et al. J. Am. Chem. Soc.* **2014**, *136*, 4369.
84. Moon, S. Y.; Liu, Y.; Hupp, J. T. & Farha, O. K. *Angew. Chem. Int. Ed.* **2015**, *54*, 6795.
85. Feng, D. *et al. Angew. Chem. Int. Ed.* **2015**, *54*, 149.
86. Schaate, A. *et al. Chem. Eur. J.* **2011**, *17*, 9320.
87. Feng, D. *et al. Angew. Chem. Int. Ed.* **2012**, *51*, 10307.
88. Mondloch, J. E. *et al. Nat. Mater.* **2015**, *14*, 512.
89. Bon, V.; Senkovskyy, V.; Senkovska, I. & Kaskel, S. *Chem. Commun.* **2012**, *48*, 8407.
90. Bon, V.; Senkovska, I.; Baburin, I. A. & Kaskel, S. *Cryst. Growth Des.* **2013**, *13*, 1231.
91. Yuan, S. *et al. J. Am. Chem. Soc.* **2015**, *137*, 3177.
92. Vo, Y. H. *et al. J. Ind. Eng. Chem.* **2018**, *64*, 107.
93. Nguyen, L. H. T.; Nguyen, T. T.; Nguyen, H. L.; Doan, T. L. H. & Tran, P. H. *Catal. Sci. Technol.* **2017**, *7*, 4346.
94. Ji, P. *et al. J. Am. Chem. Soc.* **2017**, *139*, 11325.
95. Ji, P.; Feng, X.; Veroneau, S. S.; Song, Y. & Lin, W. *J. Am. Chem. Soc.* **2017**, *139*, 15600.
96. Moon, S. Y.; Liu, Y.; Hupp, J. T. & Farha, O. K. *Angew. Chem. Int. Ed.* **2015**, *54*, 6795.
97. Kalinovskyy, Y.; Cooper, N. J.; Main, M. J.; Holder, S. J. & Blight, B. A. *Dalt. Trans.* **2017**, *46*, 15704.
98. Koning, M. C. de; Grol, M. van & Breijaert, T. *Inorg. Chem.* **2017**, *56*, 11804.
99. Plonka, A. M. *et al. J. Am. Chem. Soc.* **2017**, *139*, 599.
100. Ly, H. G. T. *et al. J. Am. Chem. Soc.* **2018**, *140*, 6325.
101. Zheng, H. Q. *et al. Inorg. Chem.* **2018**, *57*, 9096.
102. Gong, J.; Katz, M. J. & Kerton, F. M. *RSC Adv.* **2018**, *8*, 31618.
103. Desidery, L.; Chaemcheun, S.; Yusubov, M. & Verpoort, F. *Catal. Commun.* **2018**, *104*, 82.
104. Yan, X. *et al. Inorg. Chem.* **2018**, *57*, 8033.
105. Ullah, L. *et al. Sci. China Chem.* **2018**, *61*, 402.

106. Valekar, A. H. *et al. Green Chem.* **2016**, *18*, 4542.

107. Plessers, E.; Fu, G.; Tan, C.; Vos, D. de & Roeffaers, M. *Catalysts* **2016**, *6*, 104.

108. Meerwein, H. & Schmidt, R. *Liebigs Ann. Chem.* **1925**, *444*, 221.

109. Verley, A. *Bull. Soc. Chim. Fr.* **1925**, *37*, 537.

110. Ponndorf, W. *Angew. Chem.* **1926**, *39*, 138.

111. Graauw, C. F. de; Peters, J. A.; Bekkum, H. van & Huskens, J. *Synthesis (Stuttg).* **1994**, *10*, 1007.

112. Oppenauer, R. V. *Recl. Trav. Chim. Pays-Bas* **1937**, *56*, 137.

113. Nakano, T.; Umano, S.; Kino, Y.; Ishii, Y. & Ogawa, M. *J. Org. Chem.* **1988**, *53*, 3752.

114. Ishii, Y. *et al. J. Org. Chem.* **1986**, *51*, 240.

115. Vinzi, F.; Zassinovich, G. & Mestroni, G. *J. Mol. Catal.* **1983**, *18*, 359.

116. Kagan, H. B. & Namy, J. L. *Tetrahedron* **1986**, *42*, 6573.

117. Woodward, R. B.; Wendler, N. L. & Brutschy, F. J. *J. Am. Chem. Soc.* **1945**, *67*, 1425.

118. Posner, G. H.; Runquist, A. W. & J., M. C. *J. Org. Chem.* **1977**, *42*, 1202.

119. Gargano, M.; D'orazio, V.; Ravasio, N. & Rossi, M. *J. Mol. Catal.* **1990**, *58*, L5.

120. Kaspar, J.; Trovarelli, A.; Lenarda, M. & Graziani, M. *Tetrahedron Lett.* **1989**, *30*, 2705.

121. Kuno, H.; Takahashi, K.; Shibagaki, M.; Shimazaki, K. & Matsushita, H. *Bull. Chem. Soc. Jpn.* **1990**, *63*, 1943.

122. Kuno, H.; Shibagaki, M.; Takahashi, K. & Matsushita, H. *Bull. Chem. Soc. Jpn.* **1991**, *64*, 312.

123. Shabtai, J.; Lazar, R. & Biron, E. *J. Mol. Catal.1* **1984**, *27*, 35.

124. Creyghton, E. J.; Ganeshie, S. D.; Downing, R. S. & Bekkum, H. van *Chem. Commun.* **1995**, *0*, 1859.

125. Waal, J. C. van der; Tan, K. & Bekkum, H. van *Catal. Lett.* **1996**, *41*, 63.

126. Waal, J. van der; Creyghton, E.; Kunkeler, P.; Tan, K. & Bekkum, H. van *Top. Catal.* **1997**, *4*, 261.

127. Corma, A.; Domine, M. E.; Nemeth, L. & Valencia, S. *J. Am. Chem. Soc.* **2002**, *124*, 3194.

128. Zhu, Y.; Chuah, G. & Jaenicke, S. *J. Catal.* **2004**, *227*, 1.

129. Zhu, Y.; Chuah, G. & Jaenicke, S. *Chem. Commun.* **2003**, *0*, 2734.

130. Corma, A.; Llabrés i Xamena, F. X.; Prestipino, C.; Renz, M. & Valencia, S. *J. Phys. Chem. C* **2009**, *113*, 11306.

131. Wu, P. & Tatsumi, T. *Catal. Surv. from Asia* **2004**, *8*, 137.

132. Lv, A. *et al. Hydrothermal synthesis of MWW-type zirconosilicate* In: Gedeon, A., Massiani, P. & Babonneau, F. (Eds.) *Zeolites and Related Materials: Trends Targets and Challenges(SET)*, Elsevier B.V., 2008, 385.

133. Guo, Q. *et al. ChemSusChem* **2013**, *6*, 1352.

134. Anwander, R.; Palm, C.; Gerstberger, G.; Groeger, O. & Engelhardt, G. *Chem. Commun.* **1998**, *5*, 1811.

135. Zhu, Y.; Jaenicke, S. & Chuah, G. K. *J. Catal.* **2003**, *218*, 396.

136. Bruyn, M. de *et al. Appl. Catal. A Gen.* **2003**, *254*, 189.

Chapter 2

Objectives

2.1. General objectives

Taking into account the aforementioned background on the catalytic application of Zr-based MOFs, the **General Objective** of the present doctoral thesis is ***to contribute to the development of novel (chemo-, regio- and diastereo-)selective heterogeneous catalysts for the Meerwein-Ponndorf-Verley (MPV) reduction of ketones based on zirconium trimesate MOF-808 compounds.***

Within this general context, specific objectives of each Chapter are the following:

2.1.1. Chapter 4

- To prepare and characterize novel defect-engineered MOF-808-type compounds by a mixed-ligand approach, by combining the original tritopic trimesic acid ligands with symmetrically equivalent ditopic defective linkers (DL) lacking one carboxylate group; *viz*., isophthalic acid (H_2IPA) pyridine-3,5-dicarboxylic acid (H_2Pydc), or 5-hydroxyisophthalic acid (5-OH-H_2IPA) and 5-aminoisophthalic acid (5-NH_2-H_2IPA).

- To compare the catalytic properties of pristine and DE MOF-808 catalysts for the MPV reduction of carbonyl compounds, with respect to the archetypical zirconium terephthalate UiO-66 compound; with particular emphasis on pore structure and availability of coordinatively unsaturated Zr^{4+} sites.

2.1.2. Chapter 5

- To analyze the catalytic performance of MOF-808 for MPV reductions of various substituted cyclohexanones, with special emphasis on diastereoselectivity of the process and the comparison with other previously reported catalysts.

- To rationalize the catalytic results obtained by a combined use of kinetic analysis and theoretical calculations.

2.1.3. Chapter 6

-To evaluate the full potential of MOF-808 as a chemo-, regio- and diastereoselective catalyst for the preparation of a number of challenging hydroxysteroids of pharmaceutical interest through MPV reduction of the corresponding oxosteroid.

Chapter 3

Synthesis and characterization techniques

3.1. Synthesis

MOF synthesis was carried out under solvothermal conditions, using either a teflon-lined stainless steel autoclave or a screw-cap glass reactor and heating in an oilbath or inside an oven. MOFs are formed by crystallization from a solution to form a three-dimensional porous structure. The formation of crystals can be described in two steps. First the formation of a nucleus and second crystal growth. First, the formation of precursors takes place, such as formation of inorganic building unis and/or deprotonated linker molecules, which leads to an increase in concentration. A nucleus is formed from small clusters, which become stable upon reaching a certain size, the so called critical size (r_c), from which point on the growth of crystallites starts. Heterogeneous nucleation typically takes place from a supersaturated solution, which lies above the thermodynamical solubility (c_s), on the glass wall, impurities, seed crystals, bubbles, *etc*. Homogeneous nucleation on the contrary occurs above the critical nucleation concentration (c^*_{min}), without preferential nucleation sites. Apart from crystal growth additional OSTWALD ripening can occur, which leads to formation of larger crystals of cost of the smaller crystals (see also LAMER diagram, Figure 3.1, below). Solvothermal synthesis can be as well applied to microwave assisted synthesis. Also the modulator synthesis was applied in the synthesis of Zirconium MOFs. Further additives can be used in the synthesis of MOFs, such as organic acids and bases or even inorganic modulators. The addition of monocarboxylic acid modulators was found to increase the crystallinity of MOFs and made MOF synthesis more reproducible. The addition of modulators was also found to influence the crystal size and morphology as well as agglomeration/aggregation. The modulator compounds are competing with the polydentate ligands, by coordinating to the metal clusters or metal ions and are typically replaced during synthesis by the linker molecule of the MOF. Although in some cases the modulator can stay to some extent incorporated in the structure of the MOF. HCl as an additive can for instance slow down the hydrolysis of metal precursors (such as $ZrCl_4$) as well as the deprotonation of organic linker molecules in solution. Therefore, a number of parameters can be varied during solvothermal synthesis and different reaction conditions can be applied for MOF synthesis.[1–5]

$$\Delta G_N = \frac{4}{3}\pi r^3 \Delta G_V + 4\pi r^2 \gamma$$

Equation 3.1

$$\Delta G = \Delta H - T\Delta S$$

Equation 3.2

The GIBBS free energy of crystallization ΔG_N for spherical particles is applied in Equation 3.1. The value ΔG_N becomes negative (exergonic process) once the critical size (r_C) of the nucleus is surpassed. The thermodynamics of the process at constant pressure is also described by the GIBBS-HELMHOLTZ equation (Equation 3.2). The entropy of a solid MOF is much lower, due to a smaller number of microstates. In solution on the contrary the entropy is much higher and application of high temperature will shift the equilibrium towards the dissolved compounds.[6]

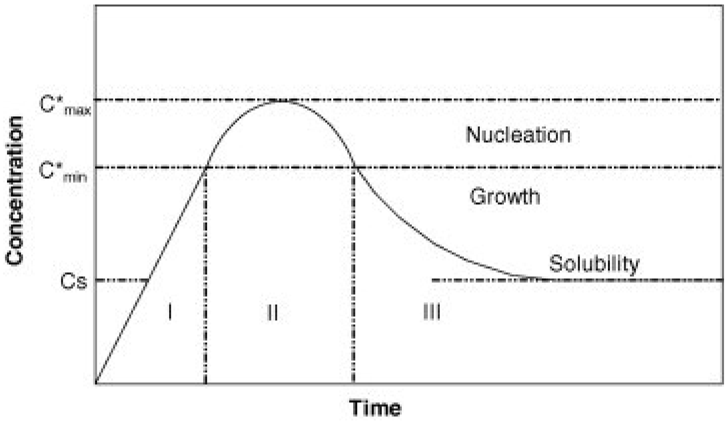

Reprinted (adapted) with permission from (*J. Am. Chem. Soc.*, **1950**, *72*, 4847–4854). Copyright (1950) American Chemical Society

Figure 3.1. LAMER diagram

3.2. X-ray powder diffraction (PXRD)

PXRD was used as a non-destructive technique for the analysis of synthesized samples. XRD allows the identification of crystalline phases and orientation of crystalline materials, their lattice parameters, strain, crystallite size and thermal expansion, which define the fingerprint of the substance. In a crystalline material, the atoms are arranged in a regular pattern. The unit cell is the smallest volume element that by repetition in three dimensions describes the crystal. The dimensions of the unit cell are described by three axes: a, b and c, as well as the angles between them: α, β and γ. The combination of these parameters results in the formation of fourteen different kinds of cells, which are covering all possible point lattices or all crystals classified by A. BRAVAIS. The fourteen BRAVAIS lattices can be represented by seven primitive lattices summarized in Table 3.1.

Table 3.1. Seven primitive lattices

System	Axial lengths and angels	Bravais lattice	Lattice symbol
Cubic	Three equal axes at right angles $a = b = c$, $\alpha = \beta = \gamma = 90°$	Simple Body-centered Face-centered	P I F
Tetragonal	Three axes at right angles, two equals $a = b \neq c$, $\alpha = \beta = \gamma = 90°$	Simple Body-centered	P I
Orthorombic	Three unequal axes at right angles $a \neq b \neq c$, $\alpha = \beta = \gamma = 90°$	Simple Body-centered Base-centered Face-centered	P I C F
Trigonal Rhombohedral	Three equal axes, equally inclined $a = b = c$, $\alpha = \beta = \gamma \neq 90°$	Simple	R
Hexagonal	Two equal coplanar axes at 120°, third axis at right angles $a = b \neq c$, $\alpha = \beta = 90°$ $\gamma = 120°$	Simple	P
Monoclinic	Three unequal axes, one pair not at right angles $a \neq b \neq c$, $\alpha \neq \gamma = 90° \neq \beta$	Simple Base-centered	P C
Triclinic	Three unequal axes, unequally inclined and none at right angles $a \neq b \neq c$, $\alpha \neq \beta \neq \gamma \neq 90°$	Simple	P

Reprinted (adapter with permission from (*X-ray Characterization of Materials* In: Lifshin, E. (Ed.) WILEY-VCH Verlag GmbH, 1999, 1). Copyright (199) WILEY-VCH Verlag GmbH

For a XRD measurement a monochromatic X-ray beam with the wavelength λ comes in contact with the sample material at a particular angle. Diffraction (constructive interference) is only produced when the distance traveled by the rays reflected from successive planes differs by a complete number of wavelengths. As shown in Figure 3.2, the diffracted angle from the family of crystallographic planes (*hkl*) has a value of 2θ, which is employed to determine the distance between layers of atoms in a sample using the BRAGG'S law (Equation 3.3).

$$n\lambda = 2d_{hkl}sin\theta \qquad \textbf{Equation 3.3}$$

Where d is the *hkl* interplanar spacing (nm), θ is the angle of incidence of X-rays (rad), λ is the wavelength of X-rays and n is an integer representing the reflection order.

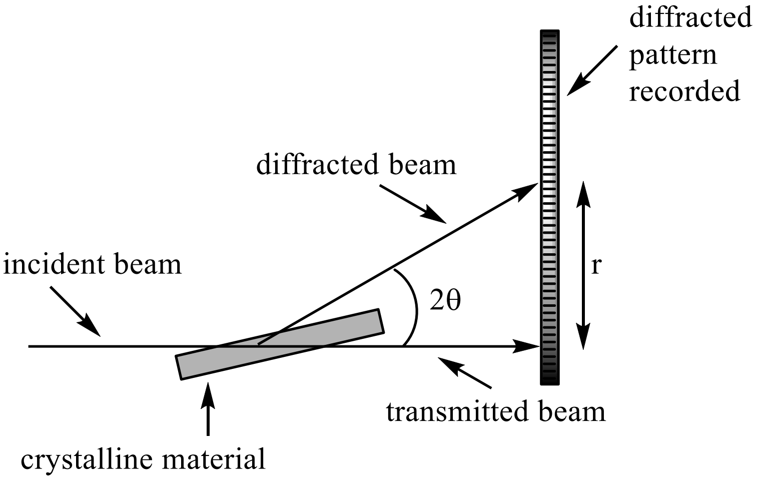

Figure 3.2. Schematic representation of a setup for the collection of a XRD pattern

By combining the BRAGG condition with the plane spacing for a system, it is feasible to directly obtain the positions of atoms in the unit cell. For example, for a cubic system the diffraction peaks satisfy the following Equation 3.4.[7]

$$\frac{sin^2\theta}{h^2+k^2+l^2}=\frac{\lambda^2}{4a^2}$$ **Equation 3.4**

Where a is the cell parameter and *h*, *k* and *l* the MILLER indices defining the plane.

XRD measurements of synthesized samples presented in this thesis were performed with a PANALYTICAL Cubix'Pro diffractometer equipped with an X'Celerator detector and automatic divergence and reception slits using Cu-Kα radiation (0.154056 nm). Measurements were carried out at angles $5 \leq 2\theta \leq 90°$.

3.3. Infrared (IR) analysis

IR spectra shown in this thesis were recorded with a THERMO FISCHER SCIENTIFIC, type NICOLET 8700 FT-IR in reflectance mode using a DTGS detector and acquiring at 4 cm^{-1} resolution. The measurements were performed in a spectral range of 400 to 4000 cm^{-1} using a mid IR-source. 32 scans were recorded for each spectrum.

Adsorption of probe molecules on the surface of materials can be used to identify the type of active sites (such as acid and base sites) on materials. The strength of adsorption can further give information about the strength of active sites, which results in a shift of IR bands recorded during adsorption. Some examples of used probe molecules are CO, NO, ammonia, pyridine or CO_2. The removal of probe molecules through thermal treatment can further elucidate how strong a certain molecule is bound to a certain active side of the material. Adsorption of probe molecules can also give information about chemical (electronic) surface properties of the material.

CO adsorption was conducted on MOF-808 and DE MOF-808-Pydc. The samples were measured in form of a pellet. Samples were further activated under vacuum with heating at 423 K for 1.5 h. At a pressure of around 10^{-5} bar samples were cooled to around 104 K and CO was added in small doses to the samples. IR spectra were recorded after each addition of CO. The background was removed prior to the CO adsorption measurements. At the end of CO addition samples were evacuated first at dynamic vacuum, followed by high vacuum using a turbomolecular pump and the process was followed by collection of IR spectra.

The dehydration of MOF-808 was followed by IR measurements. The sample was measured as a pellet as in the previous cases. The sample was measured under vacuum using a turbomolecular pump. The background was removed from measured samples and IR spectra were further collected at ambient temperature, 373 K, 423 K, 473 K, 573 K and 673 K holding each temperature for 45 min.

3.4. N_2-adsorption/desorption experiments

N_2-adsorption/desorption isotherms were collected on a Micromeritics Gemini V gas adsorption analyzer at 77 K, after degassing the samples at 393-423 K overnight in a Micromeritics Flow prep 060 system with nitrogen flux gas. The surface areas were calculated from the adsorption branch of the isotherm according to the BET method (Equation 3.5).[8] Following equation is typically used for determining the BET surface area.

$$\frac{1}{W\left(\left(\frac{P_0}{P}\right)-1\right)} = \frac{1}{W_m C} + \frac{C-1}{w_m C}\left(\frac{P}{P_0}\right) \qquad \textbf{Equation 3.5}$$

Where W is the weight of gas adsorbed at a relative pressure P/P_0 and W_m is the weight of the adsorbate constituting a monolayer of surface coverage. The term C is related to the energy of adsorption in the first adsorbed layer and its value shows the magnitude of the adsorbent/adsorbate interactions. The method is usually used for nonporous, micro- and mesoporous materials. Compared to materials with big mesopores, it is more difficult to distinguish between sorption on the surface and pore filling by condensation in microporous materials. The negative C value in the measurements indicates that the method induces a certain error and the use of a method suggested recently by Rouquerol *et al.*[9] or a direct method suggested by Lange *et. al.,*[10] to avoid negative C values might give more reliable surface areas, as shown for other microporous materials already. All samples were further measured in powder form. The micropore volume was derived from the t-plot of the N_2-sorption experiments. The pore size distribution was calculated from the Dubinin-Stoeckli equation.[11]

3.5. Thermogravimetric analysis (TGA)

Chemical and thermal stability of materials can be studied by TG technique, which is commonly used to investigate decomposition, dehydration, oxidation/reduction reactions, reaction pathways, kinetics of reactions and the quantity of specific component that occurs accompanied by a mass change. The TG device registers the mass change undergone by the sample as a function of temperature, time and atmosphere. Experiments can be conducted in a specific atmosphere, such as reducing, oxidizing or inert atmosphere. When combined with differential thermal analysis (DTA), exothermic or endothermic processes can be recorded, that enclose transformations in the material when compared with an inert reference material. DTA is mainly used for studying transitions, chemical reactions, adsorption, crystallization, melting and sublimation. In addition it is possible to measure the heat of reaction and to determine kinetic parameters.

In the current study, TGA experiments were mainly used to study the stability (removal of linker molecules) and composition (such as linker to metal ratio) of MOF materials. Further TGA can be an indicator of porosity by removal of adsorbed guest molecules at comparable low temperatures. Experiments were usually conducted in an air flow and with thermal heating at 10 $Kmin^{-1}$ until complete decomposition of materials. TGA was performed using a METTLER TOLEDO TGA/SDATA851e thermo balance under air from room temperature to 1073 K and a heating rate of 10 $Kmin^{-1}$.

3.6. Nuclear magnetic resonance spectroscopy (NMR) analysis

In NMR spectroscopy a probe molecule is exposed to an external magnetic field. A NMR signal is produced through excitation of nuclei into nuclear magnetic resonance, which is detected by sensitive radio receivers. The resonance frequency is characteristic to the intramolecular magnetic field around an atom, which allows to gain information about the electronic structure and individual functional groups of a molecule. As a nucleus can interact with neighboring nuclei (J-coupling or scalar coupling) a signal can split up into a n+1 multiplet (n = number of equivalent nuclei; spin = 1/2). The intensities of the multiplet peaks follow the PASCAL'S triangle. Coupling is usually observed between nuclei distances up to three bonds. Further, coupling to chemically equivalent nuclei leads to no change in NMR signal. The coupling constant is the distance between two neighboring signals in a multiplet and is measured in Hertz (Hz). NMR is used for paramagnetic nuclei. ^{1}H is the most commonly used nucleus for NMR measurements but it can be also applied to for instance: ^{13}C, ^{15}N or ^{31}P nuclei. Liquid NMR was used for the characterization of organic molecules. ^{1}H and ^{13}C NMR were recorded on a BRUKER 300 spectrometer and the chemical shifts are reported in ppm relative to residual proton solvents signals. Data for ^{1}H NMR spectra are reported as follows: chemical shift (δ, ppm); multiplicity (s = singlet, d = doublet, t = triplet, q = quartet, m = multiplet, dd = double doublets); coupling constant and integration. Data for ^{13}C NMR spectra are reported in chemical shift (δ, ppm) (Equation 3.6). Determination of CH_x groups was done by distorsionless enhancement by polarization transfer (DEPT) measurements (135°/90°).

$$\Delta\nu = J = \Delta\delta * \nu_0$$ **Equation 3.6**

Where ν_0 is the frequency of the NMR spectrometer.

For the reduction steroids, the crude product was dissolved in DMSO-d_6 and analyzed by ^{1}H-NMR. Parent MOF-808 and DE MOF-808-x materials (10 mg) were first dissolved in D_2SO_4 (0.1 mL) for liquid NMR. To dissolved samples, DMSO-d_6 (0.6 mL) was added and the samples were analyzed by ^{1}H-NMR.

3.7. Gas Chromatography (GC)

GC analysis was carried out on a VARIAN CP-3800 equipped with a Flame Ionization Detector (FID) and a DB-WAX (15 m x 0.32 mm x 0.25 µm) column, on an AGILENT 7890A equipped with a FID and with a DB5 (30 m x 0.25 mm x 0.25 µm) column and on a VARIAN 3900 equipped with a FID and with a HP5 (30 m x 0.25 mm x 0.25 µm) column.

Taking into account that the ionization detectors give a signal proportional to the mass product analyzed through the chromatographic area, the use of corrected areas using response factors of each analyte, allows the concentration calculation of each component in the mixture (Equation 3.7).

$$n_i = \frac{A_i * n_{S_i}}{A_{S_i * R_i}}$$ **Equation 3.7**

Where n_i is the mols of the i compound

A_i is the chromatographic area of the i compound

n_{S_i} is the mols of the internal standard

A_{S_i} is the chromatographic area of the internal standard

R_i is the response factor of the i compound

Thus, knowing the number of initial mols of the reagent ($n_{r,0}$) and the mols of this substrate at a determined time ($n_{r,t}$), the conversion at this time is determined by the following equation.

$$\text{Conv}_t(\%) = \frac{n_{r,0} - n_{r,t}}{n_{r,0}} * 100$$ **Equation 3.8**

$$\text{Yield}_{i,t}(\%) = \frac{n_{sit}}{n_{r,0}} * 100, \quad \text{Selec}_{i,t}(\%) = \frac{n_{sit}}{n_{r,0}-n_{r,t}} * 100$$ **Equation 3.9 & 3.10**

Where n_{sit} is the number of mols a compound in a time a.

3.7.1. Gas chromatography coupled with mass spectrometry (GC-MS)

GC-MS was carried out on an AGILENT 6890N equipped with an AGILENT 5973 Network, Mass Selective Detector and with a HP5 (30 m x 0.25 mm x 0.25 µm) ultra-inert column.

3.8. Scanning electron microscopy (SEM)

SEM allows for high-resolution imaging of surfaces by using high-energy electrons (1.5-20 KeV) generated by a heated tungsten filament. SEM has a magnification about six orders of magnitude and great depth of field. For that purpose, an incident beam of monochromatic electrons causes a secondary emission across the sample surface, which is collected to form an image of the surface. Quality and contrast obtained in the image depends mainly on the conductivity and surface topography of the sample. By detecting different emissions of the sample, it is possible to obtain diverse contrast images, *i.e.*, backscattered electrons (BSE), Auger electrons and Energy dispersive x-ray spectroscopy (EDS). BSE causes different contrast subjected to the atomic number, Z, of the elements, so changes in composition of the volume analyzed. It is performed in conjunction with a SEM, but uses the X-rays that are emitted from the sample due to the electron beam. The combination of SEM with EDS allows the analysis of the sample morphology and the composition of the different phases that are present. The minimum detection limits are about 0.1 weight percent, depending on the element and the matrix.

Conducting materials that allow the transport of the incident beam electrons do not need any handling of the sample. However, for poor conductors or insulators a conducting layer that does not modify the topography needs to be added. This is achieved by coating the sample in vacuum with Au or graphite (for EDS) using a sputter coater.

SEM measurements were conducted on a JEOL JSM 5400. EDX microanalyses were carried out with a detector from OXFORD INSTRUMENTS. FESEM measurements were conducted on a ZEISS Ultra55. FESEM works at lower potentials (0.02-5 kV). For the generation of electrons a field emission gun is used, which leads to a better signal-to-noise ratio and spatial resolution.

3.9. Catalytic reactions

Catalytic reactions were performed in a reinforced glass reactor made at the Instituto de Tecnología Química (ITQ). The reactor is composed of a conical vial made of reinforced glass. The reactor is closed by a screw cap or a manometer and is equipped with a stirring bar. The reactor can be heated in a silicon bath or a metal block on a magnetic stirring plate. Detailed procedures used in each case are also provided in the corresponding section of Chapter 8. Annexes.

3.10. References

1. Schaate, A. *et al. Chem. Eur. J.* **2011**, *17*, 6643.
2. Diring, S.; Furukawa, S.; Takashima, Y.; Tsuruoka, T. & Kitagawa, S. *Chem. Mater.* **2010**, *22*, 4531.
3. Tsuruoka, T. *et al. Angew. Chem. Int. Ed.* **2009**, *48*, 4739.
4. Park, J.; Wang, Z. U.; Sun, L. B.; Chen, Y. P. & Zhou, H. C. *J. Am. Chem. Soc.* **2012**, *134*, 20110.
5. Yang, Q. *et al. Chem. Eur. J.* **2011**, *17*, 8882.
6. Stock, N.; Reinsch, H. & Schilling, L. *CHAPTER 2 Synthesis of MOFs* In: Llabrés i Xamena, F. & Gascon, J. (Eds.) *Metal Organic Frameworks as Heterogeneous Catalysts*, The Royal Society of Chemistry, Cambridge, 2013, 9.
7. *X-ray Characterization of Materials* In: Lifshin, E. (Ed.) WILEY-VCH Verlag GmbH, 1999, 1.
8. Brunauer, S.; Emmett, P. H. & Teller, E. *J. Am. Chem. Soc.* **1938**, *60*, 309.
9. Rouquerol, J.; Llewellyn, P. & Rouquerol, F. *Is the BET equation applicable to microporous adsorbents?* In: Llewellyn, P., Rodriguez-Reinoso, F., Rouquerol, J. & Seaton, N. (Eds.) *Characterization of Porous Solids VII",Studies in Surface Science and Catalysis, V 160*, Elsevier, Amsterdam and Oxford, 2007, 49.
10. Lange, M. F. de; Vlugt, T. J. H.; Gascon, J. & Kapteijn, F. *Microporous Mesoporous Mater.* **2014**, *200*, 199.
11. Dubinin, M. M.; Polyakov, N. . & Kataeva, L. *Carbon N. Y.* **1991**, *29*, 481.

Chapter 4

Catalytic properties of pristine and DE MOF-808 materials

4.1. Introduction

As mentioned earlier, MOFs feature some properties which make them ideal candidates for heterogeneous catalysis. The crystalline 3-dimensional structure leads to high porosity and large surface areas and creates well defined catalytic sites within the structure. Metal-organic frameworks can be prepared with a large number of different metals. The chemical environment around the metal center can be further tuned by for instance introducing functional groups on the organic linker molecules. Isoreticular synthesis and post synthesis modification allow also incorporation of additional functionalities and active sites. The pore size and shape can be tailored by the choice of organic linker as for instance in case of expanded structures using elongated linker molecules. In other crystalline porous solids, the number of building units is rather limited, such as [SiO_4] and [AlO_4] tetrahedral units, found in zeolites or [AlO_4] and [PO_4] units in aluminophosphates. In sharp contrast, the connectivity of secondary bulding units (inorganic bricks) and organic ligands used in MOF synthesis is much richer, and so are the possible architectures that can be constructed from them.[1]

Zr-containing MOFs attracted especially interest due to their high chemical and thermal stability, which was rarely found within MOFs before the discovering of UiO-66.[2] Since then, a lot of effort has been made to further expand the family of Zr-MOFs, which led to the formation of modified and different structures containing Zr-SBUs. Although UiO-66 can be readily used in a number of reactions as catalyst showing remarkable activity, it has some limitations. On the one hand, the rather small size of pores and pore openings limit the applicability to small substrates. On the other hand, the fully coordinated Zr_6-cluster leads to its dependency on defects as active sites for catalysis. According to this, different strategies have been used to create defects within UiO-66 to increase its catalytic activity and applicability. Further, effort has been made to create new structures with more open frameworks and lower connectivity on the Zr_6-cluster to improve the catalytic activity of Zr-MOFs. A large number of Zr-MOFs has been prepared so far, such as NU-1000,[3] PCN-222,[4] PCN-700,[5] DUT-51[6] or PIZOFs.[7] However, the syntheses of these wider, low-connected Zr-MOFs often require expensive linkers or additional steps due to preparation of non-commercial linkers, which also elevates the cost of these materials. MOF-808, using cheap and readily available trimesate ligands, is a clear exception.

Among the various strategies used to increase the number of defects (and thus, the amount of potential catalytic sites), in the case of copper HKUST-1 and its Ru-analogue, a mixed linker approach was used. The idea consists in introducing different defective linkers having the same geometry as the pristine trimesate (BTC) linker but otherwise lacking one (or more) carboxylate groups connecting to the Cu and Ru paddlewheel units. The defective linkers create totally new properties that are not present in pristine materials. In some cases the formation of mesopores is observed and additional defects on the SBU lead to improved catalytic activity, which was shown in different reactions such as the hydroxylation of toluene,[8] olefin hydrogenation,[9] ethylene dimerization and PAAL-KNORR reaction.[10] A similar strategy has not been applied so far to the controlled synthesis of defect engineered MOF-808 (hereafter DE MOF-808).

The MEERWEIN-PONNDORF-VERLEY reduction is known since 1925[11–13] for the reduction of aldehydes and ketones to the corresponding primary or secondary alcohols, respectively. It is of particular interest due to its high chemoselectivity, where reducible groups, such as alkenes, alkynes, halogens, nitriles or alkoxy groups are being tolerated. Compared to other reducing methods, the MPV reduction proceeds under mild reaction conditions and avoids the use of precious metals and the use of molecular hydrogen and high pressures. Commonly used catalysts for this reaction are for instance aluminium or zirconium alkoxides. The drawback of such catalysts is, that they are used under homogeneous conditions and that an excess amount of catalyst has to be applied.[14] Heterogeneous systems have been developed as well, as for instance magnesium oxide[15], phosphates,[16] hydrous zirconium oxide,[14] zeolites,[17–21] mesoporous materials[22] or grafted alkoxides.[23]

In this chapter, the use of MOF-808 as an efficient catalyst in the MPV reduction of carbonyl compounds will be discussed. MOF-808 will be compared with other Zr-containing catalysts, such as UiO-66[24] and DUT-67, featuring a different connectivity at the Zr_6-clusters. The advantage of MOF-808 having a large pore system and a high number of open metal sites will be described. A number of DE MOF-808-x materials will be compared, where small amounts of BTC linker of parent MOF-808 are replaced by defective linker molecules, such as IPA, Pydc, 5-OH-IPA or 5-NH_2-IPA. The effect of defective linker molecules on the materials catalytic properties will be shown.

4.2. MPV reduction of cyclohexanone (CH)

The catalytic activity of pristine MOF-808 and DE MOF-808-x materials was evaluated for the MPV reduction of carbonyl compounds. As a first example the reduction of cyclohexanone (CH) to cyclohexanol (CHol) was conducted (see Scheme 4.1) and the results were compared with other Zr-MOFs, namely UiO-66 and DUT-67. Detailed reaction conditions are given in the Annexes (Section 8.2). For the MPV reduction, ^{i}PrOH was used as both solvent and reducing agent. The high excess of reducing agent

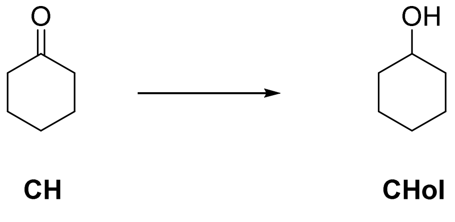

Scheme 4.1. MPV reduction of CH to corresponding alcohol CHol

also shifts the equilibrium towards the alcohol formation as all steps in the reaction cycle are reversible. The back reaction is known as the OPPENAUER-oxidation, which leads to the MEERWEIN-PONNDORF-VERLEY-OPPENAUER (MPVO) redox equilibrium. The adapted mechanism for the reaction of CH on a Zr-MOF is shown in Scheme 4.2.

It is generally accepted, that the reaction occurs through adsorption and deprotonation of the alcohol and subsequent adsorption of the carbonyl compound on a LEWIS acid site, which is provided by the zirconium open metal sites of the MOF. Adsorbed compounds form a six-membered cyclic TS, from which a hydride shift from the alcoholate towards the carbonyl carbon atom occurs. Desorption of the keton is followed by protonation of the alkoxide, leading to product formation, which is finally desorpted as shown in Scheme 4.2 for CH with ^{i}PrOH as reducing agent. The reaction mechanism is also in contrast to the stepwise transfer hydrogenation on for instance Ru and Ir catalysts, where a metal-hydride species is formed through β-hydride elimination of alcohols.

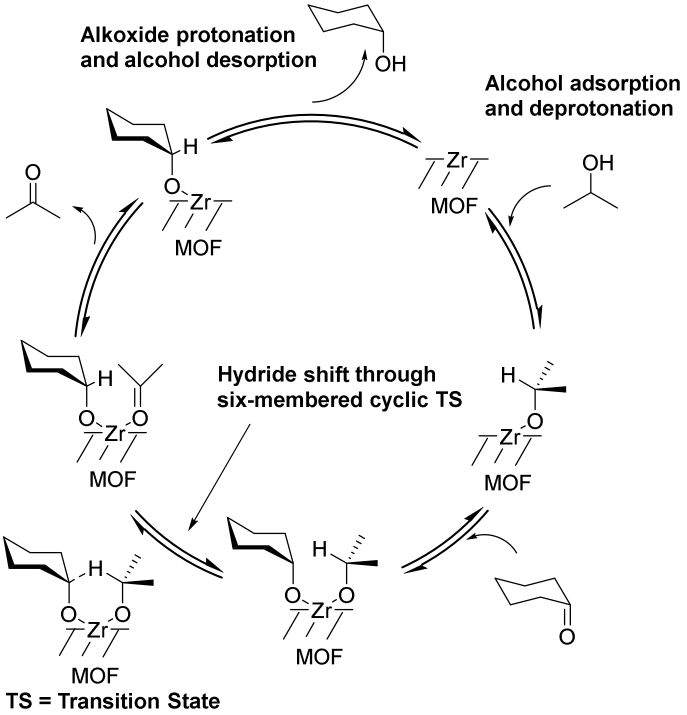
Alkoxide protonation
and alcohol desorption
OH
Alcohol adsorption
and deprotonation
H
O
Zr
MOF
OH
O
Hydride shift through
six-membered cyclic TS
TS = Transition State

Scheme 4.2. Reaction cycle for the MPV reduction of CH on a Zr-MOF

4.3. DE MOF-808-x materials

Pristine and DE MOF-808-x materials, as well as UiO-66 and DUT-67 materials used for comparison, were prepared as described in the Annexes (Section 8.2). DE MOF-808-

x materials were synthesized by replacing 10 mol% of H_3BTC by defective linker molecules (isophthalic acid (H_2IPA), pyridine-3,5-dicarboxylic acid (H_2Pydc), 5-hydroxyisophthalic acid (5-OH-H_2IPA) or 5-aminoisophthalic acid (5-NH_2-H_2IPA) for MOF-808-IPA, MOF-808-Pydc, MOF-808-OH and MOF-808-NH_2, respectively (see Figure 4.2 below).

PXRD was used to determine the crystalline structure and phase purity of materials. From the XRD patterns it is observed, that after incorporation of small amounts of defective linker molecules, the overall structure of the materials is well maintained. No additional phases were formed during any step of catalyst preparation. Therefore, the typical XRD pattern known for pristine MOF-808 is observed, indicating that DE MOF-808-x materials are structural analogous to MOF-808 (see Figure 4.1).

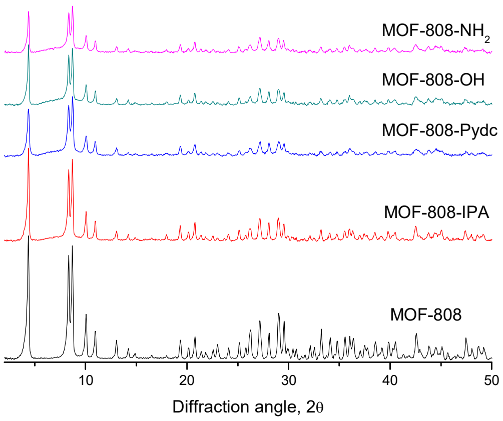

Reprinted (adapted) with permission from (*Catal. Sci. Technol.* **2018**, *8*, 3610-3616). Copyright (2018) The Royal Society of Chemistry

Figure 4.1. PXRD pattern of pristine MOF-808 and DE MOF-808-x materials

The structure of MOF-808 is described already in the literature in detail.[25,26] The incorporation of defective linker molecules creates defects on the Zr_6-cluster, due to one missing coordination group of defective linker molecules compared to the BTC linker. The exact nature of these defects cannot be revealed at this point and further research would be necessary for more detailed information. Defective linkers are missing one negative charge from the absence of one coordinating group. It can be assumed that charge neutrality is achieved by either deprotonation on the Zr_6-cluster, coordination of additional anions, such as –OH/H_2O pairs or partial reduction on the Zr_6-cluster (SBU) as observed in DE Ru-MOFs[9,10] and DE Cu-MOFs.[27,28] From ^{1}H-NMR analysis of digested samples, it was observed that all formate ions used as modulator ligand during MOF synthesis are removed from the Zr_6-cluster. Thus, it can be assumed that the materials were fully activated and Zr^{4+} (*cus*) metal sites are coordinated by –OH/H_2O pairs. Only in some cases small traces of formate ions still present on the Zr_6-cluster were observed in the ^{1}H-NMR spectra of few samples, though these solids were never used in the ensuing catalytic studies. The ^{1}H-NMR of digested samples was further used to determine the quantities of defective linkers present in DE MOF-808-x materials (see Table 4.1).

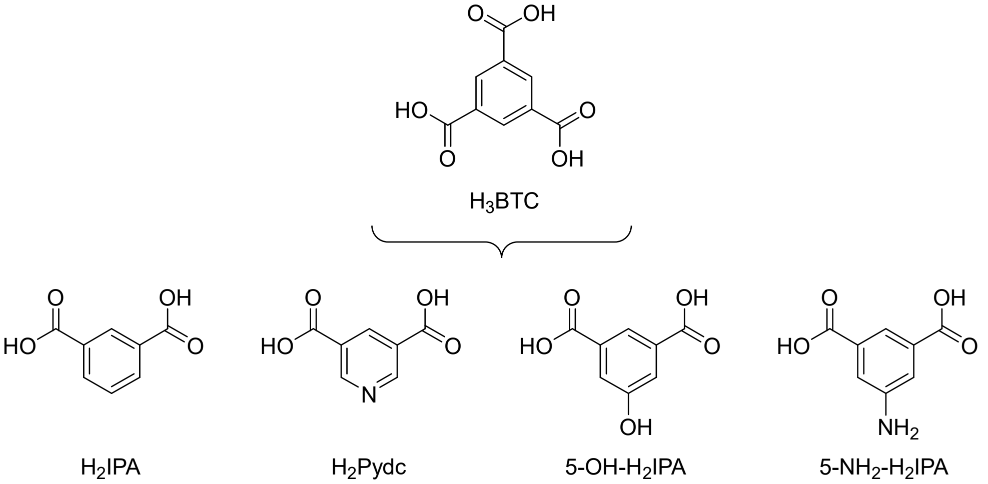

Figure 4.2. Combination of H_3BTC with various ditopic linkers (H_2IPA, H_2Pydc, 5-OH-H_2IPA and 5-NH_2-H_2IPA) for the preparation of DE MOF-808-x materials

Table 4.1. Incorporation of defective linkers in DE MOF-808-x materials as determined from ^{1}H-NMR

Sample	% Defective linker
MOF-808-IPA	3%
MOF-808-Pydc	~2%
MOF-808-OH	7%
MOF-808-NH_2	4%

Reprinted (adapted) with permission from (*Catal. Sci. Technol.* **2018**, *8*, 3610-3616).Copyright (2018) The Royal Society of Chemistry

4.3.1. Catalytic results for the MPV reduction of CH using pristine and DE MOF-808 materials

For MOF-808 a distinct increase in catalytic activity was observed compared to a defective UiO-66 sample for the MPV reduction of CH using ^{i}PrOH as hydrogen source. Thus, the amount of CH converted after 1 h was 12% in the case of UiO-66 and 69% in

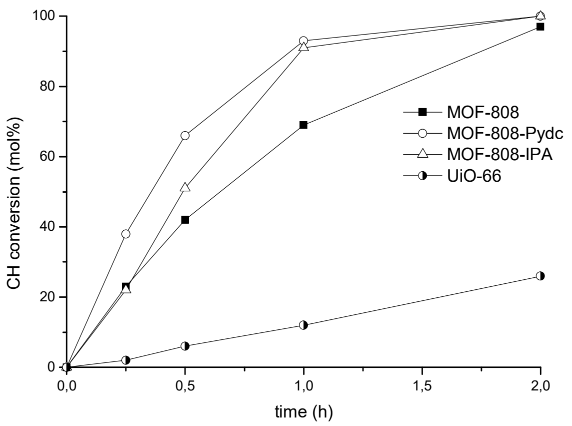

Reprinted (adapted) with permission from (*Catal. Sci. Technol.* **2018**, *8*, 3610-3616).Copyright (2018) The Royal Society of Chemistry

Figure 4.3. CH conversion plot for the MPV reduction of CH using different Zr-MOFs

Table 4.2. Comparison of different Zr-MOFs for the MPV reduction of CH at specified reaction times

Entry	Catalyst	Time (h)	Conversion (mol%)
1	UiO-66	1	12
2		24	>99
3	MOF-808	1	69
4		2	97
5	MOF-808-IPA	1	91
6		2	>99
7	MOF-808-Pydc	1	93
8		2	>99

Reprinted (adapted) with permission from (*Catal. Sci. Technol.* **2018**, *8*, 3610-3616). Copyright (2018) The Royal Society of Chemistry

MOF-808. The selectivity towards CHol was in all cases >99%. MOF-808 reached full conversion after 6 h and for UiO-66 full conversion was obtained after 24 h. For DE samples, a further increase in activity was found, attaining 91% and 93% CH conversion after 1 h for MOF-808-IPA and MOF-808-Pydc, respectively, while both materials afforded full CH conversion after only 2 h (see Table 4.2 and Figure 4.3).

In the case of pristine MOF-808, the increase in catalytic activity can be assigned to the high number of open metal sites on the Zr_6-cluster of MOF-808. As only six BTC linker molecules are coordinating to the SBU of MOF-808, every Zr atom is available for catalysis. In the case of UiO-66 on the contrary, the SBU is fully coordinated by twelve BDC linker molecules and open metal sites are depending on missing linker defects, which are much less abundant. The amount of missing linkers on UiO-66 was calculated from the TGA analysis (metal/linker ratio) following a method proposed by VALENZANO *et al.*[29] and was estimated to be *ca.* 7%. This means that only 14% of the total Zr^{4+} ions are accessible (each missing linker molecule creates two *cus* Zr^{4+} sites.[30]

Note also CH is small enough to pass through the triangular windows of UiO-66, as shown in Figure 4.4. Therefore, the lower catalytic activity observed for UiO-66 is not attributed to diffusion problems, since all Zr^{4+} sites located at both internal and external surfaces of UiO-66 are accessible and are all expected to contribute to the catalytic reaction. Differences in particle size are not expected to have a large impact, since all the materials tested have similar particle size, according to the SEM images (see Annexes, Section 8.2). Therefore, the higher activity of MOF-808 with respect to UiO-66 has been attributed (mainly) to a different amount of *cus* Zr^{4+} sites.

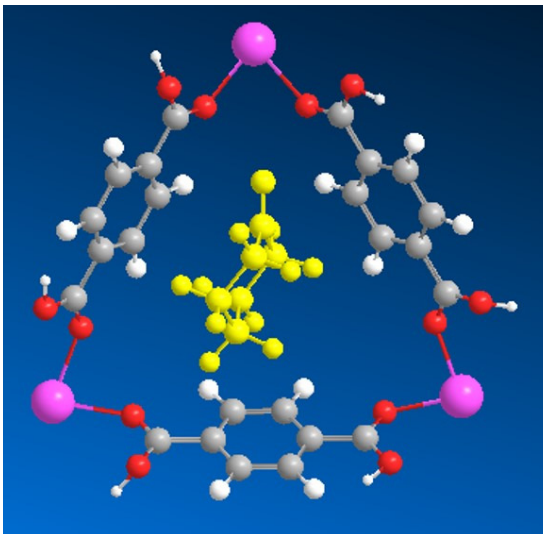

Reprinted (adapted) with permission from (*Catal. Sci. Technol.* **2018**, *8*, 3610-3616): Copyright (2018) The Rpyal Society of Chemistry

Figure 4.4. Dimensions of CH relative to the pore openings of UiO-66. The CH molecule (in yellow) is placed at the center of the triangular window of the Zr-MOF. All the atoms of the MOF have been fixed at the crystallographic positions and the CH molecule has been optimized with the MM2 force field as implemented in Chem3D Pro 12.0. Color code: C, grey; O, red; H, white; Zr, pink

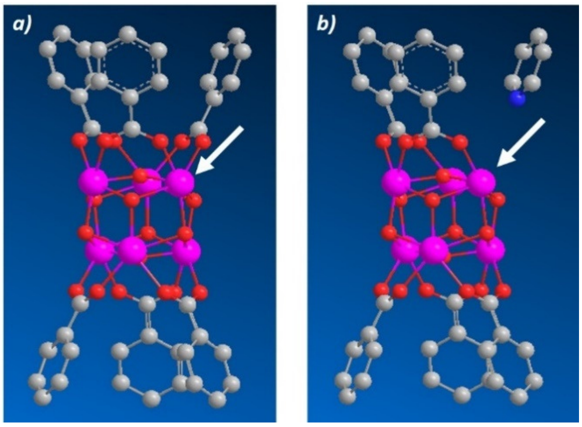

Reprinted (adapted) with permission from (*Catal. Sci. Technol.* **2018**, *8*, 3610-3616). Copyright (2018) The Royal Society of Chemistry

Figure 4.5. Comparison of Zr_6-oxoaggregates in a) pristine MOF-808 and b) MOF-808-Pydc, evidencing the less sterically crowded environment of the Zr^{4+} ions (indicated with a white arrow) in the latter materials. Color code: C, grey; O, red; Zr, pink. H atoms are omitted for clarity

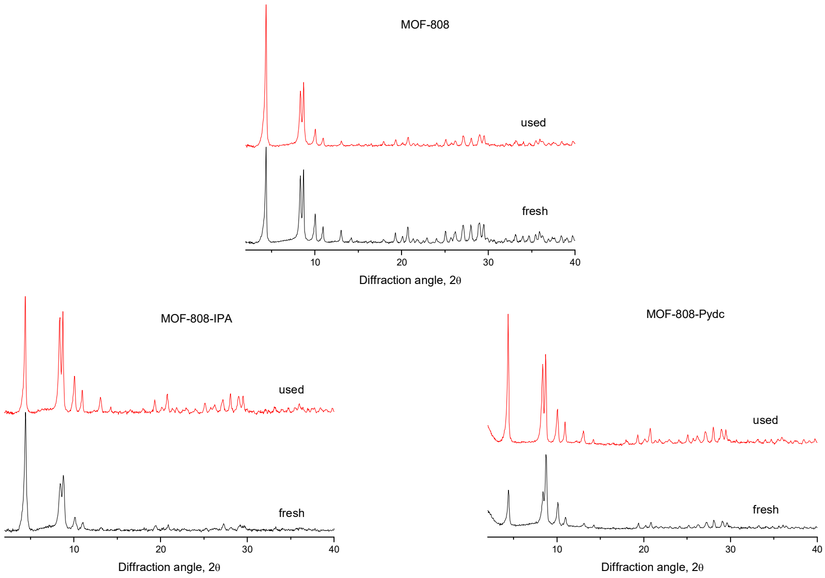

Reprinted (adapted) with permission from (*Catal. Sci. Technol.* **2018**, *8*, 3610-3616). Copyright (2018) The Royal Society of Chemistry

Figure 4.6. Comparison of the catalyst before and after reaction by PXRD analysis

For MOF-808-IPA and MOF-808-Pydc the increase in catalytic activity is induced by the introduction of defective linker molecules, which leak one coordination site if compared to BTC linker in pristine MOF-808. The missing coordination site leaves less crowded metal sites on the Zr_6-cluster (Figure 4.5), which facilitate the formation of the TS (see also Scheme 4.1).

In order to assess the stability of MOF-808 and DE MOF-808-x materials under reaction conditions, the crystallinity of materials (MOF-808, MOF-808-IPA and MOF-808-Pydc) was also analyzed after reaction. From the PXRD pattern (Figure 4.6) it can be seen that all three materials were stable under the reaction conditions and fully retained their crystallinity. Consequently, no significant decrease in catalytic activity was observed upon reuse of the materials for at least four consecutive cycles.

Unlike MOF-808-IPA and MOF-808-Pydc, the other two DE MOF-808 compounds prepared, DE MOF-808-OH and MOF-808-NH_2, showed no significant differences with respect to pristine MOF-808 for the MPV reduction of CH, as seen in Figure 4.7. This is probably due to the steric effect on the Zr^{4+} ions introduced by the amino and hydroxyl groups in position 5 of the linker, similar to the one found in pristine MOF-808.

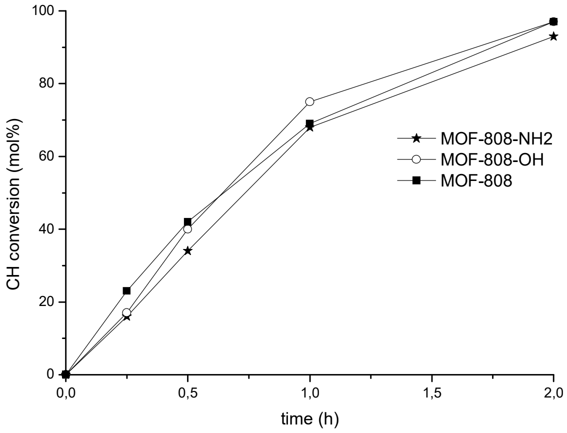

Reprinted (adapted) with permission from (*Catal. Sci. Technol.* **2018**, *8*, 3610-3616). Copyright (2018) The Royal Society of Chemistry

Figure 4.7. Comparison of DE MOF-808-OH and MOF-808-NH_2 materials with pristine MOF-808 for the MPV reduction of CH

To further investigate in the effect of open metal sites on the Zr_6-cluster on the catalytic activity, DUT-67 was tested in the MPV reduction of CH. DUT-67 consists of similar Zr_6-cluster as UiO-66 and MOF-808 but has a **reo** topology, where the SBUs are eight connected. Thus, featuring four open metal sites per inorganic SBU available for catalysis. The catalytic activity of DUT-67 was compared with UiO-66 and MOF-808 as shown in Figure 4.8.

From the catalytic results it is observed that the catalytic activity increases with an increasing number of open metal sites available on the SBU of the MOF. MOF-808 (6-conneced) > DUT-67 (8-connected) > UiO-66 (12-connected, with *ca.* 7% missing linker defects). As the Zr metal sites are the active sites for the MPV reduction, such a trend is expected.

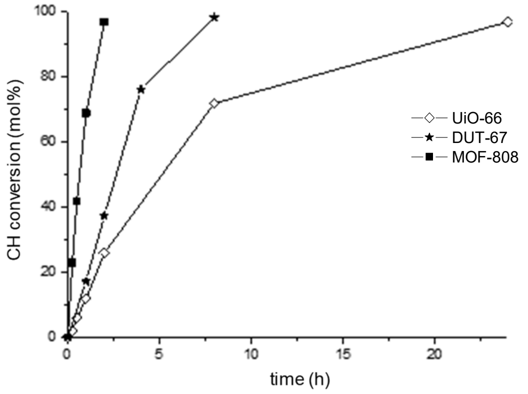

Reprinted (adapted) with permission from (*Catal. Sci. Technol.* **2018**, *8*, 3610-3616). Copyright (2018) The Royal Society of Chemistry

Figure 4.8. Comparison of different Zr-MOFs with different connectivity on the Zr_6-cluster for the MPV reduction of CH

4.3.2. Catalytic results for the MPV reduction of estrone (E1)

The catalytic activity of pristine MOF-808 and MOF-808-Pydc was further tested in the reduction of estrone (E1) to estradiol (E2) and compared with UiO-66. Reaction conditions are given in the Annexes (Section 8.2).

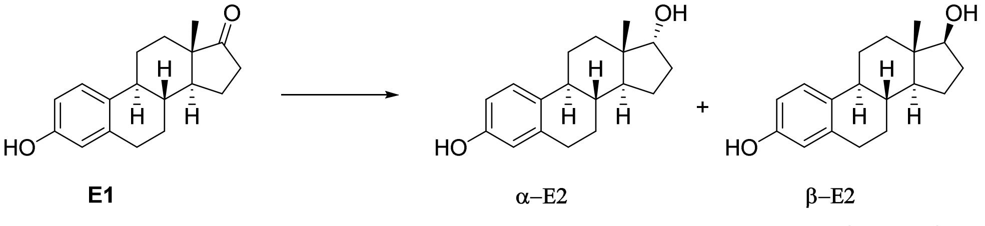

Scheme 4.3. MPV reduction of E1 to diastereoisomers α-E2 (17α-estradiol) and β-E2 (17β-estradiol)

As commented above, a second advantage of MOF-808 compared to UiO-66 is the more open framework. The adamantane-shaped pores in MOF-808 have an internal pore and aperture diameter of 18.4 and 14 Å, respectively, which is significantly bigger than in the case of UiO-66, with triangular windows of ~5-7 Å and tetrahedral and octahedral pores of 8 and 11 Å, respectively. As most of the active sites are located at the internal surface area, the pore openings become a restricting factor for bulkier substrates such as E1. The dimensions of E1 are shown in Figure 4.9.

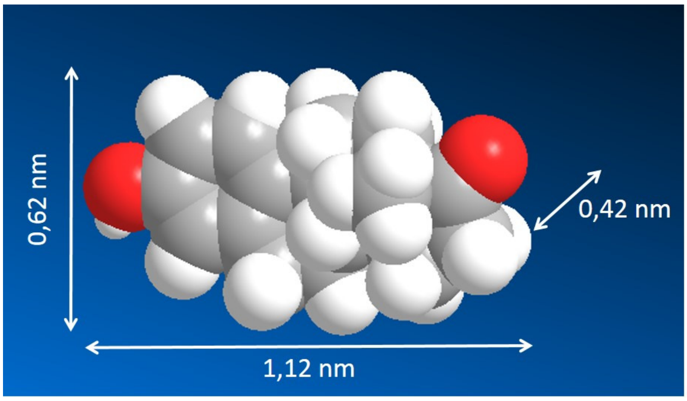

Reprinted (adapted) with permission from (*Catal. Sci. Technol.* **2018**, *8*, 3610-3616). Copyright (2018) The Royal Society of Chemistry

Figure 4.9. Approximate dimensions of E1, as obtained from the optimized structure using MOPAC2016

As expected from the dimensions of E1 relative to the pore opening of the material, UiO-66 shows almost no catalytic activity in the MPV reduction of E1, with a conversion of only 2% after 48 hours. As UiO-66 was shown to be active in the reduction of CH, the low activity is mostly assigned to diffusion limitations, which leaves most of the active sites inaccessible for the substrate. Larger dimensions of the molecule prevent crossing the rather small triangular windows and make the active sites located at the internal surface area inaccessible. Therefore, reactions can only occur on the external surface of particles. In sharp contrast with this lack of activity, when both pristine MOF-808 and MOF-808-Pydc were used, E1 conversion increased to 87% and 91% after 24 hours, respectively. An increase in catalytic activity was also observed for MOF-808-Pydc when comparing the conversion at four hours, with 24% and 61% for pristine MOF-808 and MOF-808-Pydc, respectively (see Table 4.3)

The diastereomeric ratio (d.r.) of 17α- and 17β-hydroxysteroids (17α- and 17β-OH) was analyzed by ^{1}H-NMR (see Table 4.3). For pristine MOF-808 and MOF-808-Pydc significant amounts of α-E2 (alfatradiol) were produced. This is especially interesting, as other reducing agents, such as $NaBH_4$ almost exclusively produce β-E2 (estradiol), due to steric hindrance induced by the C-18 CH_3 group and more complex synthesis

Table 4.3. Conversion and d.r. for the MPV reduction of E1 over different Zr-MOFs

Entry	Catalyst	Time (h)	Conversion	d.r. (α-E2/β-E2)
1	UiO-66	48	2	n.d.
2	MOF-808	4	24	
3		24	87	40/60
4	MOF-808-Pydc	4	61	
5		24	91	38/62

Reprinted (adapted) with permission from (*Catal. Sci. Technol.* **2018**, *8*, 3610-3616). Copyright (2018) The Royal Society of Chemistry

procedures are necessary for the production of the alpha-isomer. A more detailed discussion on the true potential of this high diastereoselectivity afforded by MOF-808 is given in Chapter 6 of this thesis.

4.4. Conclusions

In this chapter we have demonstrated that MOF-808 can be used as an efficient catalyst for the MPV reduction of carbonyl compounds as it has been shown on the case of CH reduction. The six-connected Zr_6-cluster with a high number of open metal sites where all zirconium atoms are available for catalysis is beneficial and results in a higher catalytic activity compared to other Zr-MOFs, such as UiO-66 and DUT-67. The catalytic activity of these three tested Zr-MOFs follows the order, MOF-808 > DUT-67 > UiO-66. This effect is not assigned to the size of the molecule or variations in external surface area, as CH is small enough to diffuse within the porous structure of all three catalysts. Further, SEM experiments revealed a comparable size of particles of UiO-66 compared to pristine MOF-808 and DE MOF-808-IPA and MOF-808-Pydc. The trend observed in the catalytic activities can thus be correlated with the connectivity of the Zr_6-SBUs (increasing in the same direction), which translate into a progressive decrease of the amount of open metal sites available for catalysis.

Defect engineered MOF-808 compounds, DE MOF-808-IPA and MOF-808-Pydc, show a further increase in catalytic activity. This is assigned to the defective linkers. Due to one missing coordination site on these molecules, the environment around the Zr_6-cluster is less crowded, which is beneficial for the formation of the TS and thus results in an increase in catalytic activity. A similar effect is not observed for the two remaining DE compounds, namely MOF-808-OH and MOF-808-NH_2, for which the presence of hydroxyl or amino groups in the linker introduced a steric hindrance similar to the one present in pristine MOF-808.

The large pores of MOF-808 allow the transformation of larger substrates, as shown on the case of E1. Due to smaller triangular windows in UiO-66, larger molecules cannot diffuse within the porous structure of UiO-66 and have no access to active sites located at the internal surface area of the material. DE MOF-808-Pydc showed again increased catalytic activity compared to pristine MOF-808.

Pristine MOF-808 and DE MOF-808-Pydc have shown to introduce some diastereoselectivity in the reduction of prochiral molecule E1. Reasonable amounts of the elusive α-E2 are produced (*ca.* 40%), resulting in a mixture of both diastereoisomers.

Pristine MOF-808 and DE MOF-808-IPA and MOF-808-Pydc were shown to be stable during the activation and reaction conditions as can be seen from the XRD analysis. Therefore, these materials served as reusable catalysts in the MPV reduction of CH.

4.5. References

1. Gascon, J.; Corma, A.; Kapteijn, F. & Llabrés i Xamena, F. X. *ACS Catal.* **2014**, *4*, 361.
2. Cavka, J. H. *et al. J. Am. Chem. Soc.* **2008**, *130*, 13850.
3. Mondloch, J. E. *et al. J. Am. Chem. Soc.* **2013**, *135*, 10294.
4. Feng, D. *et al. Angew. Chem. Int. Ed.* **2012**, *51*, 10307.
5. Yuan, S. *et al. J. Am. Chem. Soc.* **2015**, *137*, 3177.
6. Bon, V.; Senkovskyy, V.; Senkovska, I. & Kaskel, S. *Chem. Commun.* **2012**, *48*, 8407.
7. Schaate, A. *et al. Chem. Eur. J.* **2011**, *17*, 9320.
8. Marx, S.; Kleist, W. & Baiker, A. *J. Catal.* **2011**, *281*, 76.
9. Kozachuk, O. *et al. Angew. Chem. Int. Ed.* **2014**, *53*, 7058.
10. Zhang, W. *et al. Chem. Eur. J.* **2016**, *22*, 14297.
11. Meerwein, H. & Schmidt, R. *Liebigs Ann. Chem.* **1925**, *444*, 221.
12. Verley, A. *Bull. Soc. Chim. Fr.* **1925**, *37*, 537.
13. Ponndorf, W. *Angew. Chem.* **1926**, *39*, 138.
14. Shibagaki, M.; Takahashi, K. & Matsushita, H. *Bull. Chem. Soc. Jpn.* **1988**, *61*, 3283.
15. Aramendía, M. A.; Borau, V.; Jiménez, C.; Marinas, J. M. & Urbano, F. J. *Appl. Catal. A Gen.* **2003**, *244*, 207.
16. Aramendía, M. A.; Borau, V.; Jiménez, C.; Marinas, J. M. & Romero, F. J. *Catal. Lett.* **1999**, *58*, 53.
17. Koehle, M. & Lobo, R. F. *Catal. Sci. Technol.* **2016**, *6*, 3018.

18. Zhu, Y.; Chuah, G. & Jaenicke, S. *Chem. Commun.* **2003**, *0*, 2734.

19. Corma, A.; Domine, M. E.; Nemeth, L. & Valencia, S. *J. Am. Chem. Soc.* **2002**, *124*, 3194.

20. Waal, J. C. van der; Tan, K. & Bekkum, H. van *Catal. Lett.* **1996**, *41*, 63.

21. Creyghton, E. J.; Ganeshie, S. D.; Downing, R. S. & Bekkum, H. van *Chem. Commun.* **1995**, *0*, 1859.

22. Corma, A.; Domine, M. E. & Valencia, S. *J. Catal.* **2003**, *215*, 294.

23. Liu, S. H.; Jaenicke, S. & Chuah, G. K. *J. Catal.* **2002**, *206*, 321.

24. Kandiah, M. *et al. Chem. Mater.* **2010**, *22*, 6632.

25. Jiang, J. *et al. J. Am. Chem. Soc.* **2014**, *136*, 12844.

26. Moon, S. Y.; Liu, Y.; Hupp, J. T. & Farha, O. K. *Angew. Chem. Int. Ed.* **2015**, *54*, 6795.

27. Marx, S.; Kleist, W. & Baiker, A. *J. Catal.* **2011**, *281*, 76.

28. Fang, Z. *et al. J. Am. Chem. Soc.* **2014**, *136*, 9627.

29. Valenzano, L. *et al. Chem. Mater. Mater.* **2011**, *23*, 1700.

30. Cirujano, F. G.; Corma, A. & Llabrés i Xamena, F. X. *Chem. Eng. Sci.* **2015**, *124*, 52.

Chapter 5

Diastereoselective MPV reduction of substituted cyclohexanones over MOF-808

5.1. Introduction

In the previous chapter, it was shown that MOF-808 serves as an efficient catalysts in the MPV reduction of carbonyl compounds to their corresponding alcohols. The more open framework of MOF-808 with wider pores of 18,4 Å and the Zr_6-cluster with only six-fold connectivity and high accessibility of Zr^{4+} ions, show several advantages compared to UiO-66. CH reacted much faster over MOF-808, due to a higher number of open metal sites. Bulkier substrate E1 is able to diffuse through the porous structure of MOF-808, leaving all the active sites located at the internal surface area accessible. This results in a much higher activity, from 2% to 87% and 91% for UiO-66, MOF-808 and MOF-808-Pydc, respectively. Interestingly, it was observed that MOF-808 and MOF-808-Pydc introduced some diastereoselectivity, leading to the production of moderate amounts of α-E2 of around 40%.

As discussed in the introduction of this thesis, MPVO reactions are of interest in organic syntheses, as they require simple organic molecules as reductants or oxidants and can be performed under mild reaction conditions. Aldehydes or ketones for instance can be reduced in the presence of other functional groups, such as alkenes, alkynes, halogens, nitriles or alkoxyl groups, which makes it a selective synthesis procedure. MPVO reactions can be performed under heterogeneous conditions, which is an important step towards the development of sustainable processes. Besides its good regio- and chemoselective properties, some success has been made in the conduction of diastereoselective and enantioselective MPVO reactions, as we will shortly review.

Diastereoselectivity and enantioselectivity can be especially of importance in the production of biologically active products. In this case, the chirality of a given molecule is the key factor towards its biological activity. KUROBOSHI and ISHIHARA used $Al(O^iPr)_3$ for the production of *anti*-diols.[1] High conversions with selectivities up to 100% towards the *anti*-product were achieved in the reduction of α,α-difluoro-β-hydroxy ketones (Scheme 5.1). The selectivity decreased when higher temperatures and larger amounts of substrates were used. *Syn*- or *anti*-1,3-diols for instance, are of importance

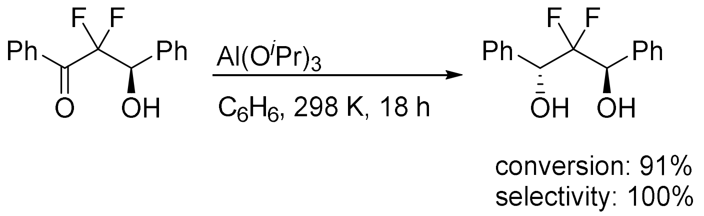

Reprinted (adapted) with permission from (*Synthesis*, **1994**, *10*, 1007-1017). Copyright (1994) Georg Thieme Verlag KG Stuttgart • New York

Scheme 5.1. Synthesis of *anti*-1,3-diols

due to their occurrence in biologically active products. Using DIBAL-H as reducing agent, reactions did not proceed with high diastereoselectivity and addition of $ZnCl_2$-TMEDA results in the production of *syn*-1,3-diols. This inversion in diastereoselectivity was explained by the $ZnCl_2$-TMEDA to work as an acid and base pair, coordinating to the α-fluorine atom of the substrate and an aluminium atom in DIBAL-H, respectively. As a consequence *syn*-1,3-diols are produced preferentially due to reduced interaction of a pseudo-axial α-fluorine with the aluminium in DIBAL-H.

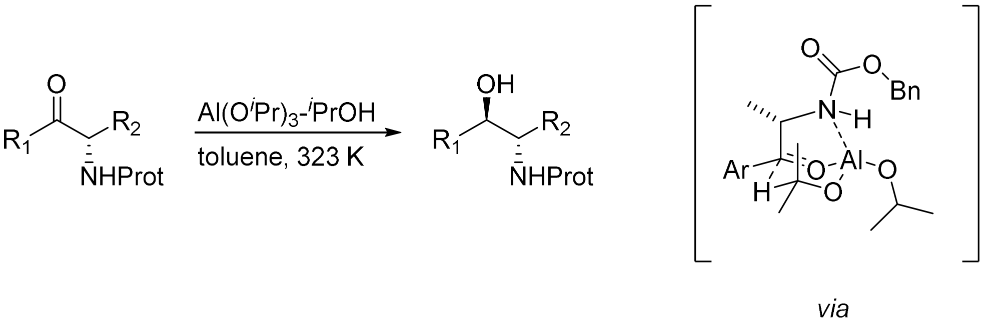

Reprinted (adapted) with permission from (*J. Org. Chem.*, **2006**, *71*, 840-843). Copyright (2006) American Chemical Society

Scheme 5.2. Synthesis of ephidrine analogues with the TS leading to *anti* products

$Al(O^iPr)_3$ has been used also in the synthesis of chiral ephedrine analogues (Scheme 5.2).[2] The high *anti*-selectivity in the reaction was achieved by the chelation ability of the nitrogen atom from the substrate to the aluminium atom of the catalyst. For the reduction of compounds without chelation control, the FELKIN-AHN-controlled *syn* product was formed. With the benzyl carbamate (Cbz) protecting group the diastereoselectivity was very high (97.6:2.4 to 99:1) with toleration of various substituents on the substrate. $Al(O^iPr)_3$ was further used in catalytic amounts for the diastereoselective reaction.

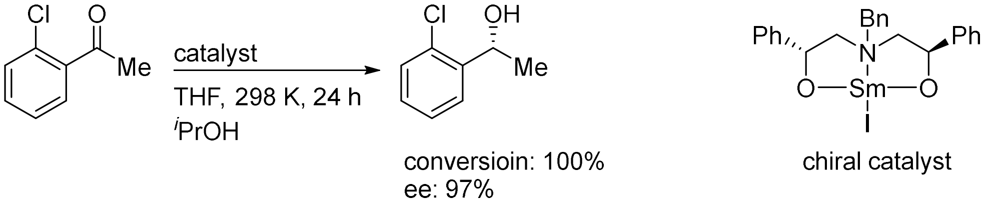

Reprinted (adapted) with permission from (*J. Am. Chem. Soc.*, **1993**, *115*, 9800-9801). Copyright (1993) American Chemical Society

Scheme 5.3. Enantioselective reduction of *α*-chloroacetophenone (left) and chiral catalyst used for the reaction (right)

Enantioselective MPV-reductions can also be performed, by for instance usage of a chiral alcohol as the reducing agent, or a chiral catalyst. EVANS *et al.* used a samarium catalyst with a chiral ligand (Scheme 5.3) in the enantioselective reduction of different arylketones.[3] The chiral ligand was synthesized by the reaction of phenylmethanamine with chiral 2-phenyloxirane and subsequent deprotonation with BuLi. The chiral catalyst was formed in situ by reaction of chiral lithium alkoxide with LnI_3 (Ln = lanthanide metal). Usually excellent conversions were achieved with selectivities above 92%. The enantioselectivity decreased when longer alkyl groups were present (e.g., Me vs. Et). In comparison with different lanthanide metals with different ionic radii, complexes of neodymium, samarium and terbium showed best enantioselectivities. Metal ions with smaller or larger radii showed lower selectivities and reduced catalytic competencies.

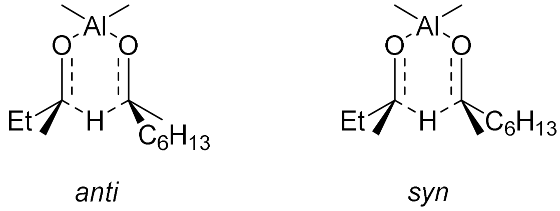

Reprinted (adapted) with permission from (*J. Am. Chem. Soc.*, **1950**, 72, 631-631). Copyright (1950) American Chemical Society

Figure 5.1. Illustration of TSs in the partially asymmetric reduction of 6-methylheptan-2-one

DOERING and YOUNG used chiral reducing agents with the corresponding *rac.* aluminium-alkoxide for the reduction of 6-methylheptan-2-one and cyclohexylethan-1-one (Figure 5.1).[4] An ee of 22% at a conversion of 60% was achieved using (+)-^{s}BuOH with *rac.* $Al(O^sBu)_3$ in the reduction of 6-methylheptan-2-one. In this reaction, (+)-6-methylheptan-2-ol was the major product of the reaction. Therefore, a steric interference between the largest groups can be assumed. The predominantly formed TS with the largest groups in *anti* position, leads to the formation of the reduced ketone with the same configuration as the reducing alcohol.

Substituted CHs have extensively been used as substrates to address diastereoselective properties of various MPV catalysts. Thus, KONISHI *et al.* used a 5,10,15,20-tetraphenylporphynatoaluminiumchloride (AlTPPCl) catalyst with *iso*-borneol as the reducing agent to convert 2-methylcyclohexanone (2MeCH) selectively to the *cis*-isomer.[5] Even though the product equilibrates towards the thermodynamically more stable product with time, the initial selectivity of 93% at a conversion of 93% was very high (Figure 5.2). The high selectivity towards the *cis*-isomer was explained by increasing steric repulsion between the 2,6-axial hydrogens of the CH ring and the porphyrin disk. Therefore, the hydrogen transfer takes place preferentially from the less sterically hindered equatorial side, which results in the formation of *cis*-2-methylcyclohexan-1-ol (*cis*-2MeCHol). With ^{i}PrOH as reducing agent, high *trans*-

selectivity was obtained, and reactivity and selectivity of AlTPPCl were significantly enhanced when compared to Al(O^{i}Pr)$_3$.

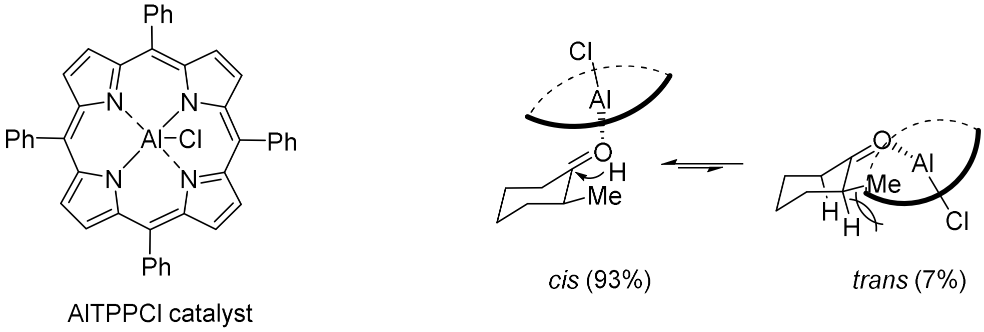

Reprinted (adapted) with permission from (*J. Chem. Soc., Chem. Commun.*, **1988**, 643-645) Copyright (1988) Royal Society of Chemistry

Figure 5.2. AlTPPCl catalyst (left) and cordination of the aldehyde leading to preferred formation of the *cis*-2MeCHol (right)

In Al-substituted zeolites[6] and different M(IV)-substituted BEA zeolites (M(IV) = Ti, Sn or Zr)[7–10] the limited pore space was used to selectively convert substituted CHs, such as 2MeCH, 3MeCH, 4MeCH and TCH to the corresponding thermodynamically less stable alcohol, with a hydroxyl group in axial position (Scheme 5.4). Due to the restricted space in the rather small channels of BEA zeolites (< 8 Å), steric constraints disfavor the formation of the TS with an axial hydride transfer.[6] The TS leading to the thermodynamically less stable product is sterically much less hindered. In this case, the molecule is aligned along the walls of the zeolite. For 2MeCH the stereoselectivity was reduced significantly. Therefore, steric interference of the CH$_3$ group at C-2 with the surface of the catalyst can be expected. For other substituted CHs, high stereoselectivities (71% and 99%) are achieved. On the other hand, different mesoporous silicates such as MCM-41,[11–13] MCM-48[14] or SBA-15 (SBA = Santa Barbara Amorphous type materials)[15] have been used to immobilize metal-alkoxides of for instance zirconium, hafnium, aluminium and indium. Interestingly, reduction of substituted CHs using these metal-alkoxide grafted mesoporous solids was reversed with respect to BEA zeolites.[16] This demonstrates the importance of the small pores in BEA zeolites on the stereoselective outcome of the reaction.

In view of the excellent activity of MOF-808 as MPV catalyst and the interesting diastereoselectivity observed in the previous chapter for the reduction of E1, in this chapter we have analyzed in more detail the potential of MOF-808 as a catalyst for diastereoselectie MPV reductions, using various CHs bearing substituents at C-2 and C-3.

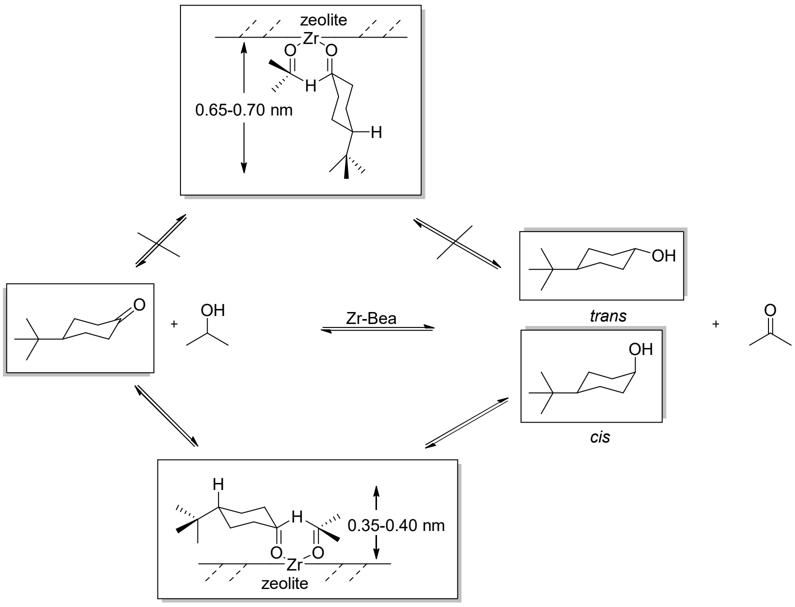

Reprinted (adapted) with permission from (*Applied Catalysis A: General*, **2015**, *493*, 112-120. Copyright (2015) Elsevier B. V.

Scheme 5.4. Synthesis of *cis*-TCHol in restricted channels of BEA zeolites

5.2. Results and discussion

The MOF-808 used in the catalytic studies described below was prepared as described in the Annexes (Section 8.1). The general procedure used for the MPV reduction of substituted CHs is also described in detail in the Annexes (Section 8.3), while specific reaction conditions are indicated in the corresponding tables and figures below. The preparation of other catalysts used for comparison purposes is also described in Chapter 8. Annexes.

5.2.1. Reduction of 3-methylcyclohexanone (3MeCH)

In 3MeCH the CH_3 group is in equatorial position, as it is more bulky than a proton and an equatorial position gives more space and decreases torsional strains. Therefore, two different TSs can be considered, as shown in Figure 5.3. In TS (a) an axial hydride transfer leads to an equatorial hydroxyl group, while in TS (b) an equatorial hydride transfer leads to an axial -OH group. Both TSs lead to the corresponding alcohol with the -OH group in *cis* or *trans* position, respectively, with respect to the CH_3 group.

Table 5.1 summarizes the main catalytic results obtained with MOF-808 and other catalysts for the MPV reduction of 3MeCH, using either ^{i}PrOH or ^{s}BuOH as reducing

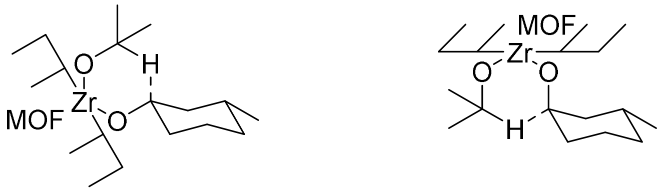

TS (a) TS (b)

Figure 5.3. Possible TSs formed in the cavities of MOF-808 leading to the corresponding *cis*-alcohol (left) and *trans*-alcohol (right)

alcohol. In all cases, 3-methylcyclohexanol (3MeCHol) was the only product observed, so the reaction was fully selective. It can be seen in Table 5.1 (entry 1), that in MOF-808 3MeCH is converted preferentially to the *cis*-alcohol (1S,3R)-3-methylcyclohexan-1-ol ((1S,3R)-3MeCHol), which is the thermodynamically more stable product. Higher diastereoselectivities (82%) towards the *cis* isomer are obtained when using ^{i}PrOH as the reducing agent. With ^{s}BuOH as reducing agent (Table 5.1, entry 2) the *cis* isomer is still the dominant product but the selectivity decreases to 68% at full conversion. Although the reaction temperature has a clear effect in the rate of 3MeCHol formation (see below), the diastereoselectivity to the *cis* alcohol was found to be almost constant within the temperature range studied (353-393 K). This lack of kinetic or thermodynamic control is in agreement with the reaction taking place inside the MOF cavities (where the Zr^{4+} are located) and being affected mainly by cavity confinement effects during formation of the TS, as we will discuss below.

The catalytic performance of Zr-containing MOF-808 was compared with that of UiO-66 under the same reaction conditions and the results are also included in Table 5.1 (entries 3 and 4). In the case of UiO-66, the reduction of 3MeCH at 353 K was very slow (3% conversion after 24 h with both ^{i}PrOH and ^{s}BuOH), and it was necessary to increase reaction temperature to 393 K to attain full conversion of the ketone in 24 h, yielding the *cis* alcohol with a 64% diastereoselectivity. The lower catalytic activity of UiO-66 with respect to MOF-808 mirrors the trend observed for CH reduction as discussed in the previous chapter and it is most likely related with: i) the lower amount of accessible Zr^{4+} sites in UiO-66 (located only at defect positions); and ii) its narrow pore system with respect to the dimensions of the reaction substrate, which hinders diffusion and formation of the TS inside the MOF cavities. The differences in catalytic activity between MOF-808 and UiO-66 are more evident in the case of 3MeCH than in CH, due to the larger dimensions of the former compound and the additional steric hindrance introduced by the CH$_3$ group substituent.

We then compared the catalytic performance of MOF-808 and UiO-66 with other catalysts reported in the literature; viz, mesoporous SBA-15 silica having grafted zirconium propoxide, Zr/SBA,[16] as well as Zr-BEA[16] and Ti-BEA zeolites[7] (Table 5.1, entries 6-8).

Zr/SBA produced *cis*-3MeCHol as the main product with 75% selectivity, in line with the diastereselectivity observed for MOF-808 and UiO-66. On the contrary, both Zr- and Ti-BEA zeolites yielded the *trans* isomer with 71% and 70% selectivity, respectively.

Table 5.1. Conversion of 3MeCH over various MPVreduction catalysts with obtained selectivities indicated for each reaction

Entry	Conditions	Conversion	Selectivity
1	MOF-808 (^{i}PrOH, 353 K)	100% (6 h)	82% (*cis*)
2	MOF-808 (^{s}BuOH, 353 K)	99% (6 h)	68% (*cis*)
3	UiO-66 (^{i}PrOH, 353 K)	3% (24 h)	74% (*cis*)
4	UiO-66 (^{s}BuOH, 353 K)	3% (24 h)	69% (*cis*)
5	UiO-66 (^{s}BuOH, 393 K)	98% (24 h)	64% (*cis*)
6	Zr-BEA (^{i}PrOH, refluxing (b.p. 355 K)[a]	54.4% (0.5 h)	71% (*trans*)
7	Ti-BEA (^{i}PrOH, refluxing (b.p. 355 K)[b]	25.8% (6 h)	70% (*trans*)
8	Zr/SBA (^{i}PrOH, refluxing (b.p. 355 K)[a]	94.1% (6 h)	75% (*cis*)

[a] Data taken from reference [16]; [b] Data taken from reference [7]

As commented earlier, in the small channels with restricted space of BEA zeolites (< 8 Å), steric constraints disfavor the formation of the TS with an axial hydride transfer, leading to the thermodynamically less stable *trans*-3MeCHol, having the -OH group in axial position. On the contrary, the wide space available inside the pores of Zr/SBA (mean pore diameter 6.5 nm) allows the formation of the other more stable TS, since the resulting -OH group occupies the thermodynamically more stable equatorial position in the final product, *cis*-3MeCHol.

Comparison of the above results obtained with Zr/SBA and Zr- and Ti-BEA zeolites illustrates the relevance of reactions taking place in confined spaces. Thus, tight fitting of the TS and the pore walls of the solid catalyst determine the type and strength of secondary (noncovalent) interactions that can be stablished, which can drive the reaction towards the formation of a given product among various possible. This transition state selectivity obtained for MPV reactions catalyzed by solid catalysts with well-defined porous systems is clearly reminiscent of enzymatic catalysis.[17]

When considered together the results summarized in Table 5.1, two groups of catalysts can be distinguished based on the preferential formation of either *trans* (Zr- and Ti-BEA zeolites) or *cis* 3MeCHol (MOF-808, UiO-66 and Zr/SBA). In the former group, limited space available inside channel-type pores prevents the formation of bulkier TS with an axial hydride transfer, resulting in the formation of the *trans* alcohol isomer, having -OH groups in axial position and in *anti* configuration with respect to the CH_3 group at C-3. In the second group of catalysts, either the wider pore channels (as in Zr/SBA) or the pore shape (in the form of cavities rather than channels, as in MOF-808 and UiO-66), allows the formation of the bulkier TS, leading to the other and more thermodynamically stable alcohol, *cis*-3MeCHol.

Therefore, the use of MOF-808 as a MPV catalyst for the reduction of 3MeCH is interesting, since this material features a catalytic activity and selectivity comparable with that of Zr- and Ti-BEA zeolites, but provides the opposite diastereoselectivity, similar to Zr/SBA. The use of UiO-66 is more limited than MOF-808, due to the lower concentration of Zr^{4+} sites and the narrow pore system, which introduce severe diffusion limitations leading to a much poorer catalytic performance.

5.2.2. Reduction of 2-methylcyclohexanone (2MeCH)

The presence of the CH_3 group at C-2 introduces a high steric interference with the surface of the catalyst. Therefore, a much lower catalytic activity can be expected as compared with 3MeCH. Accordingly, with UiO-66 the conversion of 2MeCH was very low, even at 393 K (13% after 24 h using ^{s}BuOH), as shown in Table 5.2 (entry 3). Conducting the reactions at lower temperatures, results in a further drop in activity. Therefore, 2MeCH cannot be converted over UiO-66 at 353 K with either ^{i}PrOH or ^{s}BuOH.

Table 5.2. Conversion of 2MeCH over various MPV reduction catalysts with obtained selectivities indicated for each reaction

Entry	Conditions	Conversion	Selectivity
1	MOF-808 (^{i}PrOH, 353 K)	96% (6 h)	53% (*trans*)
2	MOF-808 (^{s}BuOH, 353 K)	100% (24 h)	61% (*cis*)
3	UiO-66 (^{s}BuOH, 393 K)	13% (24 h)	58% (*cis*)
4	Zr-BEA (^{i}PrOH, refluxing (b.p. 355 K)[a]	6.1% (0.5 h)	55% (*cis*)
5	Ti-BEA (^{i}PrOH, refluxing (b.p. 355 K)[b]	8.8% (6 h)	60% (*cis*)
6	Zr/SBA (^{i}PrOH, refluxing (b.p. 355 K)[a]	3.6% (6 h)	58% (*trans*)

[a] Data taken from reference [16]; [b] Data taken from reference [7]

In line with the results found with UiO-66, the reported catalytic activity for 2MeCH reduction over Zr/SBA and Zr- and Ti-BEA zeolites was considerably low with respect to the 3MeCH isomer (compare results in Tables 5.1 and 5.2): 3.6% *vs* 94.1% conversion after 6 h for Zr/SBA; 6.1% *vs* 54.4% conversion after 0.5 h over Zr-BEA; and 8.8% *vs* 25.8% conversion after 6 h for Ti-BEA. In spite of this lower activity, the diastereoselectivity of the reaction is still governed by a similar transition state selectivity as that found for 3MeCH: i.e., formation of the less bulky TS with hydride transfer in equatorial position takes place inside the channels of BEA zeolites, while the opposite situation is found in Zr/SBA. In the case of 2MeCH, this TS leads to the preferential formation of *cis*-2MeCHol in Zr- and Ti-BEA, and formation of *trans*-2MeCHol in the case of Zr/SBA.

Coming to MOF-808 (Table 5.2, entries 1 and 2), it is first worth noting that the catalytic activity for the reduction of 2MeCH was practically the same than in the case of 3MeCH when ^{i}PrOH was used as reducing agent: full conversion of the ketone was attained in both cases after 6 h. Similar to Zr/SBA, *trans*-2MeCHol was the main product formed, although the selectivity in this case was very low, only 53%. Despite a certain decrease of activity with ^{s}BuOH, it was still possible to reach full conversion of 2MeCH after 24 h. Interestingly, the selectivity was inversed and the *cis* product *via* an equatorial hydride transfer was the major product (61% at full conversion). A similar inversion of selectivity depending on the size of the reducing alcohol has been observed before, as for instance in the report by KONISHI *et al.* using AlTPPCl catalyst and *iso*-borneol or ^{i}PrOH as the reducing agent, as commented in the introduction of this chapter.

To the best of our knowledge, the catalytic performance of MOF-808 for the reduction of 2MeCH is considerably better than any other solid catalysts reported so far. Thus, it seems that in MOF-808 an optimal interplay is found between structure of the active sites and cavity effects that allows converting strongly hindered ketones (such as ketones with a CH_3 group in *ortho* position) very efficiently.

When comparing the results summarized in Tables 5.1 and 5.2, it is worth mentioning that the diastereoselectivities obtained for 2MeCH (55-60%) are in all cases significantly lower than in the case of 3MeCHol (70-75%). Moreover, in the case of MOF-808 we have even observed an inverse selectivity depending on the size of the secondary alcohol used (from 53% (*trans*) to 61% (*cis*) for ^{i}PrOH and ^{s}BuOH, respectively), while a similar effect was not observed in the case of 3MeCH reduction. These findings evidence that the interplay between secondary interactions between the reaction substrates (ketone and alcohol), the catalytic active site and the pore walls of the solid are further complicated by the close proximity of the CH_3 group at C-2 to the carbonyl group that is transformed.

5.2.3. Reduction of 2-phenylcyclohexanone (2PhCH)

In order to analyze further the effect of substituents at C-2 in the MPV reduction of substituted CHs, we have considered the introduction of a more bulky substituent, a Ph group. Thus, Table 5.3 summarizes the catalytic results obtained for the reduction of 2-phenylcyclohexanone (2PhCH).

Despite the presence of the bulky Ph ring at C-2, MOF-808 was readily able to catalyze the MPV reduction of 2PhCH with ^{i}PrOH, attaining full conversion after 24 h of reaction and an excellent diastereoselectivity (90%) to *cis*-2-phenylcyclohexan-1-ol (*cis*-2PhCHol). Very similar results were obtained when ^{i}PrOH was replaced by ^{s}BuOH (full conversion after 24 h and 94% selectivity to *cis*-2PhCHol). Increasing the reaction temperature to 393 K produced a clear increase of the reaction rate (compare conversions at 6 h in Table 5.3, entries 2 and 3), while preserving the excellent *cis* selectivity.

Table 5.3. Conversion of 2PhCH over various MPV reduction catalysts with obtained selectivities indicated for each reaction

Entry	Conditions	Conversion	Selectivity
1	MOF-808 (^{i}PrOH, 353 K)	36% (6 h) 96% (24 h)	90% (*cis*)
2	MOF-808 (^{s}BuOH, 353 K)	28% (6 h) 97% (24 h)	94% (*cis*)
3	MOF-808 (^{s}BuOH, 393 K)	26% (0.5 h) 100% (6 h)	90% (*cis*)
4	$Al(O^iPr)_3$ (^{s}BuOH, 393 K)	43% (24 h)	74% (*cis*)
5	UiO-66 (^{s}BuOH, 393 K)	4% (24 h)	76% (*cis*)
6	Zr-BEA (^{s}BuOH, 393 K)	12% (24 h)	72% (*cis*)
7	ZrO_2 nanopowder (^{s}BuOH, 393 K)	- (24 h)	-
8	$Zr(O^iPr)_4{*}^iPrOH$ (^{s}BuOH, 393 K)	- (24 h)	-
9	$NaBH_4$ (EtOH, r.t.)	100% (2 h)	62% (*trans*)

$Al(O^iPr)_3$ was reported earlier in the literature[2] to convert 2PhCH with high diastereoselectivity towards *cis*-2PhCHol: 100% conversion after 19 h of reaction, with 83% selectivity to *cis*-2PhCHol. The reaction was performed in a 4:6 (v/v) mixture of ^{i}PrOH/toluene as solvent and 323 K. However, all our attempts to reproduce these results failed (no conversion of 2PhCH was obtained). In our hands, using $Al(O^iPr)_3$ with pure ^{s}BuOH at 393 K gave slightly lower *cis* diastereoselectivity (74%) compared to the reported results in the literature and still the activity of the catalyst was not very high (43% conversion after 24 h) as compared with MOF-808 (Table 5.3, entry 4).

For the sake of comparison, and to put the results obtained with MOF-808 into perspective, further reactions were carried out with other solid catalysts. Thus, UiO-66 afforded a very low conversion of 2PhCH and a considerably lower *cis* selectivity (76%, Table 5.3, entry 5). A Zr-BEA zeolite produced only slightly higher conversion and similar selectivity: 12% conversion after 24 h and 72% selectivity to *cis*-2PhCHol. Meanwhile, other zirconium catalysts, such as commercial ZrO_2 nanopowder (Sigma-Aldrich <100 nm and $Zr(O^iPr)_4{*}^iPrOH$ did not produce any sensible amount of 2PhCHol after 24 h of reaction (Table 5.3, entry 7 and 8).

Finally, reduction of 2PhCH was carried out using $NaBH_4$ as reducing agent (reaction conditions detailed in the Annexes, Section 8.3), which produced full conversion and a moderate (62%) inversed selectivity to the other alcohol; i.e., *trans*-2PhCHol. Therefore, a preferential axial attack of the hydride takes place when using $NaBH_4$ as a reducing agent. On the contrary, when $Al(O^iPr)_3$ or MOF-808 are used as catalysts, 2PhCH is preferentially converted to the *cis* product *via* an equatorial hydride transfer, according to a FELKIN-AHN control (*i.e.*, the attack comes from the less hindered side). These differences between $NaBH_4$ reduction and catalytic MPV reduction are better appreciated in the corresponding NEWMAN projection shown in Scheme 5.5.

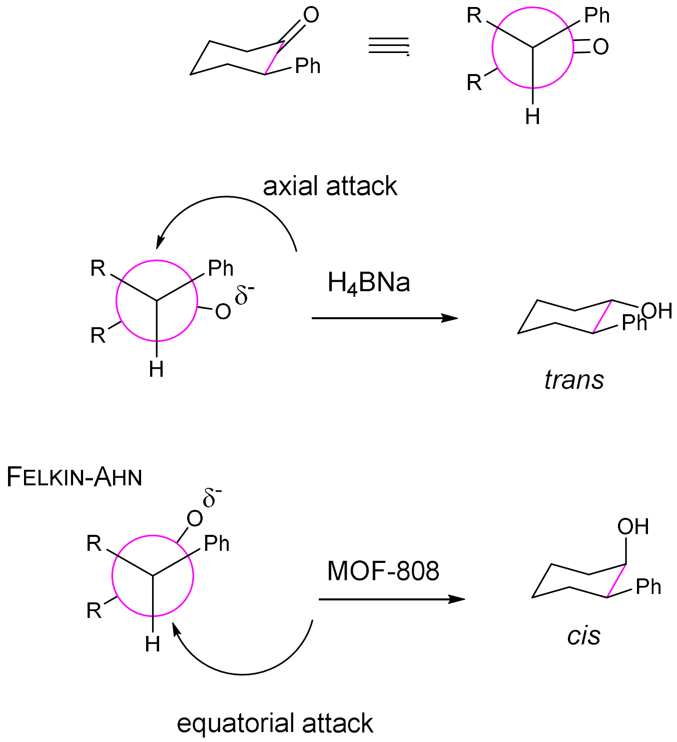

Scheme 5.5. NEWMAN projection of 2PhCH and preferred orientation for the hydride transfer (either axial or equatorial)

5.2.4. Kinetic analysis

In order to gain further insights into the diastereoselective properties of MOF-808 for the MPV reduction of substituted CHs, we carried out the reduction of 2MeCH and 3MeCH in the temperature range 353-393 K using either ^{i}PrOH or ^{s}BuOH as reducing agents. In all cases, increasing the reaction temperature produced a clear acceleration of the MPV reaction. Interestingly, the diastereomeric ratio between the resulting *cis* and *trans* alcohols remained constant and independent of the temperature thus evidencing the lack of kinetic control of the reaction.

Catalytic results of 2MeCH and 3MeCH reduction using ^{i}PrOH or ^{s}BuOH in the 353-393 K range were further used to calculate kinetic rate constants k_{cis} and k_{trans}, for the respective couple of diastereoisomers. The detailed procedure used is given in the Annexes (Section 8.3).

In general, calculated apparent activation energies and pre-exponential factors for ^{s}BuOH are higher than for ^{i}PrOH for both 2MeCH and 3MeCH, which reflects the slower conversion rate observed for the bulkier alcohol (see Annexes, Section 8.3). In the particular case of 2MeCH, the differences in both E_a and k_0 between *cis* and *trans* isomers are very small: $\Delta E_{a,cis\text{-}trans}$ = 1.9 and 0.2 kJmol^{-1} for ^{i}PrOH and ^{s}BuOH, respectively and k_0 of the same order of magnitude for both alcohols. These results are in line with the low diastereoselectivity observed in the MPV reaction (53%-*trans* and 61%-*cis*, respectively, for ^{i}PrOH and ^{s}BuOH, see Table 5.2). On the contrary, the differences in apparent activation energy are much higher for 3MeCH reduction ($\Delta E_{a,cis\text{-}trans}$ = 7.2 and 6.5 kJ mol^{-1} for ^{i}PrOH and ^{s}BuOH), though they are partially balanced by somewhat higher k_0 values of the less favored isomers.

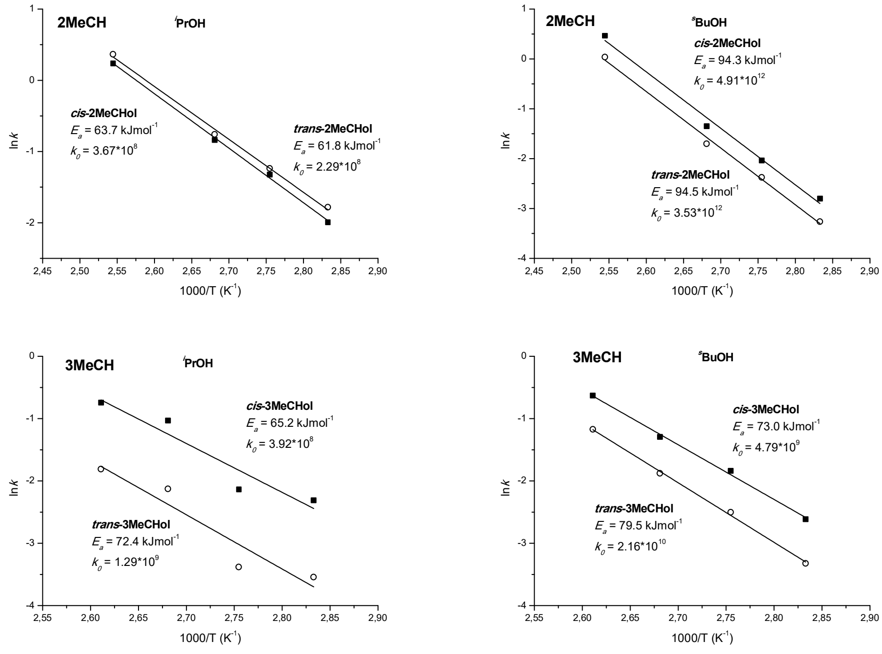

Figure 5.4. Arrhenius plots obtained for 2MeCH (top) and 3MeCH (bottom) reduction over MOF-808 using either ^{i}PrOH or ^{s}BuOH, as indicated. Calculated apparent activation energies (E_a) and pre-exponential factors (k_0) for each compound are indicated

The EYRING-POLANYI equation was then used to derive thermodynamic properties from the kinetic data. Thus, entropy ($\Delta S^{\ddagger}$), enthalpy ($\Delta H^{\ddagger}$) and GIBBS free energy ($\Delta G^{\ddagger}$) of activation can be extracted from the corresponding plots shown in the Annexes (Section

8.3). These thermodynamic properties correspond to variations in energy upon formation of the TS complex leading to *cis* or *trans* isomers during the reaction. Table 5.4 and Table 5.5 summarize the calculated values and the difference between *cis* and *trans* isomers in each case.

In general, the differences in energy between TSs leading to *cis* and *trans* isomers are very small; less than 3.5 kJmol^{-1} (in terms of $\Delta G^{\ddagger}$) in the most favorable case of 3MeCH reduction with ^{i}PrOH. This is the reason for the relatively low diastereoselectivity attained, which in the best case is 82%. Therefore, any analysis of the thermodynamic properties extracted from the EYRING-POLANYI plot must be viewed with caution. Still, some general trends are observed that are worth mentioning.

First, in the case of 3MeCH reduction (Table 5.4), it can be observed that the enthalpic contribution ($\Delta H^{\ddagger}$) is more favorable for the *cis* isomer by 7.2 and 6.5 kJmol^{-1} in ^{i}PrOH and ^{s}BuOH, respectively. However, the formation of an activated complex towards the *trans* isomer requires a lower entropy loss than in the case of the *cis* isomer: -80.6 vs -90.5 Jmol^{-1}K^{-1} in the case of ^{i}PrOH, and -57.1 vs -69.7 Jmol^{-1}K^{-1} in ^{s}BuOH. Note, that a more negative $\Delta S^{\ddagger}$ means a higher loss of entropy and thus a more ordered TS complex. Therefore, the enthalpic ($\Delta H^{\ddagger}$) and the entropic ($-T\Delta S^{\ddagger}$) contributions to the difference between both TSs have opposite signs, so the two terms are counterbalanced to some extent. As a result, the differences of the overall $\Delta G^{\ddagger}$ between both TSs are small and the resulting diastereoselectivity is relatively low.

Table 5.4. Enthalpy ($\Delta H^{\ddagger}$), entropy ($\Delta S^{\ddagger}$) and GIBBS free energy ($\Delta G^{\ddagger}$) of activation for the formation of *cis* and *trans* isomers of 3MeCHol over MOF-808 using ^{i}PrOH or ^{s}BuOH. The table also shows the differences in energy of the TSs leading to *cis* and *trans* isomers in terms of GIBBS free energy, and the corresponding enthalpic ($\Delta H^{\ddagger}$) and entropic contributions ($-T\Delta S^{\ddagger}$)

		$\Delta S^{\ddagger}$ (Jmol^{-1}K^{-1})	$-T\Delta S^{\ddagger a}$ (kJmol^{-1})	$\Delta H^{\ddagger}$ (kJmol^{-1})	$\Delta G^{\ddagger a}$ (kJmol^{-1})
^{i}PrOH	*cis*-3MeCHol	-90.5	33.7	62.2	95.9
	trans-3MeCHol	-80.6	30.0	69.4	99.4
^{s}BuOH	*cis*-3MeCHol	-69.7	25.9	70.0	95.9
	trans-3MeCHol	-57.1	21.3	76.5	97.8
		$\Delta S^{\ddagger}$ (Jmol^{-1}K^{-1})	**$-T\Delta S^{\ddagger a}$ (kJmol^{-1})**	**$\Delta H^{\ddagger}$ (kJmol^{-1})**	**$\Delta G^{\ddagger a}$ (kJmol^{-1})**
cis-trans	^{i}PrOH	-9.9	+3.7	-7.2	-3.5
	^{s}BuOH	-12.6	+4.6	-6.5	-1.9

^{a} Calculated at 373 K

In the case of 2MeCH reduction, the energy differences are still smaller than in the case of 3MeCH, and the alcohol used determines which one is the most stable isomer: *trans*-

2MeCHol in ^{i}PrOH and *cis*-2MeCHol in ^{s}BuOH, although the stabilization of one TS with respect to the other is rather small.

Table 5.5. Enthalpy ($\Delta H^\ddagger$), entropy ($\Delta S^\ddagger$) and GIBBS free energy ($\Delta G^\ddagger$) of activation for the formation of *cis* and *trans* isomers of 2MeCHol over MOF-808 using ^{i}PrOH or ^{s}BuOH. The table also shows the differences in energy of the TSs leading to *cis* and *trans* isomers in terms of GIBBS free energy, and the corresponding enthalpic ($\Delta H^\ddagger$) and entropic contributions ($-T\Delta S^\ddagger$)

		$\Delta S^\ddagger$ ($Jmol^{-1}K^{-1}$)	$-T\Delta S^{\ddagger a}$ ($kJmol^{-1}$)	$\Delta H^\ddagger$ ($kJmol^{-1}$)	$\Delta G^{\ddagger a}$ ($kJmol^{-1}$)
^{i}PrOH	*cis*-2MeCHol	-91.1	34.0	60.6	94.6
	trans-2MeCHol	-95.1	35.5	58.7	94.2
^{s}BuOH	*cis*-2MeCHol	-12.1	4.5	91.2	95.7
	trans-2MeCHol	-14.9	5.5	91.4	96.9
		$\Delta S^\ddagger$ ($Jmol^{-1}K^{-1}$)	$-T\Delta S^{\ddagger a}$ ($kJmol^{-1}$)	$\Delta H^\ddagger$ ($kJmol^{-1}$)	$\Delta G^{\ddagger a}$ ($kJmol^{-1}$)
cis-trans	^{i}PrOH	+4.0	-1.5	+1.9	-0.4
	^{s}BuOH	+2.8	-1.0	-0.2	-1.2

^{a} Calculated at 373 K

5.2.5. Computational study

In order to gain further details on the main factors influencing the interesting diastereoselective properties of MOF-808 for the MPV reduction of substituted CHs, we have started a computational study of the reaction in collaboration with Prof. G. SASTRE, from the ITQ. This research is still in progress and the results showed below, as well as the conclusions derived from them, are only preliminary findings. The study combined quantum semiempirical (PM7) partial geometry optimization and force field methodology, as described in detail in the Annexes (Section 8.3).

Figure 5.5 depicts a schematic view of the catalytic process for a generic CH compound and ^{i}PrOH as reducing agent. Calculations were first performed on MOF-808 in which both reactions substrates, substituted CH and deprotonated alcohol, are adsorbed simultaneously onto the same Zr^{4+} site (configuration $\mathbf{1}_{cis}$ and $\mathbf{1}_{trans}$ in Figure 5.5). Note that at this stage of the investigation, previous steps of the reaction dealing with adsorption and deprotonation of the alcohol have not been considered. In activated MOF-808, once formate ions are removed, each Zr^{4+} ion is coordinated to one -OH group to keep the electrical neutrality of the system. Upon adsorption of the alcohol, it is expected that deprotonation takes place leading to the formation of the alcoholate, which remains adsorbed onto the Zr^{4+} site, while the former –OH group leaves the solid in the form of H_2O. A similar process has been recently described by HAKEK *et al.* on a related UiO-66 compound.[18] In a next step, the corresponding *cis* and *trans* TS was calculated and the energy differences between configurations 1 and TS were determined in each case, as summarized in Table 5.6.

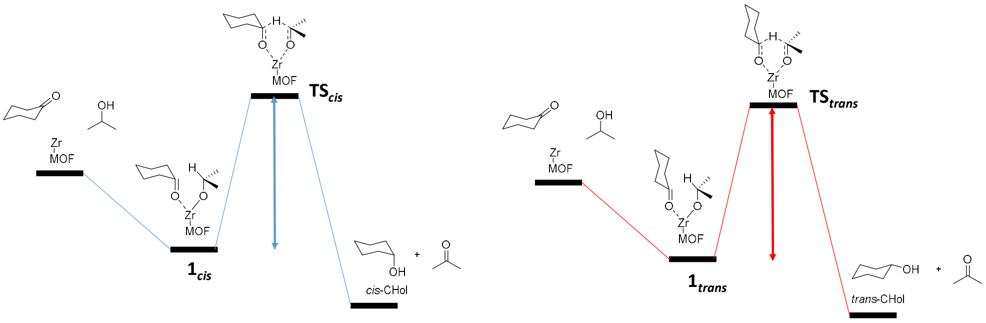

Figure 5.5. Schematic view of the catalytic reaction leading to both CHol isomers

Although these are only preliminary results, it is worth mentioning that, despite the fact that the energy differences between the reaction pathways leading to *cis* and *trans* isomers are very low, the theoretical calculations presented here are able to predict which will be the preferred isomer that will be formed in the reduction of both 2MeCH and 3MeCH. Further calculations are already underway to confirm these results and to allow a more accurate estimation of the energies by properly accounting for noncovalent and dispersive forces into play, which are decisive in determining the resulting diastereoselectivity in chemical transformations such as MPV reductions studied here.

Table 5.6. Calculated energy differences between adsorbed and TSs of 2MeCH and 3MeCH with ^{i}PrOH as reducing agent. Relative energies are given with respect to *cis*-3MeCH:^{i}PrOH, which is the configuration having the lowest energy difference

	Energy difference (kJmol^{-1}) Ts-adsorbed state	Predicted most stable isomer	Observed selectivity[a]
cis-2MeCH:^{i}PrOH	153.4	*trans*	53% (*trans*)
trans-2MeCH:^{i}PrOH	22.2		
cis-3MeCH:^{i}PrOH	0.0	*cis*	82% (*cis*)
trans-3MeCH:^{i}PrOH	116.7		

[a] Diastereoselectivity determined from the catalytic study, as shown in Table 5.1 and 5.2

5.3. Conclusions

Herein, we have continued the research introduced in the previous chapter, which evidenced the excellent performance of MOF-808 as a MPV heterogeneous catalyst. The studies have been extended to various substituted CHs and special emphasis have been put in determining the diastereoselectivity of the catalytic process.

The presence of a CH_3 group at C-3 does not obstruct the MPV reduction of CH, so that the reaction proceeds smoothly. However, this substituent has a clear directing role towards the selective formation of *cis*-3MeCHol, in which the CH_3 group and the resulting –OH group are both in equatorial position and in *syn* configuration. This compound is formed through a TS in which an axial hydride transfer takes place. Conversely, the opposite selectivity has been reported for Zr- and Ti-BEA zeolites, which has been explained by the restricted pore space available inside the channels of BEA zeolites. The wide space available inside MOF-808 pores allows forming the bulkier TS leading to the more thermodynamically stable alcohol, in line with previous reports on mesoporous Zr/SBA catalysts.

Reduction of 2MeCH produces a significantly lower diastereoselectivity to *cis* or *trans* alcohols, which depends on the particular alcohol used as reducing agent. In line with previous results reported by KONISHI *et al.*,[5] the use of a bulky alcohol (^{s}BuOH in our case) favors the formation of the less hindered TS, leading to formation of *cis*-2MeCHol; whereas the other isomer is formed when a smaller alcohol (^{i}PrOH) is used.

A similar effect of the presence of substituents at C-2 has also been observed for the reduction of 2PhCH. Although in this case, the larger size of the Ph group induces a higher diastereoselectivity than the CH_3 group (up to 94% selectivity to *cis*-2PhCHol) and the process is not sensitive to the alcohol used as reducing agent. Interestingly, the catalytic activity of MOF-808 for the reduction of 2PhCH is by far higher than that of other solid catalysts, such as BEA zeolites, ZrO_2, or Al- and Zr-alkoxides.

A more detailed variable temperature kinetic study has been carried out for the reduction of 2MeCH and 3MeCH. The corresponding apparent activation energies (E_a) and pre-exponential factors (k_0), as well as the enthalpy ($\Delta H^{\ddagger}$), entropy ($\Delta S^{\ddagger}$) and GIBBS free energy ($\Delta G^{\ddagger}$) of activation, have been calculated and analyzed from the respective ARRHENIUS and EYRING-POLANYI plots and correlated with the observed catalytic activity and diastereoselectivity. This analysis is largely complicated by the very low energy differences observed for the *cis* and *trans* isomers in all cases, in line with the moderate selectivities obtained (82% in the most favorable case).

Finally, we have discussed some preliminary results obtained from theoretical calculations, in an attempt to rationalize the experimental findings and to determine the influence of the different factors affecting the diastereoselectivity of the catalytic process. Despite the limitations of the procedure used so far, the theoretical calculations are able to predict which is the isomer with the lowest energy barrier in the reduction of both, 2MeCH and 3MeCH.

5.4. References

1. Kuroboshi, M. & Ishihara, T. *Bull. Chem. Soc. Jpn.* **1990**, *63*, 1185.
2. Yin, J.; Huffman, M. A.; Conrad, K. M. & Armstrong, J. D. *J. Org. Chem.* **2006**, *71*,

840.

3. Evans, D. A.; Nelson, S. G.; Gagné, M. R. & Muci, A. R. *J. Am. Chem. Soc.* **1993**, *115*, 9800.

4. Doering, W. V. E. & Young, R. W. *J. Am. Chem. Soc.* **1950**, *72*, 631.

5. Konishi, K.; Makita, K.; Aida, T. & Inoue, S. *Chem. Commun.* **1988**, 643.

6. Creyghton, E. J.; Ganeshie, S. D.; Downing, R. S. & Bekkum, H. van *Chem. Commun.* **1995**, *0*, 1859.

7. Waal, J. C. van der; Tan, K. & Bekkum, H. van *Catal. Lett.* **1996**, *41*, 63.

8. Waal, J. van der; Creyghton, E.; Kunkeler, P.; Tan, K. & Bekkum, H. van *Top. Catal.* **1997**, *4*, 261.

9. Corma, A.; Domine, M. E.; Nemeth, L. & Valencia, S. *J. Am. Chem. Soc.* **2002**, *124*, 3194.

10. Zhu, Y.; Chuah, G. & Jaenicke, S. *Chem. Commun.* **2003**, *0*, 2734.

11. Anwander, R.; Palm, C.; Gerstberger, G.; Groeger, O. & Engelhardt, G. *Chem. Commun.* **1998**, *5*, 1811.

12. Karatas, B. U.; Oksal, B. S. & Karatas, E. *J. Incl. Phenom. Macrocycl. Chem.* **2017**, *87*, 85.

13. Bruyn, M. de; Vos, D. de & Jacobs, P. A. *Adv. Synth. Catal.* **2002**, *344*, 1120.

14. Morey, M. S.; Stucky, G. D.; Schwarz, S. & Fröba, M. *J. Phys. Chem. B.* **1999**, *103*, 2037.

15. Zhu, Y.; Jaenicke, S. & Chuah, G. K. *J. Catal.* **2003**, *218*, 396.

16. Zhu, Y.; Chuah, G. & Jaenicke, S. *J. Catal.* **2004**, *227*, 1.

17. Csicsery, S. M. *Zeolites* **1984**, *4*, 202.

18. Hajek, J.; Bueken, B.; Waroquier, M.; Vos, D. de & Speybroeck, V. van *ChemCatChem* **2017**, *9*, 2203.

Chapter 6

One-step chemo-, regio- and stereoselective reduction of ketosteroids to hydroxysteroids over MOF-808

6.1. Introduction

Steroids are a class of chemical compounds that can be found in many organisms, such as plants, fungi and animals. They are of significant importance being responsible for many biochemical processes. Steroids share a 17-carbon atom tetracyclic ring structure, composed of three six-membered rings and one 5-membered ring. Fused rings are denoted as A-D and numbered as shown in Figure 6.1 below.[1] Various groups can be attached to the skeleton at different positions and with different configurations. Small changes in the structure of steroids can have significant impact on their biological activity. Therefore, chemo-, regio- and stereoselective (bio)transformations towards steroid structures with pharmacological activity is an area of active research. This includes synthesis of natural steroids as well as synthetic analogues. Easily available molecules can be further modified specifically, to improve their biological activity. Δ^4-androstene-3,17-dione (A4) for instance can be obtained through a stepwise degradation and transformation of sitosterol using microorganisms.[2,3] Sitosterol (Figure 6.1) is a common steroid that can be found in plants and is used as a starting material for many steroids. Ketosteroids (or oxosteroids) are steroids in which at least one hydrogen atom on the steroid nucleus is replaced by a keto group (C=O), such as Glucocorticosteroids and corticoids in general. Glucocorticosteroids have anti-inflammatory and immunosuppressive effect and are used in the treatment of a wide variety of symptoms, such as asthma and allergic rhinitis, rheumatic diseases, eczema or in Crohn's disease. Despite their successful use in pharmacology, these compounds also have drawbacks connected with adverse effects that need to be to addressed (see Figure 6.2).[4]

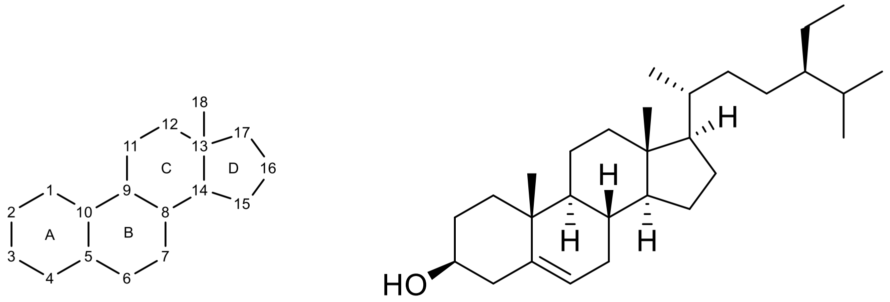

Figure 6.1. Steroid backbone with nomenclature (left) and structure of β-sitosterol (right)

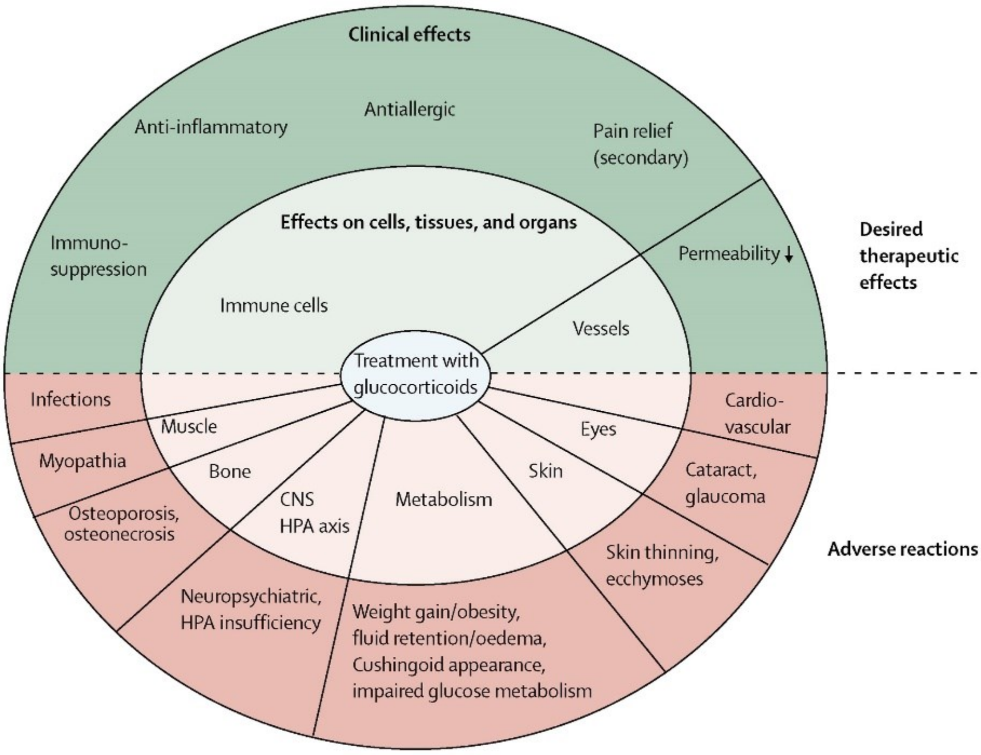
Clinical effects
Anti-inflammatory
Antiallergic
Pain relief (secondary)
Immuno-suppression
Effects on cells, tissues, and organs
Permeability ↓
Desired therapeutic effects
Immune cells
Vessels
Treatment with glucocorticoids
Infections
Cardio-vascular
Muscle
Eyes
Myopathia
Bone
Skin
Cataract, glaucoma
Osteoporosis, osteonecrosis
CNS HPA axis
Metabolism
Adverse reactions
Skin thinning, ecchymoses
Neuropsychiatric, HPA insufficiency
Weight gain/obesity, fluid retention/oedema, Cushingoid appearance, impaired glucose metabolism

Reprinted (adapted) with permission from (*Lancet*, **2005**, *365*, 801-803). Copyright (2005) Elsevier Ltd.

Figure 6.2. Most important clinical effects of glucocorticoids resulting from actions on cells, tissues and organs

Hydroxysteroids especially with a hydroxyl group at C-17 are also of importance in pharmaceutical industry. Steroids with a beta hydroxyl group at C-17, such as dihydrotestosterone (DHT), testosterone (T) or beta-estradiol (β-E2) are well known, that are responsible for reproductive tissues and secondary sex characteristics. β-E2 has a strong affinity to bind to estrogen receptors, while DHT and T can bind to and activate the androgen receptor. Still the interactions of steroids within the organism are rather diverse. Possible interactions include genomic actions of classical receptors, nongenomic actions of classical receptors as well as nongenomic actions of nonclassical receptors. Some signaling pathways can lead to indirect modulation of gene expression by modulation of transcription factors (see also Figure 6.3).[5] α-E2 was treated for a long time as the inactive isomer of estrogen β-E2, due to its low affinity towards the classical ERα and ERβ receptors.[6,7] By now, it has been shown that α-E2 is indeed an active steroid, such as in the rapid activation of MPAK/ERK with high potential.[8,9] A plasma membrane-associated estrogen receptor (ER-X), which was activated by α-E2 at a dose 100 fold lower than required for activation by β-E2 was found. α-E2 further protects a wide variety of cell types from different stressors and forestalls cell death. It is considered to be of therapeutic benefits concerning inflammation, Alzheimer's disease, Parkinson's disease, FRIEDREICH'S ataxia and amyotrophic lateral sclerosis.[10–13] Estrogens influence neuronal differentiation, survival and plasticity throughout life. Estrogens like E1 together with other synthetic estrogens are used in the treatment of osteoporosis and symptoms associated to the menopause.

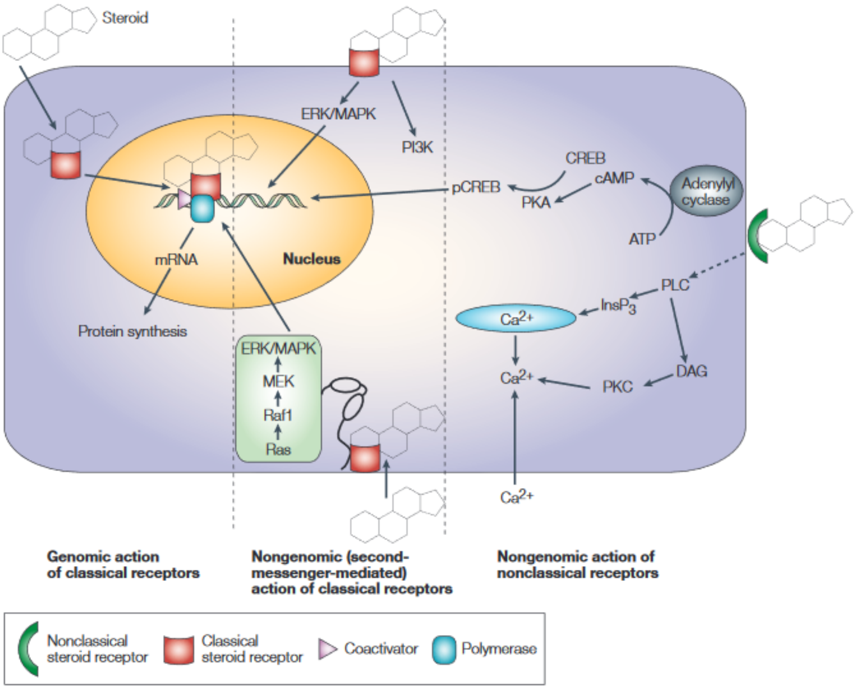
Steroid
ERK/MAPK
PI3K
CREB
cAMP
pCREB
PKA
Adenylyl cyclase
ATP
Nucleus
mRNA
Protein synthesis
PLC
InsP3
Ca2+
DAG
Ca2+
PKC
ERK/MAPK
MEK
Raf1
Ras
Ca2+
Genomic action of classical receptors
Nongenomic (second-messenger-mediated) action of classical receptors
Nongenomic action of nonclassical receptors
Nonclassical steroid receptor
Classical steroid receptor
Coactivator
Polymerase

Reprinted (adapted) with permission from (*Nat. Rev. Mol. Cell Biol.* **2003**, *4*, 46-56). Copyright (2003) Nature Publishing Group

Figure 6.3. Numerous actions of steroids by different pathways

The term ANGELS (Activators of Non-Genomic Estrogen-Like Signaling) was coined by MANOLAGAS *et al.* for small molecules that mimic the non-genomic interactions of estrogens. These ANGELS compounds lack the masculinizing or feminizing effects of hormonally more active analogues but are active in the formation of bone, including different 17α-hydroxysteroids (17α-OHs).[14,15] Estren (Δ^4-estren-3α,17β-diol) was reported as one particular example to increase bone mass without affecting reproductive organs or classical transcription. Whether estren is indeed an ANGELS compound is still controversial. It was shown in several experiments that the dissociation between genomic

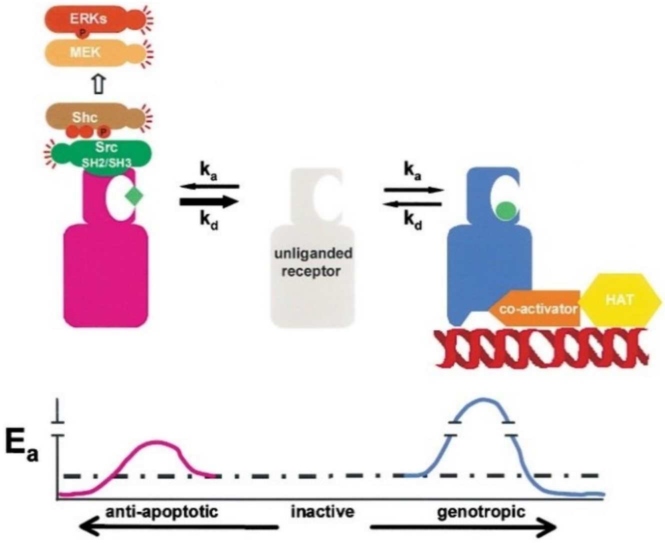

Reprinted (adapted) with permission from (*Mol. Pharmacol.* **2003**, *64*, 1428-1433). Copyright (2003) The American Society for Pharmacology and Experimental Therapeutics

Figure 6.4. Proposed model for ligand-induced dissociation of antiapoptotic from classical genotropic activity of sex steroid receptors

and nongenomic action is not achieved with this compound. Rather, it acts as an endrogen with comparable activity to β-E2.[16] Therefore, the search for selective ligands is still ongoing. In a different study, androstane-3β,17α-diol (α-EPIAdiol) was found to have anti-androgenic properties.[17,18] Anti-androgens and anti-endrogens are used in the treatment of certain tumours. Epitestosterone (E) is known to block androgenic action by inhibition of the 5α-reductase enzyme,[19] therefore, preventing the formation of more active DHT from T. E can be used as an internal standard for the assessment of unusual high levels of T in anti-doping tests,[20] through detection of the E/T ratio. E was further found to be an efficient agonist of OR51E2 receptor and was used in treating or preventing the progression of prostate cancer.[21] Still, less is known about its biological actions compared to the 17β-epimer T.

17-hydroxysteroids (17-OHs) can be directly derived through a hydrogenation of 17-oxosteroids 17-OXOs) using microorganisms.[22] This is especially true in the formation of 17β-OHs, whereas the formation of 17α-OHs is rather rare and only known for some individual compounds, such as 16,16-difluoro-17-ketosteroids.[23] Beside microorganisms, chemical reducing agents can be used in the reduction of ketosteroids. Biotransformation using microorganisms can be advantageous concerning stereo- and enantiospecificity for the production of chiral molecules. Biotransformations can be also cheaper than chemical transformations from the economic point of view. Nevertheless, it has been also observed that the reduction using microorganisms leads to the formation of various side products. Besides reduction of keto groups, additional hydroxylation or reduction of C=C bonds can occur on the steroid skeleton, leading to a decrease in final yield of the desired target steroid and complicating the purification and isolation of products. Working in aqueous media using biotransformations can lead to complications, due to low solubility of reaction substrates. The use of NADH or NAHPH as hydrogen source requires further regeneration procedures.

Formation of side products during reduction of ketosteroids is well documented. Thus, reduction of $\Delta^{1,4}$-Androstadiene-3,17-dione (ADD) at C-17 in the formation of Δ^1-testosterone (Δ^1-T) using *Mucor racemosus* was accompanied by hydroxylation at C-6β, C-14α and C-15α. Therefore, a number of side products was formed during reduction of ADD (see Figure 6.5).[24]

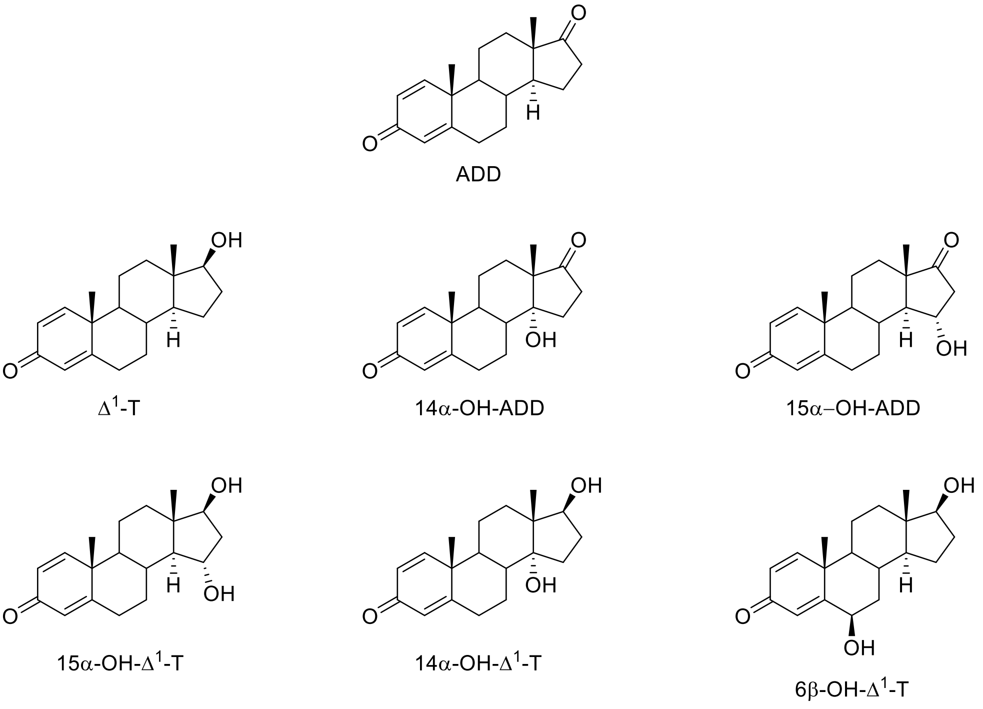

Reprinted (adapted) with permission from (*J. Chem. Technol. Biotechnol.* **2009**, *84*, 1021-1025). Copyright (2009) Society of Chemical Industry

Figure 6.5. ADD and products formed from reduction using *Mucor racemosus*

Using *Microbacterium sp.* NRRL B-3683 in the reduction of ADD led to a double reduction of both, the keto group at C-17 and 1,2 C=C bond. Cholesterol was converted to A4 and T as the main products reported by LIU *et al.* HUNG *et al.* also found that A4 is not converted directly to form T (see Scheme 6.1, below). Rather an equilibrium is formed between ADD and A4. T is formed from ADD through an intermediate compound, which is assumed to be Δ^1-T.[25,26]

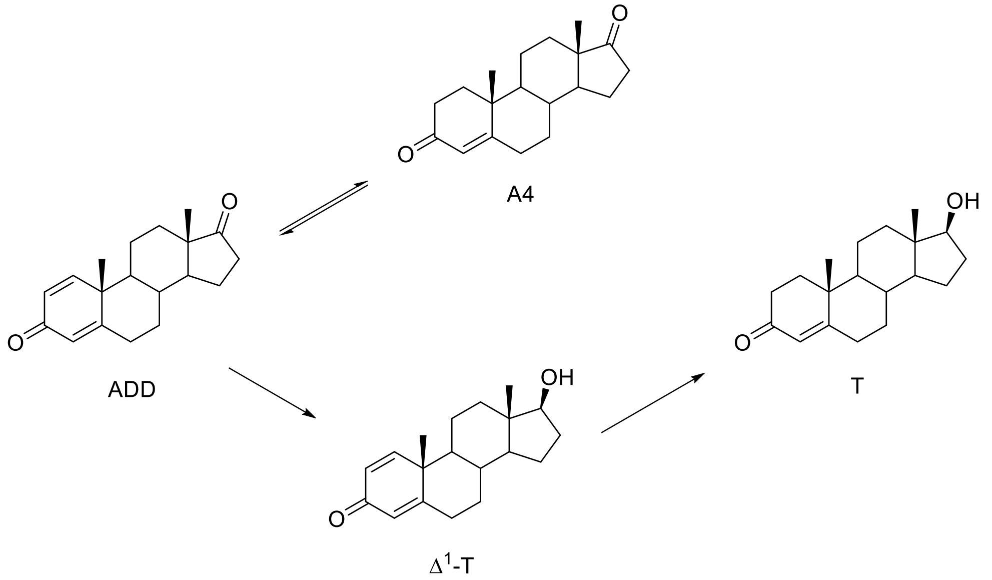

Reprinted (adapted) with permission from (Biotechnol. Lett. **1994**, *16*, 497-500). Copyright (1994) Kluwer Academic Publishers

Scheme 6.1. Proposed reaction pathway for the formation of T from ADD using *Microbacterium sp.* NRRL B-3683

Various side products are observed in the reduction of A4 using *Bacillus sp.* leading to a complex mixture of products. Besides hydrogenation of the keto group at C-17, leading to the formation of T, additional monohydroxylation at C-6, C-7, C-11 and C-14 was observed. Products that can be assigned to a posible reaction pathway are depicted in Scheme 6.2 below.[27]

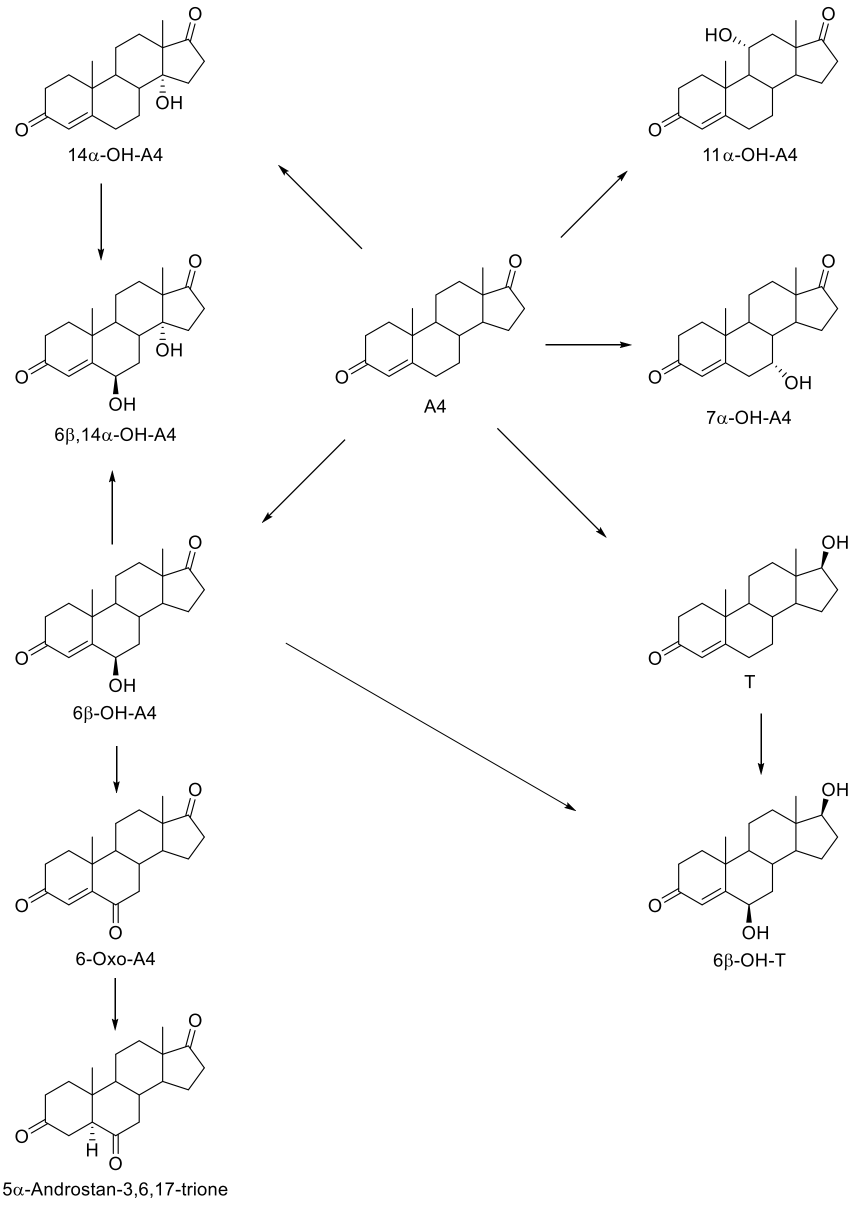
14α-OH-A4
11α-OH-A4
6β,14α-OH-A4
A4
7α-OH-A4
6β-OH-A4
T
6-Oxo-A4
6β-OH-T
5α-Androstan-3,6,17-trione

Reprinted (adapted) with permission from (*J. Steroid Biochem. Mol. Biol.* **1998**, *67*, 451-465). Copyright (1999) Elsevier Ltd.

Scheme 6.2. Formation of various products during reduction of A4 with proposed reaction pathway, using *bacillus sp.*

Besides biotransformation, chemical routes can also be used for reduction of ketosteroids. In particular, reduction of 17-OXOs using chemical reducing agents, such as $NaBH_4$ or $LiAlH_4$ leads exclusively to the formation of the corresponding 17β-OH (Scheme 6.3).[28] Concerning the synthesis of 17α-OHs, most efforts have been put into the inversion of the 17β-OH group, using MITSUNOBU reactions[29,30] or the displacement of sulfonyl ester.[31–33] These procedures however introduce additional reaction steps, which further complicate the preparation of the desired target molecules and decrease the final yields. In addition, protection/deprotection reactions include the use of expensive or non-commercial reagents. Using chemical reducing agents, it is observed that the keto group at C-3 is much more reactive than a keto group at C-17 or C-20.[34] This leads to decreased regioselectivities when the 17-OH compound is sought and additional keto groups, especially at C-3, are present in the substrate.

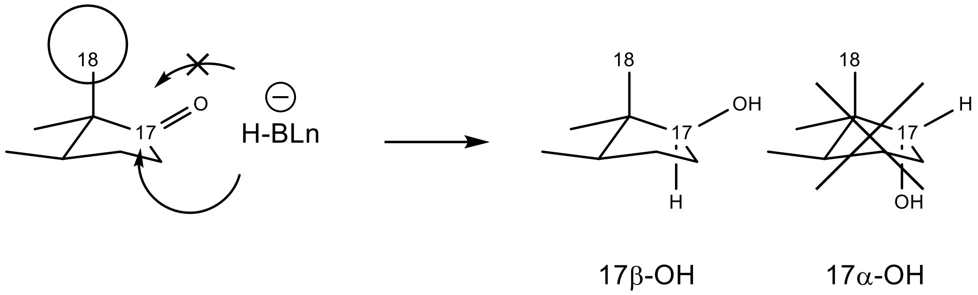

Scheme 6.3. Stereoselective reduction of 17-OXOs by $NaBH_4$ *via* an axial hydride attack

In Chapter 4 of this thesis, MOF-808 was shown to be an active catalyst in the MPV reduction of ketones to their corresponding alcohols. Its catalytic activity was higher compared to the UiO-66 MOF. This higher activity was attributed to the larger number of Zr^{4+} *cus*, which are created upon removal of formate ions from the SBU during the activation of the catalyst. The wider structure of the framework with pore openings of 14 Å and large adamantane shaped cavities of 18.4 Å enables the conversion of bulkier substrates, which can diffuse within the porous network of the material. As we have shown in Chapter 4, E1 with dimensions of approximately 11.2 x 6.2 x 4.2 Å can be readily reduced using MOF-808 as the catalyst, while UiO-66 stayed almost completely inactive. It was further observed, that the MOF structure introduces diastereoselectivity in the conversion of E1 and a number of substituted CHs (see Chapter 5). This diastereoselectivity not only depends on the type and position of substituents on the substrate. Also the reducing agent (^{i}PrOH or ^{s}BuOH) used in the reduction of ketones was found to influence the d.r. of products. In previous experiments, α-E2 was synthesized through a MPV reaction with a d.r. of 40%, using ^{i}PrOH as the reducing agent. Although the diastereoselectivity towards the α-isomer was only moderate, it has to be pointed out, that α-E2 was prepared in a single step through the reduction of E1. Avoiding additional protection/deprotection steps as required for instance in the

MITSUNOBU type process. In view of these interesting results, herein, we investigate in more detail the MPV reduction of E1 using MOF-808 as the catalyst. Studies are also extended to other 17-OH compounds of pharmaceutical interest, as mentioned above in the introduction.

6.2. Catalytic results (reduction of 17-OXOs)

The catalytic properties of MOF-808 were evaluated in the reduction of a series of 17-OXOs (E1, EPIA and A4, Scheme 6.4). The results were compared with different Zr-containing catalysts and other well-known MPV reduction catalysts. Different reducing alcohols were studied and the influence of the reaction temperature on the catalytic results was evaluated. The MOF-808 used in the following catalytic studies described below was prepared as described in the Annexes (Section 8.1). The general procedure used for the MPV reduction of steroids is also described in detail in the Annexes (Section 8.4), while specific reaction conditions are indicated in the corresponding tables and figures below.

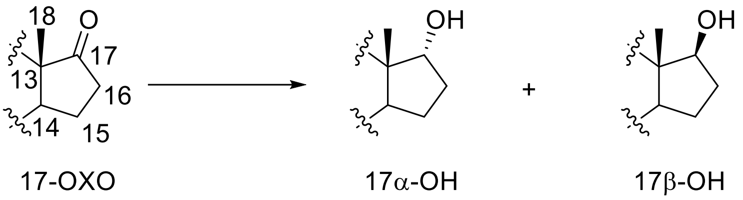

Scheme 6.4. General representation for the reduction of 17-OXOs to their 17α-OH and 17β-OH diastereoisomers

6.2.1. Diastereoselective reduction of estrone (E1)

E1 can be readily converted by MOF-808 as the catalyst, yielding in the formation of two epimers α-E2 and β-E2 (Scheme 6.5). Therefore, the newly formed -OH group at C-17 can be in axial or equatorial position for α-E2 and β-E2, respectively; i.e., in *anti* or *syn* configuration with respect to the 18-CH_3 group. The 5-membered D-ring forms a C-13-β-envelope for α-E2 and β-E2, which was studied by GUO *et al.* using liquid NMR analysis and restrained molecular dynamics. Steric interactions between the C-18 CH_3 and C-17 -OH groups in β-E2 give a slight distortion of C18-C13-C17 with respect to α-E2.[35]

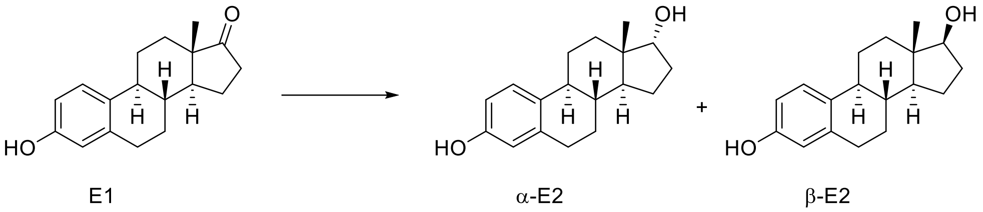

Scheme 6.5. Diasereoselective reduction of E1

When conducting the reduction of E1 in ^{i}PrOH almost full conversion is achieved after 8 h (97%). The corresponding turnover frequency (TOF) derived at short reaction times is calculated as 2.44 h^{-1}. When conducting the reduction in ^{s}BuOH, the reaction proceeds slightly slower but almost full conversion is achieved after 8 h (91%) and a TOF of 1.33 h^{-1} is obtained. The reaction also proceeds smoothly in pentan-2-ol (^{s}PentOH) and 1-phenylethan-1-ol. α-E2 and β-E2 derived through reduction of the carbonyl group at C-

Table 6.1. Summary of catalytic results for the MPV reduction of E1 over various catalysts

Entry	Catalyst	Alcohol	Conv. (time)[a]	TOF (h^{-1})[b]	d.r.[c] (α-E2/β-E2)
1	MOF-808	^{i}PrOH	97% (8 h)	2.44	60/40
			100% (24 h)		
2	MOF-808	^{s}BuOH	91% (8 h)	1.33	87/13
			100% (24 h)		
3	MOF-808	^{s}PentOH	92% (8 h)	2.11	73/28
4	MOF-808	1-phenylethan-1-ol	97% (8 h)	2.77	60/40
5	ZrO_2	^{s}BuOH	2% (24 h)	-	44/56
6	$ZrCl_4$	^{s}BuOH	13% (24 h)	-	50/50
7	Zr-BEA[d]	^{s}BuOH	2% (24 h)	-	65/35
8	Zr-MCM-41[d]	^{s}BuOH	2% (24 h)	-	52/48
9	$Zr(O^{i}Pr)_4$*^{i}PrOH	^{s}BuOH	2% (24 h)	-	50/50
10	$Al(O^{i}Pr)_3$	^{s}BuOH	11% (24 h)	-	34/66
11	$NaBH_4$		99% (24 h)	-	3/97

[a] Determined by GC; [b] moles of E1 converted per mol of Zr and per hour of reaction; [c] determined by ^{1}H-NMR and [d] for preparation and characterization of catalysts see Annexes, (Section 8.4).

17 were the only products detected in any case and a selectivity of 100% can be ascribed to this process (see Table 6.1, entry 1-4).

Different Zr-containing catalysts (Table 6.1, entry 5-8) and established MPV reduction catalysts (Table 6.1, entry 9 and 10) were compared using optimized reaction conditions for MOF-808 towards α-E2. As can be seen, activities of tested catalysts were much lower compared to MOF-808 under the same reaction conditions. E1 reduction using $NaBH_4$ forms as expected almost exclusively β-E2 (Table 6.1, entry 11). To determine the d.r. (α-E2/β-E2, Table 6.1), the crude product was also analyzed by ^{1}H-NMR at the end of the reaction as detailed in the Annexes (Section 8.4). In the previous Chapter 4, MOF-808 afforded a diastereoselectivity of 40% towards α-E2 using ^{i}PrOH at 353 K. Hence, the diastereoselectivity in the present case with ^{i}PrOH at 393 K is considerably higher with a α-E2/β-E2 ratio of 60/40, leaving α-E2 the major product of the reaction (see also Table 6.1, entry 1). This enhanced diastereoselectivity is probably related with improvements in the preparation and washing procedure used and corresponding removal of formate ions from the catalyst. As it will be shown later, the reaction temperature does not have a major impact on the diastereoselectivity of the reaction. The diastereoselectivity is further improved, when conducting the reaction in ^{s}BuOH. The α-E2/β-E2 ratio increased to 87/13 (Table 6.1, entry 2) at a conversion of 91%, corresponding to the reaction progress at 8 h. The stability and reusability of MOF-808 was, therefore, tested at optimized conditions, using ^{s}BuOH at 393 K. MOF-808 could be used for at least six consecutive runs without loss of crystallinity. The activity and diastereoselectivity was maintained for all catalytic cycles as can be seen from Figure 6.6.

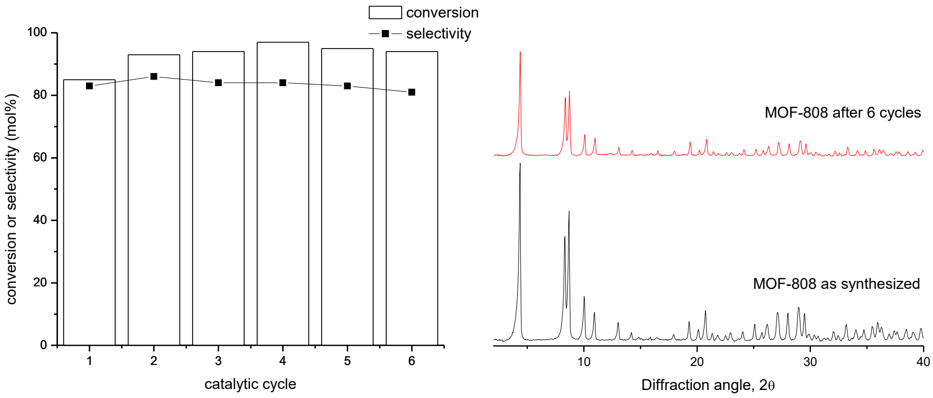

Figure 6.6. Reusability of MOF-808 in the reduction of E1 and diastereoselectivity towards α-E2 (left) and X-ray powder diffraction pattern of MOF-808 before reaction and after six consecutive runs (right)

6.2.1.1 *Influence of the reaction temperature*

The influence of the reaction temperature in the reduction of E1 was assessed. Therefore, the reaction kinetics were followed in the temperature range of 353-403 K (see Figure 6.7). The d.r. was determined by ^{1}H-NMR after each reaction. Independent of the alcohol used a distinct increase in activity was observed when raising the temperature from 353 K to 403 K. For ^{i}PrOH full conversion was achieved after 4 h at 403 K, while the conversion reached 83% at 353 K after 48 h. Thus, the TOF increased from 0.78 h^{-1} to 9.11 h^{-1} in ^{i}PrOH in the range of 353-403 K. The same trend is observed when the reaction is conducted in ^{s}BuOH. Full conversion is achieved at 403 K after 8 h, while the reaction proceeds significantly slower, reaching a conversion of 68% at 353 K after 48 h. Thus, the TOF is increasing from 0.33 h^{-1} to 3.78 h^{-1} at 353 K and 403 K, respectively. Apart from the alcohol used, the diastereoselectivity stays almost unchanged over the 353-403 K temperature range (see insets in Figure 6.7). The diastereoselectivity is mainly influenced by the choice of alcohol (^{i}PrOH or ^{s}BuOH). This further suggests that the reaction takes place at the reactive Zr^{4+} sites inside the cavities of MOF-808 and that the diastereoselectivity is primary driven by cavity confinement effects through transition state selectivity.

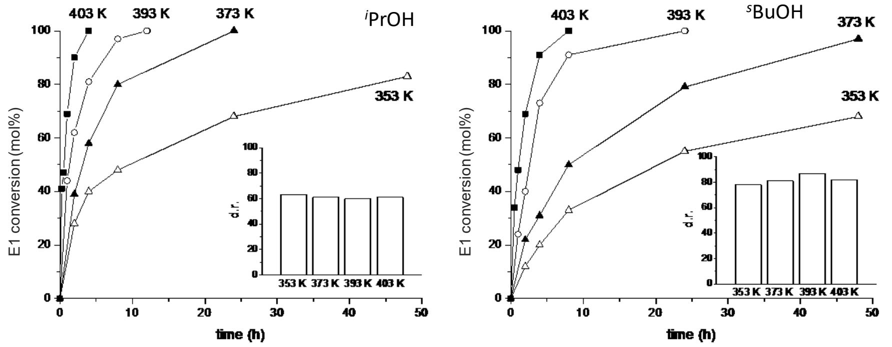

Figure 6.7. Time conversion plots for the MPV reduction of E1 over MOF-808 using ^{i}PrOH (left) or ^{s}BuOH (right) in the temperature range 353-403 K. In each plot, the inset shows the d.r. of the reaction (α-E2/β-E2)

a) Kinetic analysis

Catalytic results using ^{i}PrOH or ^{s}BuOH in the 353-403 K range were further used to calculate kinetic rate constants k_α and k_β, for both diastereoisomers, α-E2 and β-E2. The detailed procedure used is given in the Annexes (Section 8.4). To determine apparent activation energies E_a for α-E2 and β-E2 the slope of the Arrhenius equation was determined. The intercept in the Arrhenius plot (see Figure 6.8) with the y-axis was further used to determine the pre-exponential factors (k_0), which are related to entropic factors. From the values obtained corresponding to E_a for α-E2 and β-E2, it can be seen

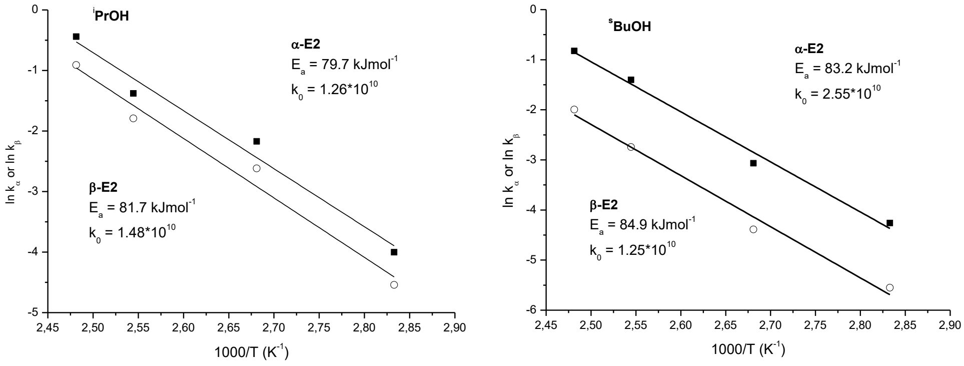

Figure 6.8. Arrhenius plots from the conversion of E1to α-E2 and β-E2 in ^{i}PrOH (left) and ^{s}BuOH (right), with calculated apparent activation energies (E_a) and pre-exponential factors (k_0) for each compound

that the differences are not very high, in both cases, for reactions conducted in ^{i}PrOH or ^{s}BuOH. Therefore, values of E_a for α-E2 and β-E2 in ^{i}PrOH are 79.7 kJmol^{-1} and 81.7 kJmol^{-1}, which gives a ΔE_a of 2 kJmol^{-1}. In ^{s}BuOH values of E_a are 83.2 kJmol^{-1} and 84.9 kJmol^{-1} for α-E2 and β-E2, respectively, which gives a ΔE_a of 1.7 kJmol^{-1}. In both cases, higher E_a values are obtained for β-E2, which is also reflected in the selectivity towards α-E2. Further, values for E_a obtained from the reaction conducted in ^{s}BuOH are higher compared to ^{i}PrOH. This is also reflected in the faster reaction kinetics, as reactions were faster if conducted in ^{i}PrOH compared to ^{s}BuOH. k_0 values obtained for α-E2 and β-E2 are 1.26*10^{10} and 1.48*10^{10} in ^{i}PrOH and 2.55*10^{10} and 1.25*10^{10} in ^{s}BuOH. Still, at this point it is difficult to say which factor drives the reaction towards preferential formation of α-E2 over β-E2.

To further investigate results concerning the diastereoselectivity, the EYRING-POLANYI equation was used, which allows the direct calculation of entropy ($\Delta S^‡$), enthalpy ($\Delta H^‡$) and GIBBS energy ($\Delta G^‡$) of activation from kinetic data (see Annexes, Section 8.4 for the E-P plots obtained). Unlike the ARRHENIUS equation, which is an empirical model, the EYRING-POLANYI equation is derived from the transition state theory and the values correlate to changes in energy upon formation of the TS complex during reaction. At this point, it has to be mentioned that the MPV reduction of E1 is expected to proceed *via* an activated complex (TS, see Figure 6.9). Upon coordination of the secondary alcohol and the carbonyl compound to the zirconium site, a six-membered cyclic TS is formed, where the hydride shift to the carbonyl carbon takes place.

As it can be seen in Table 6.2, in the case of ^{s}BuOH at 393 K the TS leading to α-E2 is clearly preferred by -4.1 kJmol^{-1} for $\Delta G^‡$. In the case of ^{i}PrOH the difference in $\Delta G^‡$ = -1.4 kJmol^{-1} is significantly lower and a higher selectivity towards α-E2 in

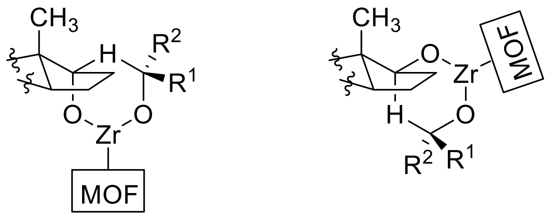

α-E2 **β-E2**

^{i}PrOH: $R^1 = R^2 = CH_3$

^{s}BuOH: $R^1 = CH_3$; $R^2 = CH_2CH_3$

Figure 6.9. Proposed structure of the two posible TSs in the MPV reduction of E1 with ^{i}PrOH or ^{s}BuOH over MOF-808

Table 6.2. Enthalpy ($\Delta H^{\ddagger}$), entropy ($\Delta S^{\ddagger}$) and Gibbs energy ($\Delta G^{\ddagger}$) of activation for the formation of α-E2 and β-E2 over MOF-808 using ^{i}PrOH and ^{s}BuOH. The bottom part of the table shows the differences in energy of the TSs leading to α-E2 and β-E2 (α-β) in terms of Gibbs energy, and the corresponding enthalpic ($\Delta H^{\ddagger}$) and entropic contributions ($T\Delta S^{\ddagger}$)

		$\Delta S^{\ddagger}$ ($Jmol^{-1}K^{-1}$)	$-T\Delta S^{\ddagger a}$ ($kJmol^{-1}$)	$\Delta H^{\ddagger}$ ($kJmol^{-1}$)	$\Delta G^{\ddagger a}$ ($kJmol^{-1}$)
^{i}PrOH	α-E2	-61.8	24.3	76.6	100.9
	β-E2	-60.5	23.8	78.5	102.3
^{s}BuOH	α-E2	-56.0	22.0	80.0	102.0
	β-E2	-61.9	24.3	81.8	106.1
		$\Delta S^{\ddagger}$ ($Jmol^{-1}K^{-1}$)	$-T\Delta S^{\ddagger a}$ ($kJmol^{-1}$)	$\Delta H^{\ddagger}$ ($kJmol^{-1}$)	$\Delta G^{\ddagger a}$ ($kJmol^{-1}$)
α-β	^{i}PrOH	-1.3	+0.5	-1.9	-1.4
	^{s}BuOH	+5.9	-2.3	-1.8	-4.1

[a] Calculated at 393 K

^{s}BuOH can be expected. In both cases, negative $\Delta S^{\ddagger}$ values are obtained, which correlates to a more ordered TS and loss in entropy. In ^{s}BuOH the loss in entropy is lower for α-E2 than for β-E2 (-56.0 vs -61.9 $Jmol^{-1}K^{-1}$), which corresponds to a difference of +5.9 $Jmol^{-1}K^{-1}$. Also changes can be seen when comparing the entropic contributions to $\Delta G^{\ddagger}$ for ^{i}PrOH and ^{s}BuOH. In the case of ^{s}BuOH the entropic and enthalpic term are lowering the energy for α-E2 compared to β-E2. In the case of ^{i}PrOH, the enthalpic term is lower for α-E2, whereas the entropic term ($-T\Delta S^{\ddagger}$ = 23.8 $kJmol^{-1}$) is lower for β-E2. This leads to decreased difference in $\Delta G^{\ddagger}$ for ^{i}PrOH, since both terms are partially counteracting each other. As a result, lower selectivity towards α-E2 is obtained with ^{i}PrOH compared to ^{s}BuOH. The results further suggest that the reaction takes place inside the cavities of MOF-808. The pore space favors the formation of the TS leading to α-E2 rather than β-E2. This effect is more pronounced when the reaction is conducted in ^{s}BuOH, compared to ^{i}PrOH. As the alcohol directly participates in the formation of the TS, it is not surprising that a relation between the alcohol and the d.r. is observed in the reduction of E1.

Following a similar approach as that described in the previous Chapter 5 for the MPV reduction of substituted CHs, we have examined the possible structures of the two TSs leading to α-E2 and β-E2 formed inside the cavities of MOF-808. A schematic view of both TSs is shown in Figure 6.10. Although more detailed calculations are already underway to estimate the energetic characteristics of the system, it can be observed that the TS leading to the α-E2 product is more tightly locked in place and stabilized by up to 4 hydrogen bonds with d(O···H) comprised between 2.4-2.6 Å (indicated by the arrows in Figure 6.10), while in the case of β-E2, there is only one such short hydrogen bond.

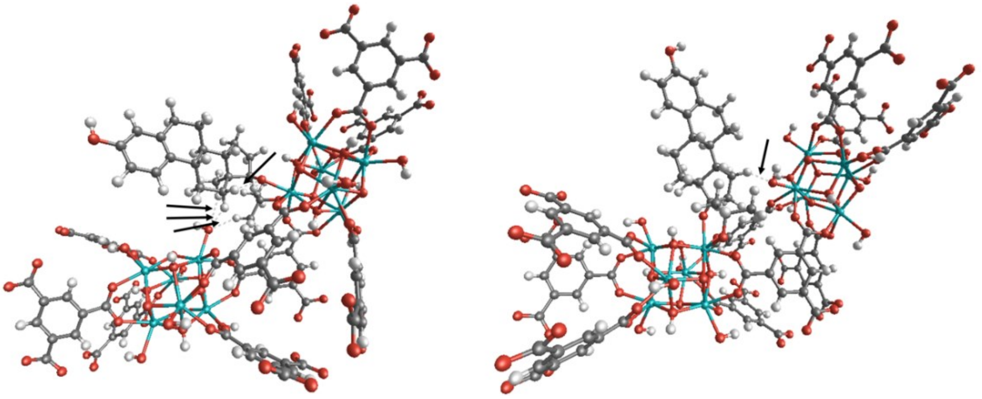

Figure 6.10. Schematic view of the two TSs formed in MOF-808 leading to α-E2 (left) and β-E2 (right). Short hydrogen bond contacts (d(O···H) = 2.4-2.6 Å) are indicated by black arrows

A schematic representation of the differences in energy for α-E2 and β-E2, using ^{i}PrOH or ^{s}BuOH is shown in Figure 6.11, below. For reactions conducted in ^{s}BuOH, the entropic term contributes in further lowering the energy of the TS, which strongly indicates, that confinement effects and steric hindrance inside the MOF pores are responsible for the preferred reaction path leading to the formation of α-E2. In the case of ^{i}PrOH, the entropic term is partly neutralizing the enthalpic term, which leads to decreased difference ($\Delta G^{\ddagger}$ = -1.4 kJmol^{-1}) in energy for α-E2 and β-E2. As a consequence, the diastereoselectivity towards α-E2 is reduced, when conducting the reaction in ^{i}PrOH compared to ^{s}BuOH.

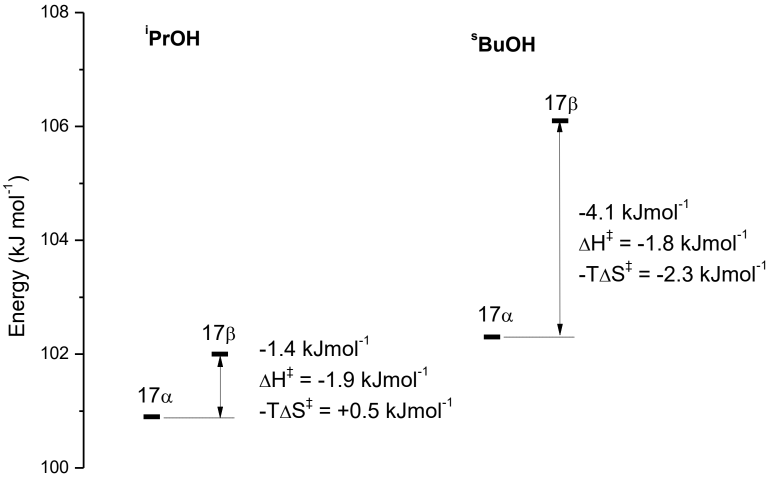

Figure 6.11. Schematic energy diagram showing the calculated energies (ΔG‡) of the activated complexes leading to α-E2 and β-E2 in ^{i}PrOH (left) and ^{s}BuOH (right) and the corresponding enthalpic and entropic contributions

6.2.2. Diastereoselective reduction of 5α-androstan-3β-ol,17-one (or epiandrosterone, EPIA)

Given the excellent diastereoselectivity obtained towards α-E2 in the reduction of E1 using MOF-808 as the catalyst, the scope of this study was further extended to the reduction of other 17-OXOs. Therefore, EPIA was considered as another example, since it contains a keto group at C-17 analogous to E1. The diastereoselectivity in the reduction

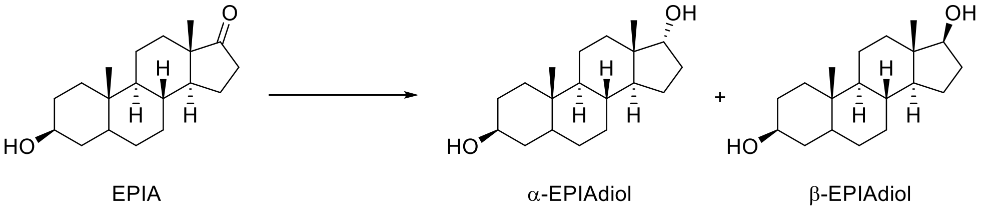

Scheme 6.6. Reduction of EPIA can yield a mixture of α-EPIAdiol and β-EPIAdiol

of EPIA was studied, regarding the conformation of the newly formed -OH group with respect to the 18-CH_3 group (see Scheme 6.6).

As it is also the case of E1, the C-18 CH_3 group is also expected to have a strong influence on the diastereoselectivity in the reduction of EPIA. For instance, the reduction with $NaBH_4$ almost exclusively leads to the formation of 5α-androstan-3β,17β-diol (β-EPIAdiol) and only traces or minor quantities of 5α-androstan-3β,17α-diol (α-EPIAdiol) are formed. Therefore, the hydride attack in most cases is preferred from the α-face, due to steric hindrance of the C-18 CH_3 group. However, as it was the case of E1 described above, the use of MOF-808 as the catalyst leads in the reduction of EPIA to the preferred formation of the α-EPIAdiol epimer. This diastereoselectivity is analogous to the reduction of E1 more pronounced when the reaction is performed in ^{s}BuOH compared to ^{i}PrOH with a d.r. of 84% and 77%, respectively (Figure 6.12). In both cases, α-EPIAdiol and β-EPIAdiol were the only products detected. The catalyst was found to be stable and reusable under the reaction conditions.

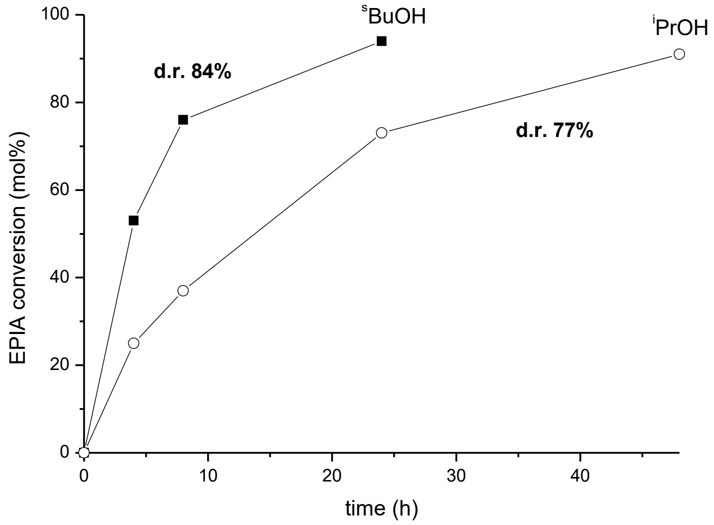

Figure 6.12. MPV reduction of EPIA to androstandiols using ^{i}PrOH and ^{s}BuOH. The obtained diastereoselectivity (d.r.) to α-EPIAdiol is indicated. d.r. was calculated by ^{1}H-NMR of the filtrate at the end of the reaction

Together with the results from the reduction of E1, it can be concluded that MOF-808 serves as a stable and reusable catalyst in the diastereoselective reduction of 17-OXOs to their corresponding 17α-OHs. Other existing hydride-transfer compounds often have to be used in stoichiometric quantities and result usually in the formation of corresponding 17β-OHs. The synthesis of 17α-OHs usually requires several synthetic steps as well as toxic and/or expensive reagents, which also leads to lower final yields. Therefore, the use of MOF-808 can serve as an attractive alternative in the preparation of 17α-OHs.

6.2.3. Regio-, chemo- and diastereoselective reduction of Δ⁴-androstene-3,17-dione (A4)

One major advantage of the MPV reduction is, that it can be applied to the reduction of keto groups, while other reducible groups, such as C=C bonds stay intact. Therefore, not only diastereoselective but also chemoselective MPV reductions can be conducted, which is highly desirable in the transformation of more complex molecules. In the presence of different keto groups, regioselectivity can become a further issue. Therefore, different mono- and polyhydroxylated compounds can be formed. This is the case if for instance an unsaturated ketone or enone is present, since more than one keto group can be reduced, which results in the formation of various diols.

To evaluate also the regio- and chemoselectivity, Δ^4-androstene-3,17-dione (A4) was choosen as a substrate, which contains a C=C bond at C-4, as well as two keto groups at C-3- and C-17.

Reactions were conducted at varying temperatures, in ^{i}PrOH or ^{s}BuOH. In all cases, no reduction at the C=C bond was observed and the reduction can be considered as fully chemoselective. Further, no monoreduction at C-3 was observed. Therefore, reduction takes places preferentially at C-17, resulting in the formation of Δ^4-androstene-17β-ol-3-one (or testosterone, T) and Δ^4-androstene-17α-ol-3-one (or epitestosterone, E). Further secondary reduction at C-3 leads to the formation of additional diol isomers (see Scheme 6.7). Due to two possible configurations of the –OH group at C-3- and C-17, four diol isomers Δ^4-androstene-3α,17α-diol, Δ^4-androstene-3α,17β-diol, Δ^4-androstene-3β,17α-diol and Δ^4-androstene-3β,17β-diol can be formed.

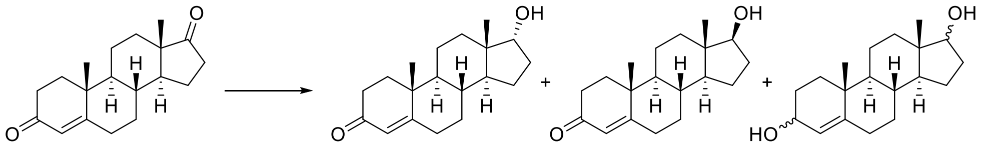

Scheme 6.7. MPV reduction of A4 over MOF-808 yields T, E and a mixture of diol isomers with various local configuration of the -OH groups at C-3- and C-17

Figure 6.12 shows the time-conversion plot for a reaction conducted in ^{s}BuOH at 353 K with the product distribution corresponding to mono- (E+T) and dihydroxylated (diol) products. An overall A4 conversion of 89% is already achieved after 8 h. Results for a reaction in ^{i}PrOH at 353 K were very similar.

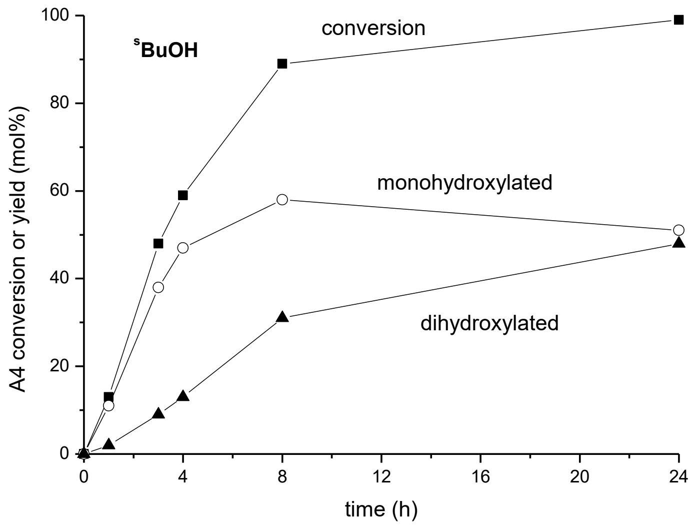

Figure 6.13. (-■-) A4 conversion; (-○-) yield of monohydroxylated products (T + E); and (-▲-) yield of dihydroxylated products obtained over MOF-808 with ^{s}BuOH at 353 K

From Figure 6.13 it can be seen, that first reduction takes place at C-17, yielding a mixture of monohydroxylated compounds (T + E). Afterwards, reduction takes also place at C-3, which results in the formation of a mixture of diol isomers. The yield of monohydroxylated products is increasing during the first 8 h, until a maximum of 58% is reached. Afterwards the ongoing formation of diol isomers at the expenses of monohydroxylated compounds leads to a decrease in final yield of monohydroxylated compounds (T + E).

The d.r. (E/T) of monohydroxylated products at C-17 was determined from ^{1}H-NMR spectra, as described in the Annexes (Section 8.4). The values obtained were very high and in all cases less than 5% of T were present. As can be seen from the reaction kinetics, the lower final yield of E also results from partial reduction at C-3 and formation of additional diol isomers.

In order to improve further the final yield of E, by minimizing the amount of diols formed during reaction, different temperatures were tested ranging from 333-393 K. Figure 6.14 shows the conversion curves for A4 and the selectivity-conversion plots obtained as a function of temperature. From Figure 6.14 it can be seen that a maximum selectivity towards monohydroxylated compounds (E + T) of around 85% is achieved at a conversion of 10–20%. Afterwards, selectivity drops continuously as the conversion

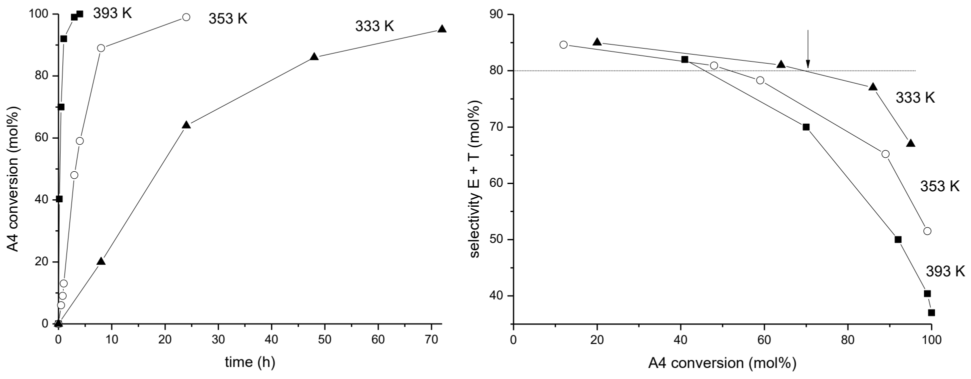

Figure 6.14. A4 conversion over MOF-808 in ^{s}BuOH at the indicated temperature (left) and selectivity to monohydroxylated products (E + T) as a function of conversion and temperature (right)

proceeds and a faster drop in selectivity is observed at higher temperatures. Therefore, increasing the reaction temperature has a clear detrimental effect on the selectivity to monohydroxylated products (T + E). Nevertheless, if the reaction temperature is kept as low as 333 K, a selectivity towards monohydroxylated compounds (E + T) of above 80% can be maintained, corresponding to a conversion of 70-80%, after 30-35 h of reaction (as indicated by an arrow in Figure 6.14). The d.r. towards E in monohydroxylated products is kept at >95%. This shows that E can be directly obtained with a very high yield and purity through reduction of A4 and points towards a preferred reduction of the keto group at C-17 to the corresponding 17α-OH, E. This is in line with the previous discussed examples of E1 and EPIA reduction, where the 17α-OH (α-E2 or α-EPIAdiol) is the major product of the reaction.

From the reduction of A4, it can be summarized that MOF-808 affords a very good selectivity towards E, according to several factors. The C=C bond at C-4 remains intact under the reaction conditions used, leading to a chemoselectivity of 100%. No products from monohydroxylation at C-3 have been detected. Therefore, the carbonyl group at C-17 is selectively reduced before the carbonyl (enone) group at C-3 leading to a regioselectivity of 100%. The diastereoselectivity during reduction at C-17 produces preferentially E, resulting in a final d.r. of E/T >95%. The 17α-OH isomer is selectively formed, as in the case of E1 and EPIA reduction, with excellent diastereoselectivity. Despite the eventual reduction of both carbonyl groups taking place at long reaction times, it is possible to minimize the formation of diols by proper selection of the reaction conditions, allowing very high A4 conversions while keeping very good selectivity (>80% to monohydroxylated compounds).

6.3. Conclusions

In the reduction of different 17-OXOs (E1, EPIA and A4) to their corresponding 17-OHs, MOF-808 served as a selective catalyst, which can be reused several times without any loss of activity and selectivity. On the one hand, the open porous structure with pores and pore openings of sufficient size, allows the conversion of bulky steroid compounds. Substrates can readily diffuse within the structure to and from the Zr^{4+} active sites. As a consequence, MOF-808 shows high activity in the MPV reduction allowing coordination of carbonyl compounds and different secondary alcohols, which are used as a hydride source in this process. On the other hand, diastereoselectivity was introduced by the MOF structure, leading to the formation of corresponding 17α-OHs. This is in contrast to most existing processes including biotransformations and chemical routes were almost exclusively the corresponding 17β-OHs are formed. Therefore, MOF-808 serves as an attractive alternative in the formation of challenging compounds, which was shown in the synthesis of three different 17α-OHs, denoted as α-E2, α-EPIAdiol and E.

The reactions were analyzed by following the kinetics at different temperatures and determining the d.r. according to the choice of alcohol. Conducting reactions in ^{s}BuOH gave highest selectivities to the corresponding 17α-OHs. Temperature dependent kinetic analysis was used in the determination of apparent activation energies, in either ^{i}PrOH or ^{s}BuOH. From a close inspection using the EYRING-POLANYI equation, it was shown that the entropic factor is crucial, concerning the diastereoselectivity towards α-E2 in the reduction of E1. Therefore, enthalpic and entropic contribtions are partially counteracting each other in the case of ^{i}PrOH, leading to a decreased d.r. (α-E2/β-E2). In the case of ^{s}BuOH, both factors are in favor for α-E2, which is also reflected in a higher d.r. towards α-E2. This supports that the secondary alcohol is directly influencing the formation of α-E2 or β-E2 during the formation of the six-membered ring TS where the carbonyl compound and the secondary alcohol are simultaneously coordinated to the active Zr^{4+} metal sites. Further, the selectivity is driven by cavity confinement effects, which are favoring the formation of α-E2 and which is more pronounced when conducting reactions in ^{s}BuOH.

In the MPV reduction of A4, excellent chemo-and regioselectivity is observed. The C=C bond at C-4 stays intact at selected reaction conditions. Further, the keto group at C-17 is selectively reduced before the keto (enone) group at C-3, giving a considerably high selectivity towards the formation of E.

6.4. References

1. Moss, G. P. *Pure. Appl. Chem.* **1989**, *61*, 1783.
2. Malaviya, A. & Gomes, J. *J. Ind. Microbiol. Biotechnol.* **2008**, *35*, 1235.
3. Kutney, J. P.; Herrington, E. J. & Spassov, G. WO 2003064674.

4. Buttgereit, F.; Burmester, G. R. & Lipworth, B. J. *Lancet* **2005**, *365*, 801.
5. Loesel, R. & Wehling, M. *Nat. Rev. Mol. Cell Biol.* **2003**, *4*, 46.
6. Nilsson, S. *et al. Endo.* **1997**, *138*, 863.
7. Snyder, M. A.; Smejkalova, T.; Forlano, P. M. & Woolley, C. S. *J Neurosci Methods.* **2010**, *188*, 226.
8. Toran-Allerand, C. D.; Tinnikov, A. A.; Singh, R. J. & Nethrapalli, I. S. *Endocrinology* **2005**, *146*, 3843.
9. Toran-Allerand, C. D. WO 2004029023.
10. Kaur, S. P.; Bansal, S. & Chopra, K. *Steroids* **2015**, *96*, 7.
11. Behl, C. *et al. Mol. Pharmacol.* **1997**, *51*, 535.
12. Dykens, J. A.; Moos, W. H. & Howell, N. *Ann. N. Y. Acad. Sci.* **2005**, *1052*, 116.
13. Santos, R. S.; Fatima, L. A. de; Frank, A. P.; Carneiro, E. M. & Clegg, D. J. *Biol. Sex Differ.* **2017**, *8*, 1.
14. Manolagas, S. C. *et al. Kidney Int.* **2004**, *66*, 41.
15. Manolagas, S. C. & Katzenellenbogen, J. A. WO2003002058.
16. Movérare, S. *et al. Mol. Pharmacol.* **2003**, *64*, 1428.
17. Bovee, T. F. H. *et al. J. Steroid Biochem. Mol. Biol.* **2010**, *118*, 85.
18. Wang, P.; Wen, Y.; Han, G. Z.; Sidhu, P. K. & Zhu, B. T. *Br. J. Pharmacol.* **2009**, *158*, 1796.
19. Nuck, B. A. & Lucky, A. W. *J Invest Dermatol.* **1987**, *89*, 209.
20. Stárka, L. *Endocr. Regul.* **1993**, *27*, 43.
21. Abaffy, T. & Matsunami, H. US 20180116992.
22. Donova, M. V.; Egorova, O. V. & Nikolayeva, V. M. *Process Biochem.* **2005**, *40*, 2253.
23. Charney, W. & Herzog, H. L. *Microbial Transformations of Steroids* In: New York, London: Academic Press, 1967, 728.
24. Faramarzi, M. A. *et al. J. Chem. Technol. Biotechnol.* **2009**, *84*, 1021.
25. Liu, W. H.; Kuo, C. W.; Wu, K. L.; Lee, C. Y. & Hsu, W. Y. *J. Ind. Microbiol.* **1994**, *13*, 167.
26. Hung, B.; Falero, A.; Llanes, N.; Pérez, C. & Ramírez, M. A. *Biotechnol. Lett.* **1994**, *16*, 497.
27. Schaaf, O. & Dettner, K. *J. Steroid Biochem. Mol. Biol.* **1998**, *67*, 451.

28. Wheeler & Wheeler. *Chapter 2 Reductions of Steroidal Ketones* In: Fried, J. & Edwards, J. A. (Eds.) *Organic Reactions in Steroid Chemistry*, Van Nostrand Reinhold Co., New York, 1972, 61.

29. Balssa, F.; Fischer, M. & Bonnaire, Y. *Steroids* **2014**, *86*, 1.

30. Dodge, J. A. & Lugar, C. W. *Bioorganic Med. Chem. Lett.* **1996**, *6*, 1.

31. Guo, P. P. & Ding, K. *Tetrahedron Lett.* **2015**, *56*, 4096.

32. Shi, X. X.; Shen, C. L.; Yao, J. Z.; Nie, L. D. & Quan, N. *Tetrahedron Asymmetry* **2010**, *21*, 277.

33. Nambara, T.; Numazawa, M. & Takahashi, H. *Chem. Pharm. Bull.* **1969**, *17*, 1725.

34. Göndös, G. & Orr, J. C. *Chem. Commun.* **1982**, *0*, 1239.

35. Jianxin Guo, Richard I. Duclos Jr., V. Kiran Vemuri, & A. M. *Tetrahedron Lett.* **2010**, *51*, 3465.

Chapter 7

Conclusions

The main conclusions that can be extracted from the results discussed in previous chapters are as follows:

1) It is possible to prepare defect-engineered MOF-808 materials (DE MOF-808) in which BTC ligands are partially replaced by dicarboxylate linkers: isophthalate (IPA), pyridine-3,5-dicarboxylate (Pydc), 5-hydroxyisophthalate (5-OH-IPA) and 5-aminoisophthalate (5-NH_2-IPA). The materials are all crystalline and isoreticular with parent MOF-808.
2) The DE MOF-808-IPA and MOF-808-Pydc materials prepared were found to be active for the MEERWEIN-PONNDORF-VERLEY (MPV) reduction of cyclohexanone (CH), with an activity higher than the pristine MOF-808, DUT-67 and UiO-66 compounds. This was attributed to a higher availability of the Zr^{4+} open metal sites due to missing coordination groups on defective linkers (DLs).
3) Unlike UiO-66, the wider pores in MOF-808 allow converting bulky substrates, as shown for the MPV reduction of estrone (E1). Interestingly, a noticeable diastereoselectivity to the elusive 17α-estradiol (α-E2) compound is observed.
4) MOF-808 is a diastereoselective catalyst for the MPV reduction of substituted cyclohexanones.
5) 3-methylcyclohexanone (3MeCH) is preferentially reduced to the corresponding *cis*-3-methylcyclohexanol (*cis*-3MeCHol) with both ^{i}PrOH and ^{s}BuOH as reducing agents. This selectivity is the opposite to found in BEA-type zeolites, which is attributed to the confinement of the reactions substrates in the cavities of MOF-808.
6) 2-methylcyclohexanone (2MeCH) is preferentially reduced by MOF-808 to the corresponding *trans*-2-methylcyclohexanol (*trans*-2MeCHol) with ^{i}PrOH reducing agents. Using ^{s}BuOH, the diastereoselectivity is inversed due to increasing bulkiness of the secondary alcohol. Again, this selectivity is the opposite to found in BEA-type zeolites, which is attributed to the confinement of the reaction substrates in the cavities of MOF-808.
7) 2-phenylcyclohexanone (2PhCH) is preferentially reduced to the corresponding *cis*-2-phenylcyclohexanol (*cis*-2PhCHol) with both ^{i}PrOH and ^{s}BuOH as reducing agent. The opposite diastereoselectivity compared to 2MeCH is most likely due to the steric effect of the large phenyl group at C-2. 2PhCH cannot be converted in BEA-zeolite.
8) The secondary alcohol directly influences the diastereoselectivity, as it participates in the formation of the transitions state (TS). From detailed kinetic study, activation energies GIBBS free energy were obtained using the EYRING-POLANYI equation. This was further confirmed by preliminary computational calculations for the reduction of 2MeCH and 3MeCH using ^{i}PrOH. It can be concluded, that the diastereoselectivity is driven by confinement effects and transition state selectivity inside the cavities of MOF-808.

9) MOF-808 can be used in the diastereoselective reduction of bulky 17-oxosteroids (17-OXO) to their corresponding 17α-hydroxysteroids (17α-OH). This was confirmed by the reduction of estrone (E1) to 17α-estadiol (α-E2) and epiandrosterone (EPIA) to 5α-androstan-3β,17α-diol. Higher diastereoselectivities to the corresponding 17α-OH are observed with ^{s}BuOH.
10) Detailed kinetic study and calculation of GIBBS free energy using the EYRING-POLANYI equation showed that enthalpic- and entropic terms are partially counteracting in the reduction of E1 with ^{i}PrOH. With ^{s}BuOH, entropic and enthalpic terms favor the formation of the TS leading to α-E2, which leads to a higher diastereoselectivity. Preliminary computational analysis suggests that short hydrogen bonds stabilize the TS leading to α-E2, which are less pronounced or absent in the TS leading to β-E2.
11) Androstenedione (A4) can be converted in a one-step chemo-, regio- and diastereoselective MPV reduction to epitestosterone (E) over MOF-808. Final yields are optimized by the choice of reaction temperatures and minimization of double-hydroxylation at C-3.

Chapter 8

Annexes

8.1. General information

8.1.1. Synthesis of materials

8.1.1.1 UiO-66: Used in Chapter 4 and 5

A two-step procedure was carried out for the synthesis of UiO-66 materials as described in the literature.[1] DMF was dried before synthesis using activated molecular sieve (4 Å, 1.6 mm pellets) and $ZrCl_4$ was dried at 373 K under vacuum (10^{-3} mbar) for 8 hours in a SCHLENK tube. Subsequently, a solution of terephthalic acid (H_2BDC) (400 mg, 2.4 mmol) in DMF (45 mL) and $ZrCl_4$ (375 mg, 1.6 mmol) were placed in a screw-cap glass reactor (200 mL). The closed reactor was heated in an oven at 353 K over night and for an additional 24 hours at 373 K. After cooling down to room temperature the MOF was collected by filtration and washed thoroughly with DMF. The MOF was soaked in fresh DMF (15 mL) over night and solvent exchanged with fresh dichloromethane (DCM, 15 mL) for 8 hours. After removal of solvent by decantation, the product was dried on air.

8.1.1.2 MOF-808: Used in Chapter 4, 5 and 6

A solution of $ZrOCl_2(H_2O)_8$ (242.5 mg, 0.75 mmol), benzene-1,3,5-tricarboxylic acid (H_3BTC) (105.4 mg, 0.5 mmol), DMF (11.25 mL) and formic acid, purity = 90%, 11.25 mL) was placed in a screw-cap glass reactor (100 mL). The reactor was closed and heated in an oilbath to 403 K for 48 hours. After cooling down to room temperature, the product was recovered by centrifugation and washed with fresh DMF (15 mL) for 3 days exchanging the solvent 2 times per day and with fresh EtOH (15 mL) for 3 days exchanging the solvent 2 times per day. The final product was recovered by centrifugation and dried on air. The synthesis procedure[2] first reported by JIANG *et al.* was adapted with slight modifications.

MOF-808 was also synthesized using a teflon-lined stainless steel autoclave (100 mL) and heating in an oven to 408 K for 48 hours. The rest of the synthesis procedure was kept as described before.

8.1.1.3 DE MOF-808-x (x = IPA, Pydc, OH or NH_2): Used in Chapter 4

DE MOF-808-x materials were synthesized by replacing 10 mol% of H_3BTC by defective linker molecules (isophthalic acid (H_2IPA), pyridine-3,5-dicarboxylic acid (H_2Pydc), 5-hydroxyisophthalic acid (5-OH-H_2IPA) or 5-aminoisophthalic acid (5-NH_2-H_2IPA) for MOF-808-IPA, MOF-808-Pydc, MOF-808-OH and MOF-808-NH_2, respectively (see Figure 8.1). Exact linker ratios for the preparation of DE MOF-808-x materials were as follows: H_3BTC/H_2IPA (94.9 mg (0.45 mmol)/8.3 mg (0.05 mmol)), H_3BTC/H_2Pydc (94.9 mg (0.45 mmol)/8.4 mg (0.05 mmol)), H_3BTC/5-OH-H_2IPA (94.9 mg (0.45 mmol)/9.1 mg (0.05 mmol)) and H_3BTC/5-NH_2-H_2IPA (94.9 mg (0.45 mmol)/9.1 mg (0.05 mmol)). A solution of linker molecules (0.5 mmol), $ZrOCl_2(H_2O)_8$

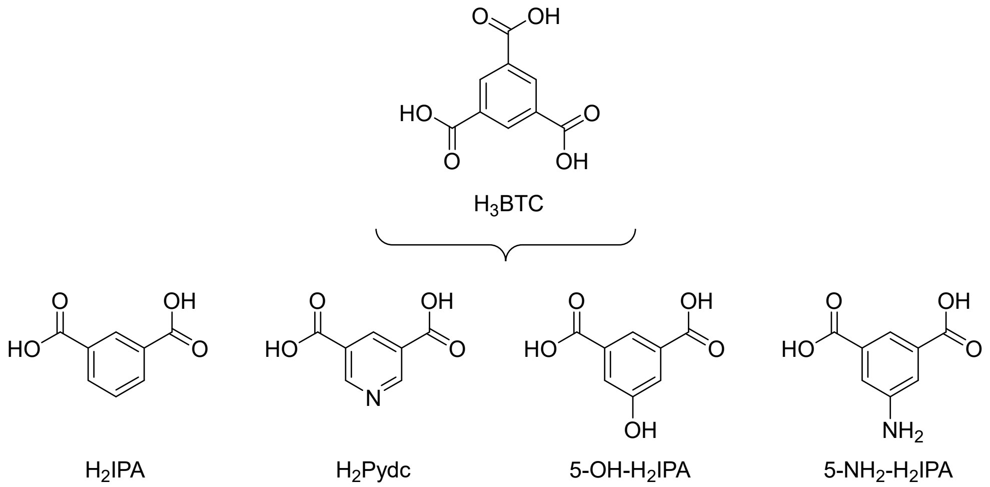

Figure 8.1. H_3BTC is combined with various ditopic ligands (H_2IPA, H_2Pydc, 5-OH-H_2IPA and 5-NH_2-H_2IPA

(242.5 mg, 0.75 mmol) DMF (11.25 mL) and formic acid, purity = 90% (11.25 mL) was placed in a screw-cap glass reactor (100 mL). The reactor was closed and heated in an oilbath to 403 K for 48 hours. After cooling down to room temperature, the product was recovered by centrifugation and washed with fresh DMF (15 mL) for 3 days exchanging the solvent 2 times per day and with fresh EtOH (15 mL) for 3 days exchanging the solvent 2 times per day. The final product was recovered by centrifugation and dried on air.

DE MOF-808-x materials were also prepared in a teflon-lined stainless steel autoclave (100 mL) and heating in an oven for 48 hours to 408 K. Further, a two step procedure was applied in DE MOF-808-x synthesis using a teflon-lined stainless steel autoclave (100 mL) and heating to 353 K for 4.5 hours and 393 K for additional 43.5 hours. The rest of the synthesis procedure was kept unchanged in all cases.

8.1.1.4 DUT-67: Used in Chapter 4

DUT-67 was kindly provided by the group of Stefan Kaskel at the TU Dresden. $ZrCl_4$(1.38 g, 6 mmol) was dissolved in 150 mL of N,N-dimethylformamide/N-methyl-2-pyrrolidone mixture (DMF/NMP, 1:1) by ultrasonication for 10 minutes. Afterwards, H_2TDC linker (0.66 g, 4 mmol) was added and the mixture was sonicated again for 5 minutes. Then formic acid (26.8 mL, 120 eq.) was added and the resulting mixture was divided into 3 parts and distributed between three Schott flasks (500 mL each) and placed inside an oven for 72 h at 358 K. The white precipitate was filtered off and washed several times with DMF.

8.1.1.5 Zr-BEA: Used in Chapter 5 and 6

a) Synthesis of dealuminated Zr-BEA seeds

First, 1.85 g of $AlCl_3(H_2O)_6$ were disolved in 4.33 g of water. To this solution, 45.2 g of tetraethylammonium hydroxide solution (TEAOH, 35 wt. % in H_2O) were added, followed by 40.0 g of tetraethyl orthosilicate (TEOS) and the mixture was stirred until evaporation of the EtOH formed by hydrolysis of TEOS. The final composition of the gel was:

SiO_2: 0.56 TEAOH: 0.02 Al_2O_3: 6.5 H_2O

The gel was transferred into a teflon lined autoclae and heated to 413 K for 3 days with stirring. The solid product was recovered by filtration, washed with distilled water and dried at 373 K. The resulting zeolite was dealuminated by treating 1 g of the solid with 60 g of HNO_3 (60 wt%) at 353 K for 24 h. The dealuminated solid was filtered, washed with water and dried at 373 K. The final Si/Al ratio of the solid was higher than 2000, as determined by elemental analysis.

b) Synthesis of aluminium-free Zr-BEA zeolite

30 g of TEOS and 33.0 g of TEAOH (35 wt. % in H_2O) were placed inside a teflon lined autoclave. To this, a solution containing 0.39 g of $ZrOCl_2(H_2O)_8$ in 2.75 g water, and the mixture was stirred until evaporation of the EtOH formed by hydrolysis of TEOS. To this solution, 3.27 g of HF (48 wt%) were added, and the resulting viscous gel was mixed with a aqueous suspension of 0.36 g of preformed dealuminated Zr-BEA seeds in 2 g of water. The final composition of the gel was:

SiO_2: 0.54 TEAOH: 0.008 ZrO_2: 0.54 HF: 7.5 H_2O

The gel was transferred into a teflon lined autoclave and heated to 413 K for 14 days with stirring. The solid product was recovered by filtration, washed with distilled water and dried at 373 K. The final Si/Zr ratio of the solid was 148, as determined by elemental analysis.

8.1.2. General procedure for the thermal activation of MOF catalysts

5 mg of catalyst were activated in a GC vial, which was placed inside a SCHLENK tube. The SCHLENK tube was closed and evacuated (10^{-3} mbar) via a SCHLENK line, while heating to 423 K in an oilbath for 24 hours. The SCHLENK tube was set under nitrogen atmosphere after activation and cooled down to room temperature.

8.2. Additional information for Chapter 4. Catalytic properties of pristine and DE MOF-808 materials

8.2.1. Characterization of catalysts

8.2.1.1 XRD

The crystallinity of prepared UiO-66 was measured by PXRD and the material was crystalline showing a PXRD pattern consistent with the reported structure earlier in the literature (see Figure 8.2).

A sample of DUT-67 which was used for comparison was provided by the group of S. KASKEL at the Dresden University of Technology. The crystallinity of used DUT-67 was analyzed by PXRD measurements and was found to be crystalline as expected for the structure and reported previously in the literature (see Figure 8.2).

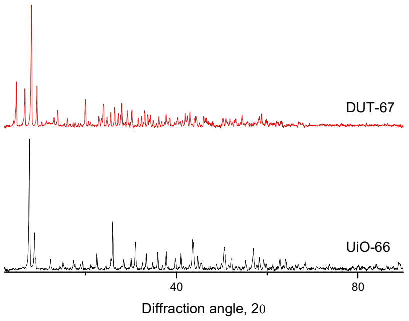

Figure 8.2. PXRD pattern of UiO-66 and DUT-67 reference materials

8.2.1.2 ^{1}H-NMR

Parent MOF-808 and DE MOF-808-x materials were also analyzed by liquid NMR experiments. NMR experiments were used for analysis of the organic part of the MOF as it can be used for detection of organic linker molecules as well as solvent and modulator compounds present in the material. The experiments show that there is no formic acid or only traces of formic acid present in DE MOF-808-x materials. It can be assumed, that $^{-}$OH/H_2O pairs are present at undercoordinated Zr-sites due to the absence of formate ions (see also Figure 8.6 & 8.7 below, CO adsorption). Further, small amounts of DMF are present in all samples, which was not fully removed during the washing and drying procedure (see Figure 8.3). For DE MOF-808-x materials characteristic signals with lower intensities can be seen by NMR analysis, indicative for small amounts of defective linker molecules (IPA, Pydc, 5-OH-IPA or 5-NH_2-IPA) present in the samples.

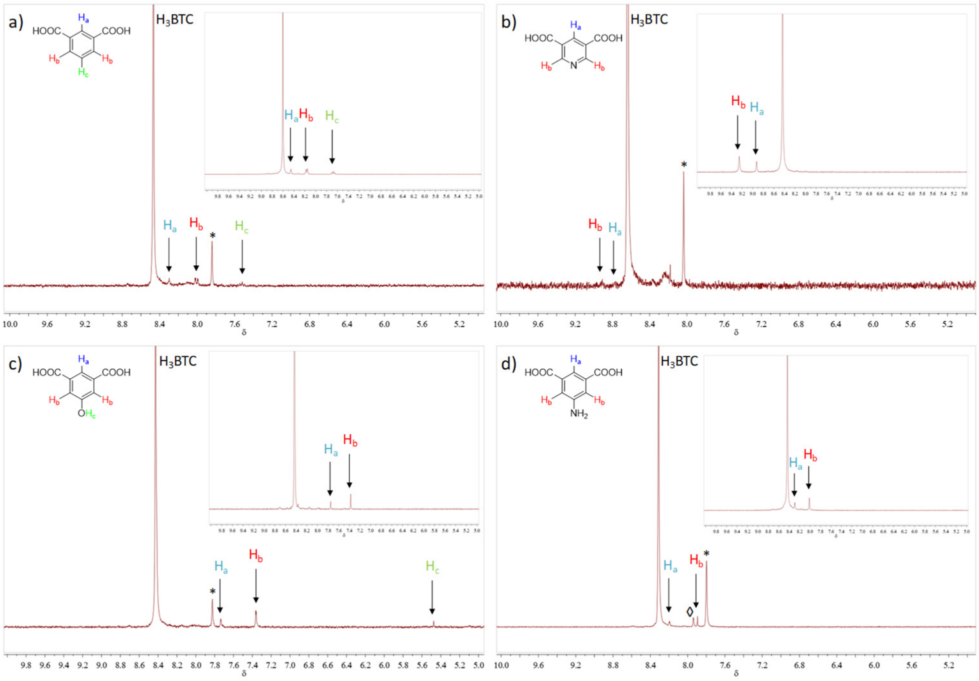

Reprinted (adapted) with permission from (*Catal. Sci. Technol.*, **2018**, *8*, 3610-3616). Copyright (2018) The Royal Society of Chemistry

Figure 8.3. ^{1}H-NMR spectra of digested DE MOF-808-x samples and a physical mixture of BTC linker with corresponding defective linkers in insets for a) MOF-808-IPA; b) MOF-808-Pydc; c) MOF-808-OH and d) MOF-808-NH_2. Traces of formic acid and DMF are marked by ◊ and *, respectively

Physical mixtures of defective linker molecules with H_3BTC were prepared as reference and the amount of defective linker molecules present in DE MOF-808-x materials was calculated using peak integrations from the NMR experiment. (shown in Chapter 4, Table 4.1)

8.2.1.3 FESM

Crystal size and morphology was examined by FESEM experiments (see Figure 8.4). Small crystals of octahedral shape can be seen for pristine MOF-808 and DE MOF-808-x materials. The crystals form big agglomerates which can be seen in the FESEM images. There are no significant variations in crystal size for measured samples. Although the crystals are not of uniform size within measured batches, rather small crystals are present in all samples with a size of around 200 nm. The images show again good crystallinity and phase purity in all samples. The materials were further compared with a UiO-66 sample, which shows crystals of comparable size.

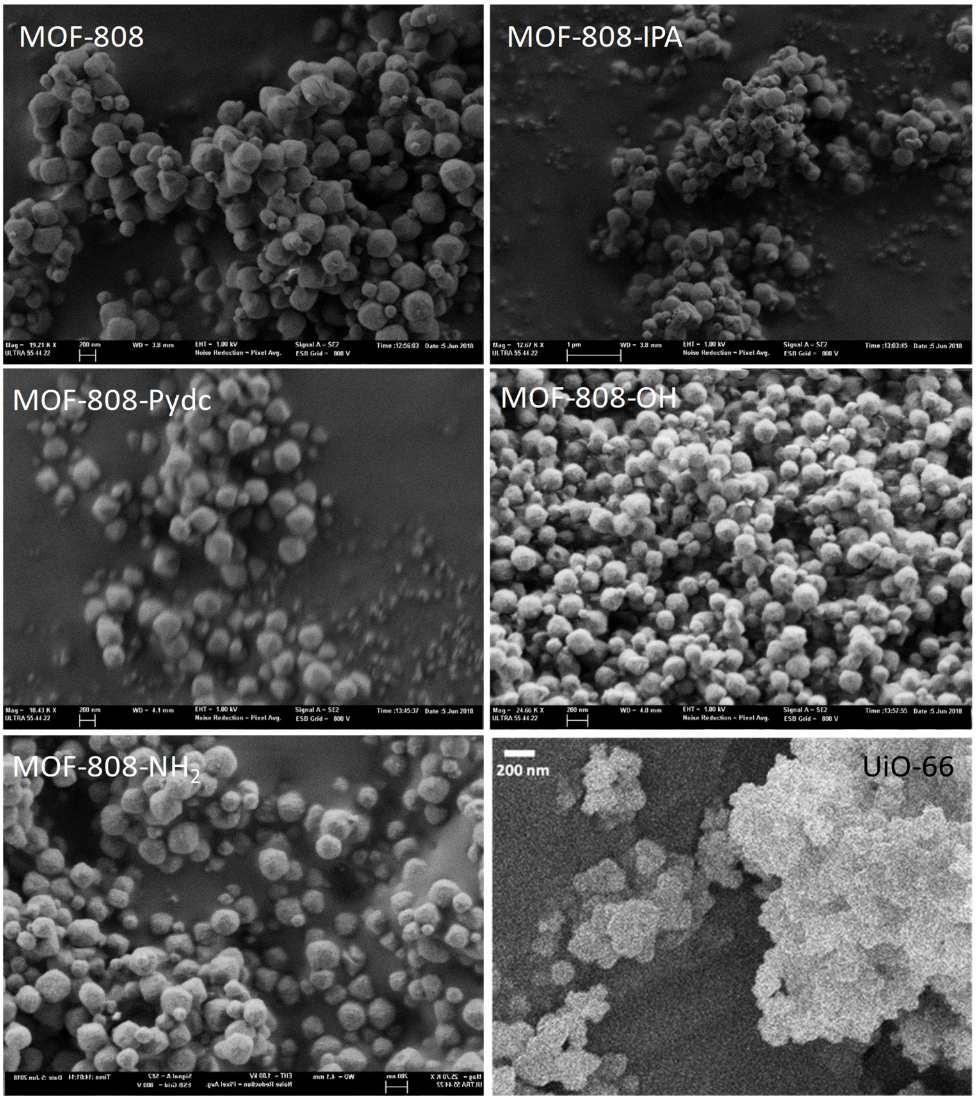
MOF-808
MOF-808-IPA
MOF-808-Pydc
MOF-808-OH
MOF-808-NH$_2$
200 nm
UiO-66

Reprinted (adapted) with permission from (*Catal. Sci. Technol.*, **2018**, *8*, 3610-3616). Copyright (2018) The Royal Society of Chemistry

Figure 8.4. FESEM images of prisine MOF-808, DE MOF-808-x materials and UiO-66

8.2.1.4 N_2-adsorption/desorption isotherms

Textural properties of pristine MOF-808 and DE MOF-808-x materials were also analyzed by N_2-adsorption/desorption experiments. The isotherms of materials are shown in Figure 8.5. Obtained results were used for the calculation of the BET surface are (S_{BET}), micropore volume (V_P) and pore size distribution (see Table 8.1). From the calculated S_{BET} values, an increase is observed for all DE MOF-808-xs compared to pristine MOF-808. The biggest increase in S_{BET} is observed for MOF-808-Pydc. The microporous volume (V_P) follows the same trend as S_{BET}, with the highest value for MOF-808-Pydc compared to MOF-808. In the pore size calculation on the contrary the reversed trend is observed, as calculated values for all DE MOF-808-x materials are below of that of pristine MOF-808. A similar effect was observed previously on DE HKUST-1 were incorporation of 5% of Pydc led to a distinct increase in surface area (S_{BET}=985.17 m^2g^{-1}) compared to pristine HKUST-1 with a S_{BET} of 723.40 m^2g^{-1}. As the pore volume also increased from 0.336 cm^3g^{-1} to 0.436 cm^3g^{-1}, the pore diameter decreased from 1.858 Å to 1.769 Å for pristine HKUST-1 and D1, respectively.[3]

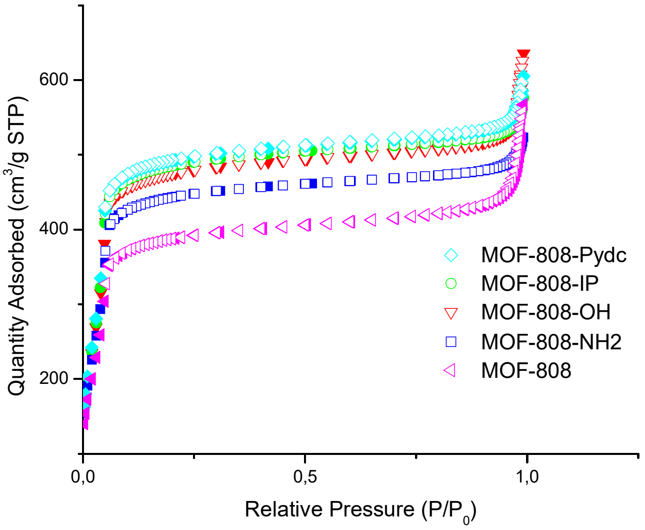

Figure 8.5. Isotherms for pristine MOF-808 and DE MOF-808-x materials obtained from the nitrogen adsorption/desorption experiments; empty symbols-adsorption, filled symbols-desorption

Table 8.1. Comparison of textural properties of pristine MOF-808 and DE MOF-808-x materials

Sample	S_{BET} (m^2g^{-1})	V_P (cm^3g^{-1})	Pore size (Å)
MOF-808	1345	0.60	18.2
MOF-808-IPA	1558	0.73	17.3
MOF-808-Pydc	1592	0.74	17.3
MOF-808-OH	1537	0.71	17.5
MOF-808-NH_2	1436	0.67	17.4

Reprinted (adapted) with permission from (*Catal. Sci. Technol.*, **2018**, *8*, 3610-3616). Copyright (2018) The Royal Society of Chemistry

8.2.1.5 FTIR and CO adsorption

FTIR spectra of CO adsorbed at 77 K were measured on pristine MOF-808 (Figure 8.6) and MOF-808-Pydc (Figure 8.7), previously activated at 393 K under vacuum. Figures are presenting the C-O and O-H stretching regions. For the lowest CO equilibrium pressure (~10^{-2} Torr), a single IR absorption band is seen at 2176 cm^{-1} which can be assigned to the C-O stretching mode of $Zr^{4+}\cdots CO$ adducts formed onto Zr^{4+} open metal sites of MOF-808. Upon increasing the equilibrium pressure of CO, the band at 2176 cm^{-1} progressively broadens and shifts towards lower wavenumbers and a new shoulder becomes visible at *ca*. 2170 cm^{-1}. (see the inset for a better definition). This new band reflects the formation of multi-carbonyl species on the Zr^{4+} open metal sites. Additionally, a new band develops at 2154 cm^{-1}, which corresponds to CO adsorbed onto the μ^3-OH groups of the Zr_6 clusters. In parts and the progressive erosion of the ν(OH) band of these OH groups at 3677 cm^{-1} and the appearance of a new, broader band at 3604 cm^{-1} (Δν(O-H) = -73 cm^{-1}) indicative of mild acid sites can be seen. Finally, at the highest CO equilibrium pressure, an additional CO absorption band is observed at 2137 cm^{-1}, corresponding to CO physisorbed inside the pores of MOF-808.

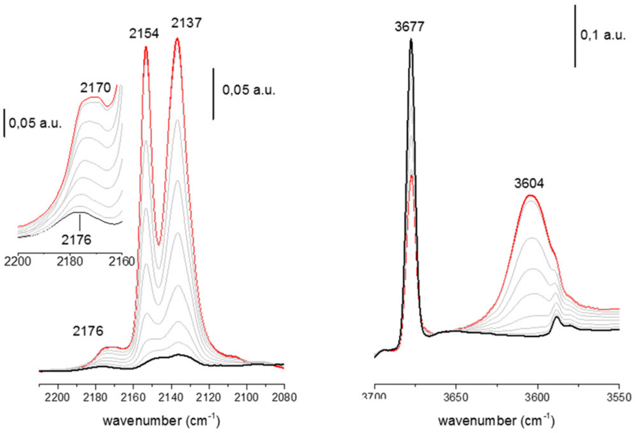

Reprinted (adapted) with permission from (*Catal. Sci. Technol.*, **2018**, *8*, 3610-3616). Copyright (2018) The Royal Society of Chemistry

Figure 8.6. CO adsorption in C-O region (left) and O-H region (right) for pristine MOF-808

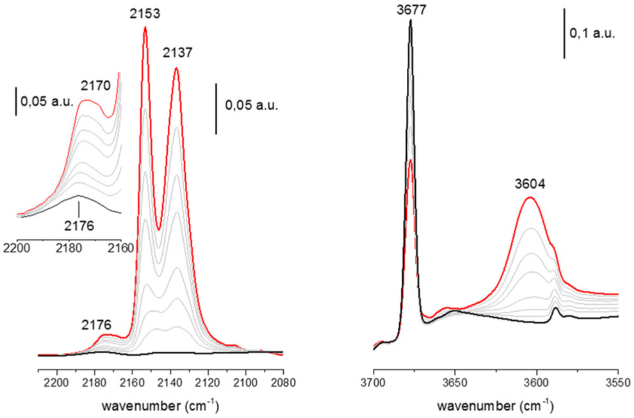

Reprinted (adapted) with permission from (*Catal. Sci. Technol.*, **2018**, *8*, 3610-3616). Copyright (2018) The Royal Society of Chemistry

Figure 8.7. CO adsorption in C-O region (left) and O-H region (right) for DE MOF-808-Pydc

8.2.2. General procedure for the reduction of cyclohexanone (CH)

10 mg (0.1 mmol) of CH were dissoloved in 0.5 mL of ^{i}PrOH. The solution was added to activated catalyst (Zr/CH ratio = 14 mol%) under nitrogen atmosphere. The mixture was transferred into a 2-mL glass batch reactor charged with a magnetic stirrer. The reactor was closed and heated in a metal heating block to 353 K while stirring. Aliquots were taken at specified reaction times and the reaction was followed by GC analysis on an AGILENT 7890A equipped with a FID detector and a DB5 (30 m x 0.25 mm x 0.25 µm) column.

8.2.3. General procedure for the reduction of estrone (E1)

20 mg (0.08 mmol) of E1 were dissolved in 1 mL of ^{i}PrOH. The solution was added to activated catalyst (Zr/E1 ratio = 18 mol%) under nitrogen atmosphere. The mixture was transferred into a 2-mL glass batch reactor charged with a magnetic stirrer. The reactor was closed and heated in a metal heating block to 353 K while stirring. Aliquots were taken at specified reaction times and the reaction was followed by GC analysis on an AGILENT 7890A equipped with a FID detector and a DB5 (30 m x 0.25 mm x 0.25 µm) column. Parameters for the separation of steroids were the following:

Table 8.2. parameters used for the separation of steroid compounds by GC analysis

Oven	Heating rate	Temperature	Hold temperature
	Injection	493 K	1 min
	10 Kmin^{-1}	523 K	0 min
	5 Kmin^{-1}	553 K	15 min

Due to overlapping of the GC peaks, a deconvolution method was applied to determine the relative amounts of reaction substrates. After completion of the reaction, the catalyst was removed from the reaction mixture and washed with ^{i}PrOH (2 x 0.5 mL). Combined liquid phases were transferred into a GC vail. The GC vial was placed inside a SCHLENK tube and the solvent was removed under vacuum (10^{-3} mbar) at room temperature via a SCHLENK line. The crude product was dissolved in DMSO-d_6 and NMR analysis was performed on a BRUKER 300 spectrometer.

8.2.4. Structural analysis of estradiols (E2) and determination of diastereoselective ratio (d.r.)

Main ^{1}H-NMR peaks observed in the corresponding spectra of α-E2 and β-E2 were as follows:

α-E2: ^{1}H NMR (300 MHz, DMSO-d_6): δ 8.96 (s, 1H), 7.05 (d, *J* = 8.4 Hz, 1H), 6.50 (dd, *J* = 8.4, 2.5 Hz, 1H), 6.43 (d, *J* = 2.3 Hz, 1H), 4.33 (d, *J* = 4.2 Hz, 1H), 3.61 – 3.54 (m, 1H), 2.71 (s, 2H), 2.27 (d, *J* = 10.1 Hz, 1H), 2.13 – 1.96 (m, 2H), 1.82 (d, *J* = 9.6 Hz, 1H), 1.77 – 1.62 (m, 2H), 1.61 – 1.49 (m, 1H), 1.49 – 1.05 (m, 6H), 0.61 (s, 3H).[4]

β-E2: ^{1}H NMR (300 MHz, DMSO-d_6): δ 8.96 (s, 1H), 7.04 (d, *J* = 8.4 Hz, 1H), 6.50 (dd, *J* = 8.3, 2.4 Hz, 1H), 6.43 (s, 1H), 4.47 (d, *J* = 4.8 Hz, 1H), 3.51 (dd, *J* = 13.0, 8.2 Hz, 1H), 2.69 (s, 2H), 2.22 (d, *J* = 12.6 Hz, 1H), 2.06 (s, 1H), 1.85 (t, *J* = 12.7 Hz, 3H), 1.57 (d, *J* = 9.1 Hz, 1H), 1.46 – 0.98 (m, 7H), 0.66 (s, 3H).

Most characteristic signals which were used for the identification of 17α- and 17β-OHs are listed in Table 8.3. Signals are representing protons of the CH_3 group at C-18, on C-17 and the –OH group at C-17. Other signals are either identical or overlap, due to the presence of both diastereoisomers in the crude product. The values of d.r. α-E2/β-E2 reported in Table 4.4 of Chapter 4 have been calculated from both, the ratios of peaks at 0.61/0.66 and 4.33/4.47, for α-E2 and β-E2.

Table 8.3. Signals used for the determination of d.r. of products by ^{1}H-NMR

Position	Chemical shift	
	α-E2	β-E2
18-H	0.61	0.66
17-H	3.57	3.51
17-OH	4.33	4.47

8.2.5. *Characterization of steroids from the reduction of E1 (^{1}H-NMR spectra of individual compounds)*

The ^{1}H-NMR spectra of α-E2 is in accordance with the spectra reported in the literature[4] (see Figure 8.8, d). Therefore, all characteristic signals from the steroid compound can be found in the ^{1}H-NMR spectra. If a mixture of α-E2 and β-E2 is present, the assignment of peaks is very difficult, due to very similar chemical shifts of many protons of both compounds. Nevertheless, some individual signals can be used to identify α-E2 and β-E2 or E1 and were used for the analysis, as described in Chapter 4.

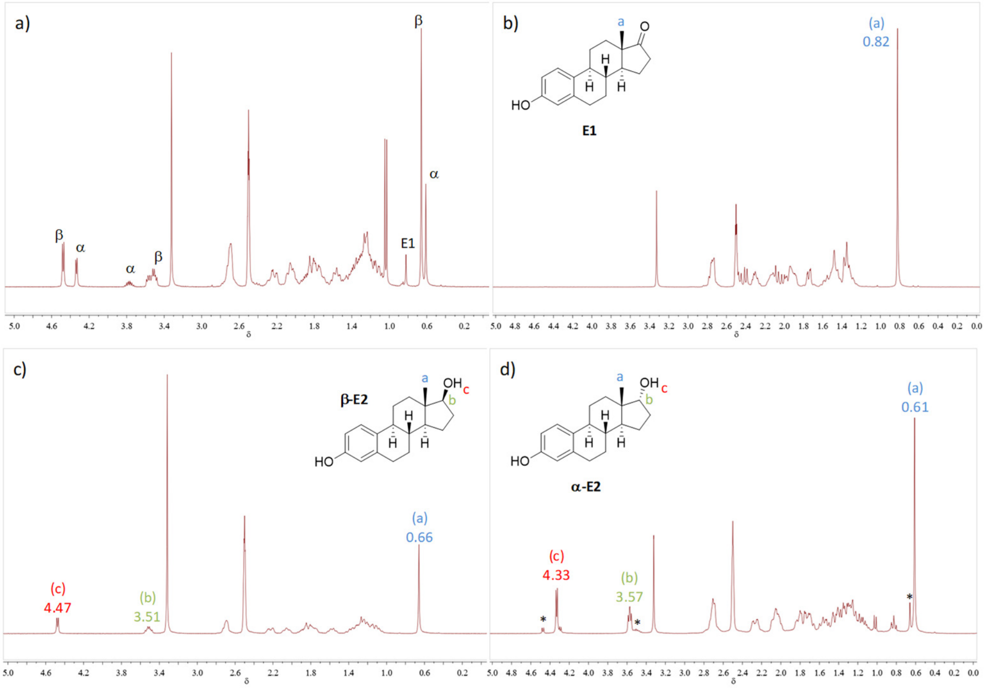

Figure 8.8. ^{1}**H NMR spectra of: a) the reaction crude obtained at almost full E1 conversion (some E1 still left, marked with E1); and reference spectra of b) E1, c) β-E2 and d) α-E2. The most prominent peaks of each compound have been indicated. In (d), the asterisks mark some traces of β-E2 detected together with α-E2**

8.3. Additional information for Chapter 5. Diastereoselective MPV reduction of substituted cyclohexanones

8.3.1. General procedure for the reduction of substituted cyclohexanones

Substituted CH (0.1 mmol) was dissolved in 0.5 mL of ^{i}PrOH. The solution was added to the catalyst (Zr/CH ratio = 14 mol%) under nitrogen atmosphere. The mixture was transferred into a 2-mL glass batch reactor charged with a magnetic stirrer. The reactor was closed and heated in a metal heating block to the desired reaction temperature while stirring. Aliquots were taken at specified reaction times and the reaction was followed by GC analysis. In the case of 2MeCH and 2PhCH, the analysis was carried out on an AGILENT 7890A equipped with a FID detector and a DB5 (30 m x 0.25 mm x 0.25 µm) column. In the case of 3MeCH, a DB-WAX (15 m x 0.32 mm x 0.25 µm) column was used.

8.3.2. NaBH$_4$ reduction of 2PhCH

2PhCH (35 mg, 0.201 mmol) was dissolved in EtOH (1 mL) and NaBH$_4$ was added (20.7 mg, 0.547 mmol) while stirring in a round botttom flask.The flask was closed with a septum and the reaction was stirred for additional 2 hours at room temperature and quenched with a saturated NH$_4$Cl solution subsequently. The product was extracted with Et$_2$O (3x10 mL) and dried over Na$_2$SO$_4$. The solution was filtered and the solvent was removed on a rotary evaporator.[5]

8.3.3. Time-conversion plots of 2MeCH and 3MeCH over MOF-808 using ^{i}PrOH or ^{s}BuOH at 353 K

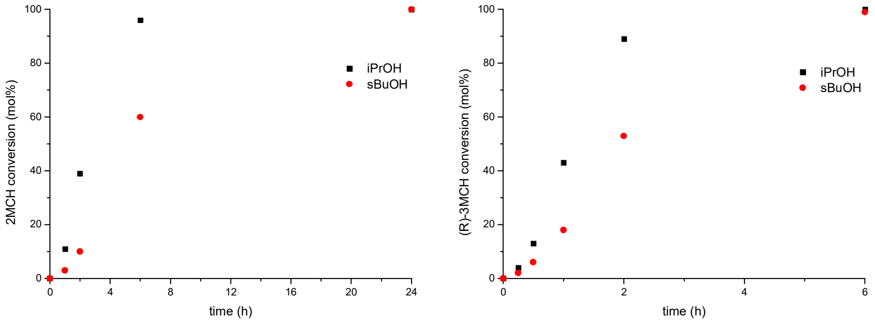

Figure 8.9. Conversion of 2MeCH (left) and (R)-3MeCH (right) using MOF-808 in either ^{i}PrOH or ^{s}BuOH at 353 K

8.3.4. Procedure for the kinetic analysis of 2MeCH and 3MeCH reduction

A diastereoselective reaction of substrate A reacting to two diastereoisomers P$_1$ and P$_2$ is formulated as shown below in Scheme 8.1. Therefore, no formation of additional by-products is considered. Further, the interconversion of products as well as the reversed reaction of products to the corresponding starting compound can be neglected.

$$\mathrm{A} \longrightarrow \mathrm{P}_1 + \mathrm{P}_2$$

Scheme 8.1. Schematic representation of a diastereoselective reduction of compound A to products P$_1$ and P$_2$

If the starting compound was not enantiomerically pure, each diastereoisomer consists of two enantiomers, which are considered as equal, product P$_1$ or P$_2$, respectively. The reducing agent (e.g., ^{i}PrOH, ^{s}BuOH, …) was used in high access, small changes in concentration in reducing agent are negligible and the reaction can be further considered as a pseudo-1st-order parallel reaction (Equation 8.1).

$$A \overset{k_1}{\rightarrow} P_1 \quad \& \quad A \overset{k_2}{\rightarrow} P_2 \qquad \textbf{Equation 8.1}$$

The reaction constants, leading to P_1 and P_2 are given as k_1 and k_2, respectively. Since the two reactions are considered independent in our approach (as indeed observed experimentally in the kinetic ratio), the $[P_1]/[P_2]$ ratio is considered being constant (Equation 8.2) during the course of reaction and is equal to the ratio of reaction constants (Equation 8.3).

$$\frac{[P_1]}{[P_2]} = const. \qquad \textbf{Equation 8.2}$$

$$\frac{[P_1]}{[P_2]} = \frac{k_1}{k_2} \qquad \textbf{Equation 8.3}$$

The global reaction constant k can be derived from the sum of k_1 and k_2.

$$k = k_1 + k_2 \qquad \textbf{Equation 8.4}$$

From Equation 8.3, k_1 can be formulated as:

$$k_1 = \frac{[P_1]}{[P_2]} * k_2 \qquad \textbf{Equation 8.5}$$

Combining Equation 8.4 and Equation 8.5, k_2 can be formulated as:

$$k_2 = k/(1 + \frac{[P_1]}{[P_2]}) \qquad \textbf{Equation 8.6}$$

The global reaction constant k is derived by plotting the experimental data of ln[A] against time. In a (pseudo)1st-order reaction a linear function is obtained, with $-k$ = slope of the equation (Equation 8.9).

After calculation of k_2 from k and the ratio $[P_1]/[P_2]$ (Equation 8.6), k_1 can be simply calculated as:

$$k_1 = k - k_2 \qquad \textbf{Equation 8.7}$$

Combining a 1st-order reaction and a parallel reaction, the reaction kinetics can be formulated as:

$$-d[A]/dt = k_1[A] + k_2[A] = (k_1 + k_2)[A] \qquad \textbf{Equation 8.8}$$

This equation can be rewritten in its integrated form (with $-k$ = slope of the equation) as:

$$\ln[A] = ln[A]_0 - k * t \qquad \textbf{Equation 8.9}$$

and further in its exponential form as:

$$[A] = [A]_0 * e^{-(k_1+k_2)t}$$ **Equation 8.10**

Next, the ARRHENIUS equation is given as:

$$k(t) = k(0) * e^{-E_a/(RT)}$$ **Equation 8.11**

In its logarithmic form and at a set of different temperatures a linear equation is obtained with an intercept = $k(0)$ and a slope = $-E_a/\mathrm{R}$, from which the activation energy (E_a) can be calculated. (R = gas constant = 8.314 JK^{-1}mol^{-1}).

$$\ln(k(t)) = \ln(k(0)) - E_a/RT$$ **Equation 8.12**

Following the transition state theory, the EYRING-POLANYI equation can be used to calculate the GIBBS energy of activation ($\Delta G^{\ddagger}$), enthalpy of activation ($\Delta H^{\ddagger}$) and entropy of activation ($\Delta S^{\ddagger}$). The EYRING-POLANYI equation is given as:

$$\ln\left(\frac{k}{T}\right) = \frac{-\Delta H^{\ddagger}}{RT} + \ln\left(\frac{k^{'}}{h}\right) + \frac{\Delta S^{\ddagger}}{R}$$ **Equation 8.13**

With a set of different temperatures a linear equation is obtained, with an intercept = $\ln\left(\frac{k'}{h}\right) + \frac{\Delta S^{\ddagger}}{R}$ and a slope = $\frac{-\Delta H^{\ddagger}}{R}$. ($k$‘ = BOLTZMANN constant = 1.38064852*10^-23 JK^{-1}, h = PLANCK constant = 6.626070150*10^-34 Js, R = gas constant = 8.314 JK^{-1}mol^{-1}, k'/h = 2.083*10^10 K^{-1}s^{-1} and $\ln(k'/h)$ = 23.760).

$\Delta G^{\ddagger}$ is calculated in the following from:

$$\Delta G^{\ddagger} = RTln\left(\frac{k'T}{h}\right) - RTln(k)$$ **Equation 8.14**

or

$$\Delta G^{\ddagger} = \Delta H^{\ddagger} - T\Delta S^{\ddagger}$$ **Equation 8.15**

8.3.5. Eyring-Polanyi plots obtained from the reduction of 2MeCH and 3MeCH over MOF-808 using ^{i}PrOH or ^{s}BuOH as reducing agent

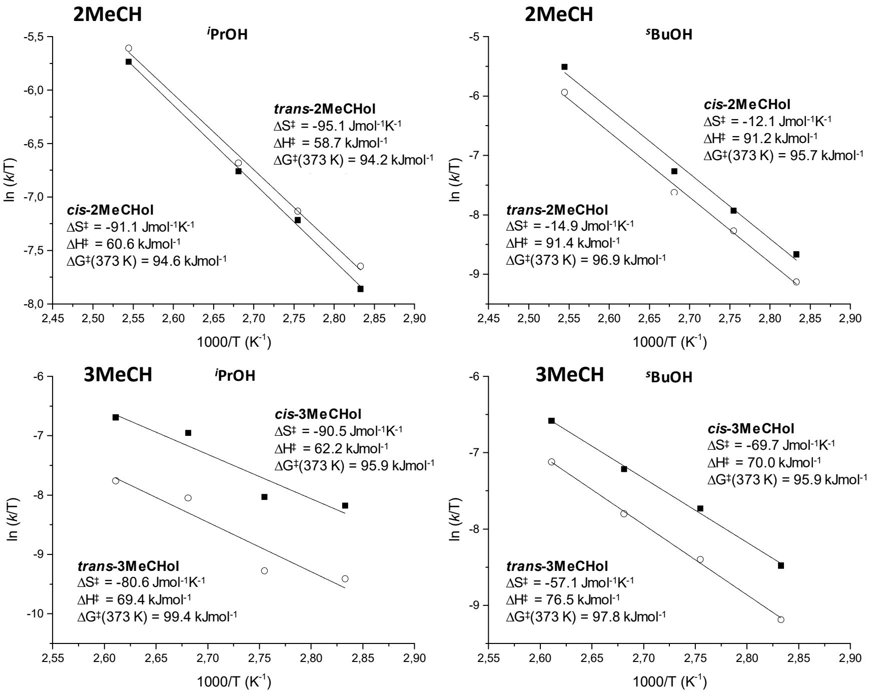

Figure 8.10. Eyring-Polanyi plots obtained from the reduction of 2MeCH (top) and 3MeCH (bottom) with calculated enthalpy- ($\Delta H^\ddagger$), entropy- ($\Delta S^\ddagger$) and Gibbs energy ($\Delta G^\ddagger$) of activiation of individual compounds

8.3.6. Computational analysis

A subset of the MOF-808 structure was chosen that has to meet the requirements of chemically feasible atom termination as well as sufficiently large number of atoms so as to represent a chemically correct representation of the active site environment. Without saturation with protons of the terminating dicarboxylate groups (which could arguably be considered a rough approximation) and by termination of one of the seven bonds of Zr with OH and by adding a proton to each of the four oxygen atoms resulting in the Zr_6 inorganic building units, a cluster of 269 atoms (including the reacting molecules) results.

A quantum semiempirical PM7[6] partial geometry optimization has been performed within the MOPAC2016[7] code. This method employs the Hartree–Fock (HF) approximation with Slater-type orbitals for the valence shell electrons and the NDDO (neglect of diatomic differential overlap) approximation for the core electrons. NDDO differs from the zero-differential overlap in that it calculates the electron repulsion between electrons at different atoms. PM7 represents an improved parametrized version of PM6 and PM3 with a wider set of reference data and enhanced functions and makes use of a modified function for the core–core interactions and a set of parametrization rules which increase the accuracy, in particular for transition metal compounds.[8] Additionally, an approach for the treatment of periodic systems has been implemented and tested with a wide set of organic and inorganic crystalline structures.

Recently, UYSAL[9] in a detailed comparison between semiempirical and DFT methods for Zr–ligand properties, found that the PM7 performance is comparable to B3LYP/LanL2dz for bond lengths, formation GIBBS free energy, HOMO-LUMO gaps and dipole moments. Such study does not compare performance between PM7 and PM3 although it can be said that, overall, PM7 maintains or improves the known quality of results for, not only PM3 but also PM6 semiempirical methods, and this is available for the simulation of nearly all atoms in the periodic table. Thus, we have used PM7 in order to extract atomic charges for the clusters indicated above in much shorter computation times than any ab-initio method.

With the above atomic charges, a force field methodology was found more convenient in terms of the high quality and efficient geometry optimization that can be employed using GULP,[10,11] using the EWALD method for summation of the long range COULOMBIC interactions, and direct summation of the short range interactions with a cut off distance of 12 Å. The BFGS (BROYDEN−FLETCHER−GOLDFARB−SHANNO)[12–15] was used as the cell minimization scheme with a convergence criterion of a gradient norm below 0.001 eV$Å^{-1}$.

The energy expression has been considered according to the Universal Force Field[16] which is widely known to perform in a well-balanced form conveying a very wide selection of atoms in the periodic table. In particular, the heptacoordination of zirconium atoms in MOF-808 has been found a stable relative minimum when the cluster above was geometry optimized without any constraint.

Transition states obtained for *cis*- and *trans*-2MeCH, and *cis*- and *trans*-3MeCH are shown below (Figure 8.11). Relative energies are referred to the TS leading to the cis-3MeCHol product, since this adduct features the lowest calculated energy difference (i.e., lowest activation energy, E_a) between adsorbed products and TS.

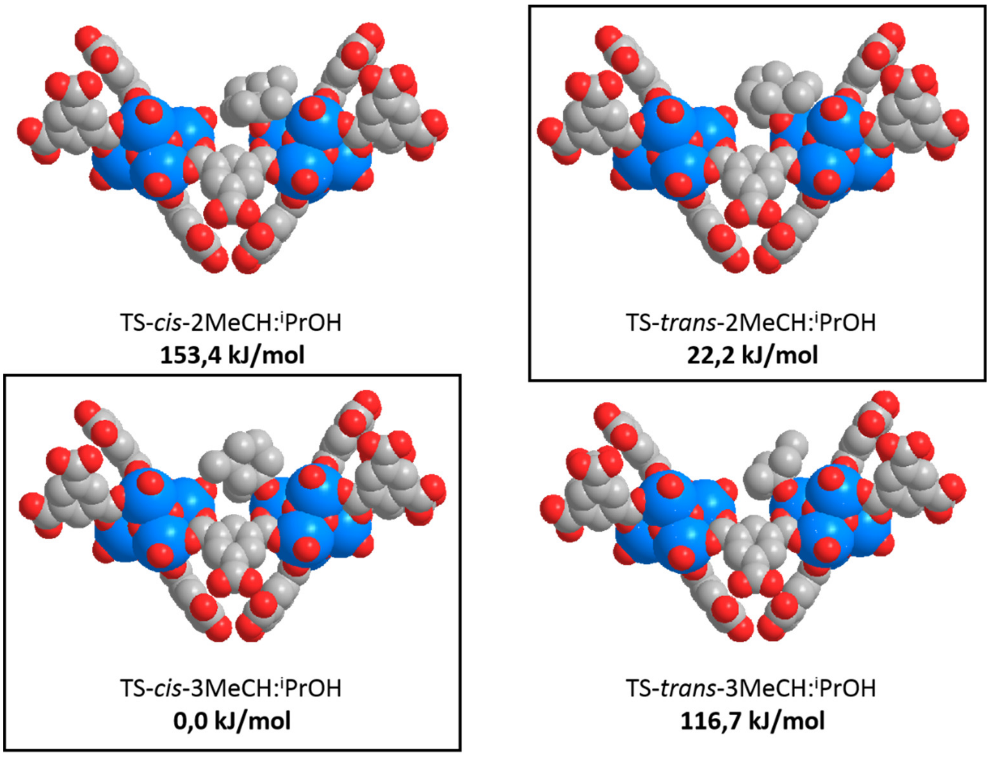

TS-*cis*-2MeCH:^{i}PrOH
153,4 kJ/mol

TS-*trans*-2MeCH:^{i}PrOH
22,2 kJ/mol

TS-*cis*-3MeCH:^{i}PrOH
0,0 kJ/mol

TS-*trans*-3MeCH:^{i}PrOH
116,7 kJ/mol

Figure 8.11. TSs (*via* equatorial or axial hydride transfer) calculated for the reduction of 2MeCH and 3MeCH with ^{i}PrOH as the secondary alcohol

8.4. Additional information for Chapter 6. One-step chemo-, regio- and stereoselective reduction of ketosteroids to hydroxysteroids

8.4.1. General procedure for the reduction of steroids

5 mg of catalyst (*ca.* 18 mol% Zr) were placed in a 2-mL glass-reactor charged with a magnetic stirrer. A solution containing 0.08 mmol of 17-OXO with reducing alcohol (1 mL) was prepared and added to the glass-reactor. The reactor was closed with a screw-cap, placed in a metal heating block and heated to the desired reaction temperature while stirring. Aliquots were taken at specified reaction times and the reaction was followed by GC analysis on an AGILENT 7890A equipped with a FID detector and a DB5 (30 m x 0.25 mm x 0.25 µm) column. Parameters for the separation of steroids are described in Chapter 4, Table 4.2. Due to overlapping of the GC peaks, a deconvolution method was applied to determine the relative amounts of reaction substrates. After completion of the reaction, the catalyst was removed from the reaction mixture and washed with reducing

alcohol (2 x 0.5 mL). Combined liquid phases were transferred into a GC vail. The GC vial was placed inside a SCHLENK tube and the solvent was removed under vacuum (10^{-3} mbar) at room temperature *via* a SCHLENK line. The crude product was dissolved in DMSO-d_6 (reduction of E1 and A4) or $CDCl_3$ (reduction of EPIA) and NMR analysis was performed on a BRUKER 300 spectrometer. The reaction of EPIA was also followed by liquid NMR analysis, due to very poor separation of reaction compounds by GC. For one sample 0.3 mL were taken from the reaction mixture. The catalyst was removed by centrifugation and washed with reducing alcohol (2 x 0.5 mL). Liquid phases were combined in a GC vial. The vial was placed in a SCHLENK tube and the solvent was removed under high vacuum at room temperature using a SCHLENK line and carefull evacuation. The remaining dry solid was dissolved in $CDCl_3$ and analyzed by ^{1}H-NMR on a BRUKER 300 spectrometer.

8.4.2. NaBH$_4$ reduction of E1 and EPIA

The procedure was adapted from ADITYA *et al.* Briefly, 0.15 mmol of 17-OXO (corresponding to 40 mg and 43 mg for E1 and EPIA, respectively) were dissolved in 5 mL of absolute EtOH at 353 K, while stirring in a 10 mL round-bottom flask. At 343 K, 1 mL of a freshly prepared 0.5 M $NaBH_4$ solution in absolute ethanol was added slowly. The mixture was stirred at 70 C° for 20 min and the temperature was raised to 353 K for an additional 10 min. The reaction was quenched with 12 mL of distilled water and cooled in an ice-water bath for 15 min. The crystallized solid product was recovered by filtration, washed with cold water and air dried on the filter.[17]

8.4.3. Procedure for the kinetic analysis of E1

The procedure used for the kinetic analysis of E1 reduction was analogous to the one described above for the reduction of substituted CHs (see Section 8.3).

8.4.4. EYRING-POLANYI plots obtained from the reduction of E1

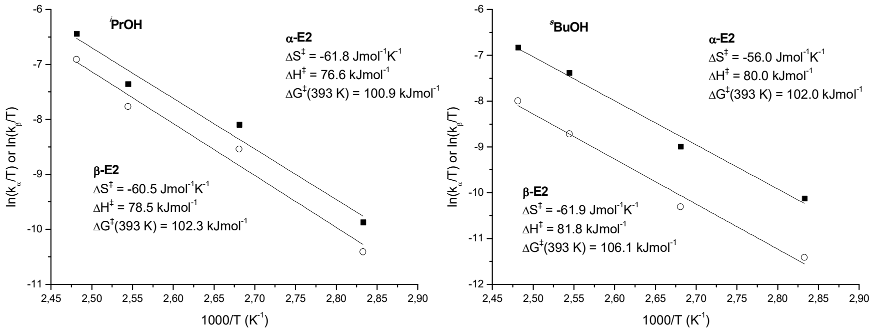

Figure 8.12. EYRING-POLANYI plots from the conversion of E1 to β-E2 and α-E2 in ^{i}PrOH (left) or ^{s}BuOH (right) with calculated enthalpy- (ΔH‡), entropy- (ΔS‡) and GIBBS energy (ΔG‡) of activiation of individual compounds

8.4.5. Structural analysis of hydroxysteroids and determination of diastereoselective ratio (d.r.)

The structural analysis of α-E2 and β-E2 is described in Chapter 4 and the compounds were analyzed by GC and ^{1}H-NMR. Most characteristic signals in ^{1}H-NMR correspond to the protons H-18 of the CH_3 group and protons H-17 as well as the –OH roup at C-17 and were used for the analysis of reaction compounds. Products from the reduction of EPIA and A4 were analyzed by their most characteristic signals present in the ^{1}H-NMR spectra. The corresponding spectra obtained experimentally are shown below (Figure 8.13, 8.15 and 8.16).

α-EPIAdiol: ^{1}H NMR (300 MHz, $CDCl_3$): δ 3.72 (dd, J = 5.7, 3.6 Hz, 1H), 3.60 (m, 1H), 0.82 (s, 3H), 0.65 (s, 3H).

β-EPIAdiol: ^{1}H NMR (300 MHz, $CDCl_3$): δ 3.60 (m, 2H), 0.82 (s, 3H), 0.73 (s, 3H).

E: ^{1}H NMR (300 MHz, DMSO-d_6): δ 4.30 (d, J = 4.1 Hz, 1H), 3.52 (dd, J = 10.7, 6.3 Hz, 1H), 1.14 (s, 3H), 0.63 (s, 3H); **^{13}C NMR** (300 MHz, DMSO-d_6): δ 198.05 (1C), 77.75 (1C).

T: ^{1}H NMR (300 MHz, DMSO-d_6): δ 4.46 (d, J = 4.8 Hz, 1H), 3.43 (dd, J = 8.4, 4.9 Hz, 1H), 1.14 (s, 3H), 0.68 (s, 3H); **^{13}C NMR** (300 MHz, DMSO-d_6): δ 198.01 (1C), 79.86 (1C).

8.4.6. Characterization of steroids from the reduction of EPIA (^{1}H-NMR spectra of individual compounds)

Analogous to the reduction of E1, characteristic signals for individual compounds (α-EPIAdiol and β-EPIAdiol) can be identified in the ^{1}H-NMR spectra of the crude product from the reduction of EPIA. Therefore, the CH_3 group (C-18) in close proximity to C-17 and the newly formed –OH group has a different chemical shift (upfield, for α-EPIAdiol) compared to β-EPIAdiol. Further, the two equatorial protons H-3 and H-17 in β-EPIAdiol have an identical chemical shift. In α-EPIAdiol two separate signals are observed where the equatorial H-17 has a slight downfield shift. These characteristics have been described in the literature previously[18] and were, therefore, used for the characterization of products. EPIA can be also identified from the ^{1}H-NMR spectra, as both CH_3 groups (C-18 and C-19) have a downfield chemical shift compared to diols (α-EPIAdiol and β-EPIAdiol).

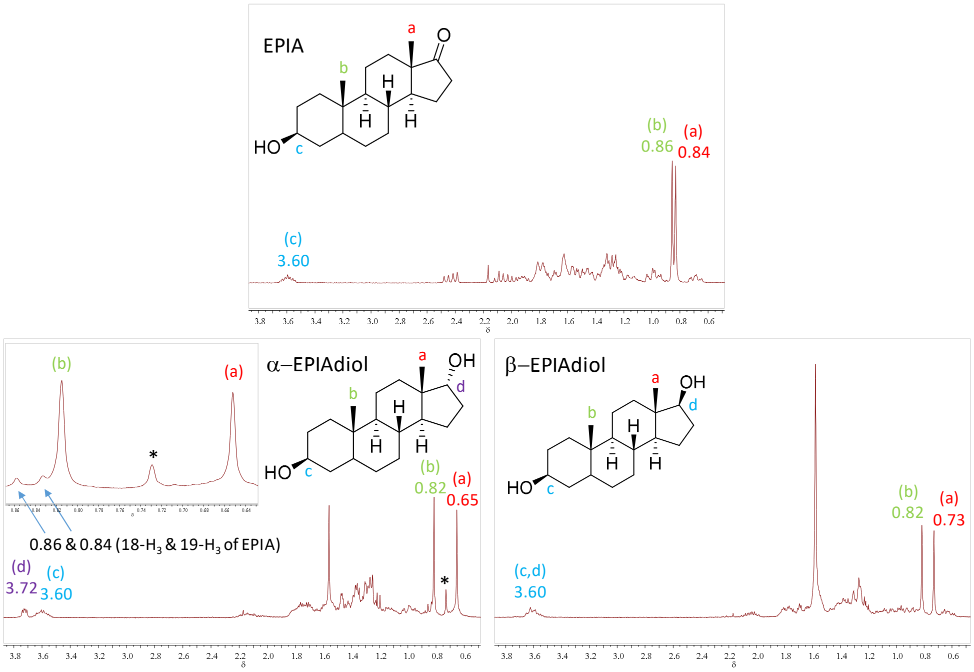

Figure 8.13. ^{1}H NMR spectra of: EPIA (top); the reaction crude obtained at almost full EPIA conversion (some EPIA still left, indicated by the arrows in inset) (bottom, left); and reference spectra of β-EPIAdiol (bottom, right). The most prominent peaks of each compound have been indicated. In the reaction crude mixture (bottom, left), the asterisk marks some traces of β-EPIAdiol detected together with α-EPIAdiol as the major product

8.4.7. Characterization of steroids from the reduction of A4 (GC analysis of reaction and ^{1}H- and ^{13}C-NMR spectra of individual compounds)

The reduction of A4 was followed by GC analysis, where the formation of E is observed as the major product. In addition, four diol isomers are formed, due to partial reduction at C-3. No products from monohydroxylation at C-3 were detected, which confirms that reduction at C-17 takes place prior to reduction at C-3. To confirm E as the major product by monohydroxylation at C-17, the reaction crude product was purified by TLC (PE/EtOAc, 4/6). From the GC analysis it can be seen that E is almost exclusively present in the fraction, which was further analyzed by ^{1}H-NMR and ^{13}C-NMR.

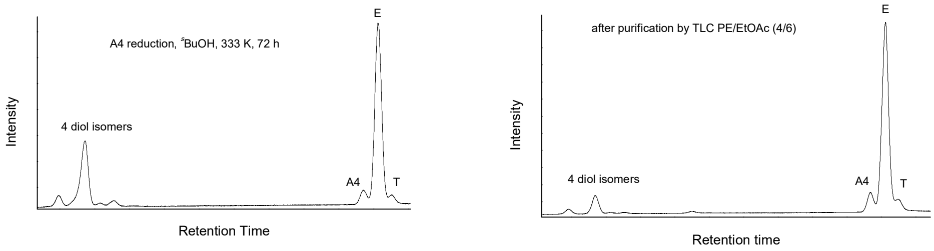

Figure 8.14. GC analysis of products from the MPV reduction of A4: crude product (left) and purified fraction (right)

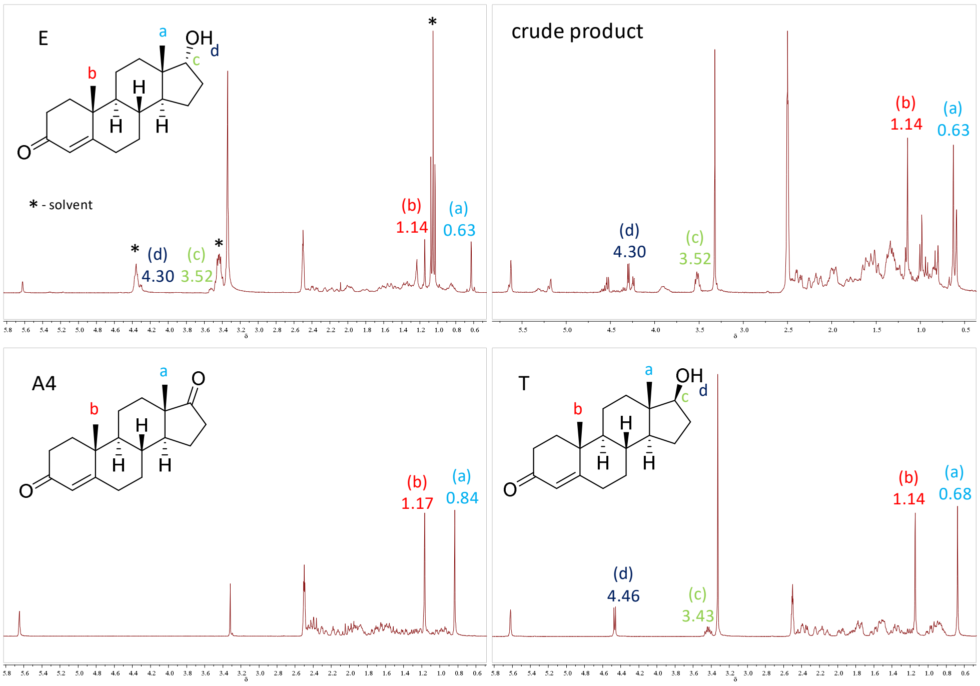

Figure 8.15. ^{1}H-NMR of: purified fraction (E) from the reduction of A4 (top, left);crude product after removal of the catalyst by centrifugation (top, right); starting compound A4 (bottom, left) and reference compound (T) (bottom, right). In the purified fraction of E (top, left) some solvent is present, which is marked by asterisks

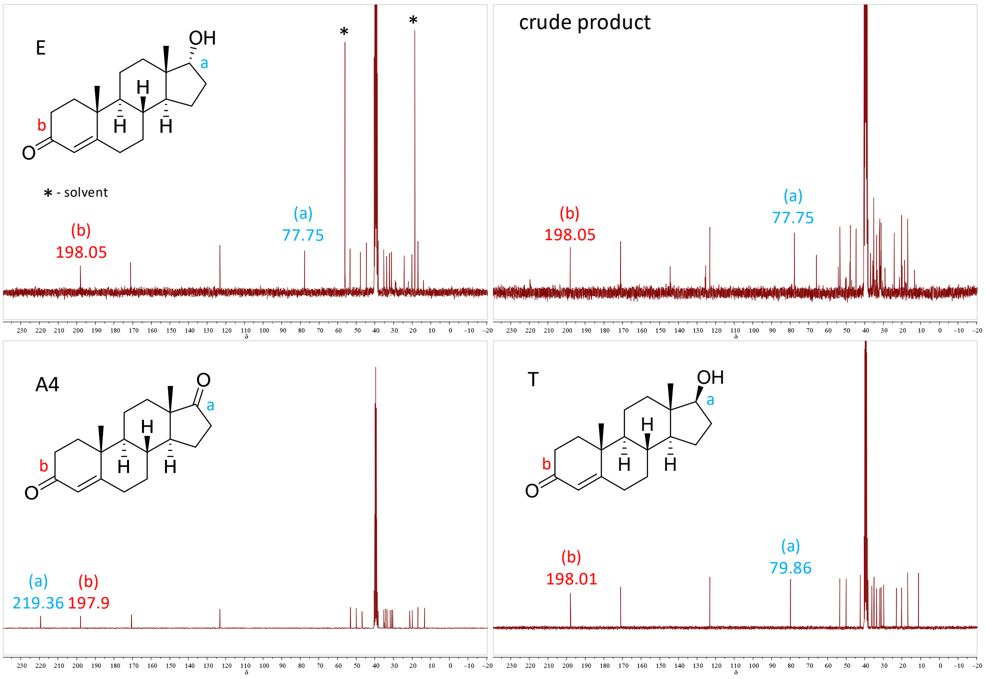

Figure 8.16. ^{13}C-NMR of: purified fraction (E) from the reduction of A4 (top, left);crude product after removal of the catalyst by centrifugation (top, right); starting compound A4 (bottom, left) and reference compound (T) (bottom,right). In the purified fraction of E (top, left) some solvent is present, which is marked by asterisks

From the ^{1}H-NMR an upfield chemical shift of the C-18 CH_3 group is observed in comparison to T. Further, H-17 and OH-17 have a downfield and upfield chemical shift, respectively. This confirms that the keto group at C-17 is reduced with very high selectivity towards the 17α isomer. From the ^{13}C-NMR of the reaction crude and the isolated product it can be seen that the C-17 has a big upfield chemical shift, due to reduction on C-17 from C=O to C-OH. With T as the reference compound, it is confirmed that E is formed as the major product, due to a slight upfield chemical shift of C-17 in E compared to T. The signals for the identification of E can be also found in the ^{1}H- and ^{13}C-NMR spectra of the crude product.

8.4.8. Computational analysis

Preliminary calculations of the two TSs leading to α-E2 and β-E2 inside MOF-808 was done by following the same approach already described for 2MeCH and 3MeCH (see Section 8.3). In this case, the total number of atoms included in the resulting clusters was 291.

8.5. References

1. Kandiah, M. *et al. Chem. Mater.* **2010**, *22*, 6632.
2. Jiang, J. *et al. J. Am. Chem. Soc.* **2014**, *136*, 12844.
3. Kozachuk, O. *et al. Angew. Chem. Int. Ed.* **2014**, *53*, 7058.
4. Guo, J.; Duclos Jr., R. I.; Vemuri, V. K. & Makriyannis, A. *Tetrahedron Lett.* **2010**, *51*, 3465.
5. Wang, L.; Akhani, R. K. & Wiskur, S. L. *Org. Lett.* **2015**, *17*, 2408.
6. Stewart, J. J. P. *J. Mol. Mod.* **2013**, *1*, 19.
7. Stewart, J. J. P. *Stewart Computational Chemistry, Colorado Springs*, Available at: http://openmopac.net.
8. Stewart, J. J. P. *J. Mol. Model.* **2007**, *25*, 1173.
9. Uysal, U. D. *Asian J. Chem.* **2013**, *25*, 2783.
10. Gale, J. D. *J. Chem. Soc. Faraday Trans.* **1997**, *93*, 629.
11. Gale, J. D. & Rohl, A. L. *Mol. Simul.* **2003**, *29*, 291.
12. Broyden, C. G. *IMA J. Appl. Math.* **1970**, *6*, 222.
13. Fletcher, R. *Comput. J.* **1970**, *13*, 317.
14. Goldfarb, D. *Math. Comput.* **1970**, *24*, 23.
15. Shanno, D. F. *Math. Comput.* **1970**, *24*, 647.
16. Rappe, A. K.; Casewit, C. J.; Colwell, K. S.; III, W. A. G. & Skiff, W. M. *J. Am. Chem. Soc.* **1992**, *114*, 10024.
17. Aditya, A.; Nichols, D. E. & Loudon, G. M. *J. Chem. Educ.* **2008**, *85*, 1535.
18. Hunter, A. C.; Collins, C.; Dodd, H. T.; Dedi, C. & Koussoroplis, S. J. *J. Steroid Biochem. Mol. Biol.* **2010**, *122*, 352.